Development of a 3D *In Vitro* Model of the Blood-Brain Barrier in Layered Microfluidic Devices

by

Jack D. Wang

A dissertation submitted in partial fulfillment
of the requirements for the degree of
Doctor of Philosophy
(Biomedical Engineering)
in the University of Michigan
2015

Doctoral Committee:

Associate Professor Mohamed E.H. ElSayed, Chair
Associate Professor Anuska V. Andjelkovic-Zochowska
Professor Joseph L. Bull
Professor Shuichi Takayama

DEDICATION

This thesis is dedicated to my loving parents Wenjie Wang and Ling Feng, who without their dedication and support I would not have been able to complete my doctoral work. Their persistent reassurance allowed me to persevere throughout the most of trying times. I would also like to extend my sincerest gratitude to my doctoral research advisor, Mohamed E.H. ElSayed for the vital training, support, and expertise he provided during my doctoral education and his important advises on career development.

Table of Contents

List of Figures

Abstract

Development of a 3D *In Vitro* Model of the Blood-Brain Barrier in Layered Microfluidic Devices

by

Jack D. Wang

Chair: Mohamed E.H. ElSayed

The endothelial cells lining the capillaries that supply the brain with oxygen and nutrients present a highly regulated transport barrier known as the blood-brain barrier (BBB). These endothelial cells are characterized by thick cell membranes, low number of endocytic vesicles, absence of fenestrae, and highly organized tight junctions that restrict molecular diffusion across the paracellular space. The integrity and function of the BBB is finely regulated by several environmental conditions including endothelial cell-to-cell contact, communication with other neural cells such as astrocytes and pericytes, and the local concentration of secreted chemical factors. Several groups have cultured primary and immortalized brain capillary endothelial cells to develop an *in vitro* model that mimics the BBB for the purpose of screening transport properties of new drug molecules designed for treatment of central nervous system (CNS) disorders. However, these *in vitro* models

generally failed to mimic the restrictive transport properties of the BBB due to the formation of "loose" tight junctions, lower expression of specific carriers, or limited cell viability. We developed a 3D *in vitro* model of the BBB by culturing brain endothelial cells with pericytes and astrocytes in layered microfluidic channels. We hypothesized that the proposed model would improve endothelial cell polarization and enhance the formation of tight junctions, provide better endothelial cell-to-cell contact that is important for barrier development, and prevent the dilution of secreted neurotrophic factors, and these conditions collectively led to the development of an *in vitro* model that can truly mimic the BBB.

Chapter 1

Introduction

1.1 What is the Blood-Brain Barrier?

The endothelial cells lining the capillaries that supply the brain with oxygen and nutrients present a highly regulated transport barrier known as the blood-brain barrier (BBB). These endothelial cells are characterized by thick cell membranes, low number of endocytic vesicles, absence of fenestrae, and highly organized tight junctions that restrict molecular diffusion across the paracellular space [1-4]. The integrity and function of the BBB is regulated by several environmental conditions including endothelial cell-to-cell contact [4], communication with other supporting cell types such as astrocytes [5, 6] and pericytes [7-9], and the local concentration of secreted neurotrophic factors [6]. Due to the presence of this highly functional barrier, only 2% of small-molecule drugs (< 500 Daltons) can across the BBB to achieve their effective concentrations and nearly none of the existing

large-molecule drugs can across the BBB [10]. Only a few central nervous system (CNS) disorders, such as depression, epilepsy, chronic pain, and affective disorders, respond to clinical treatments by the 2% of small-molecule drugs that we have; on the other hand, many more serious CNS disorders cannot be effectively treated by these small therapeutic molecules including Alzheimer disease, Huntington disease, stroke, brain cancer, brain and spinal cord injury, HIV infection of the brain, etc [10]. Because of limitations of the currently available drug molecules, the CNS pharmaceutics market needs to grow more than 500% to reach the cardiovascular drug market despite the fact that there are 4 times more people afflicted with CNS disorders than cardiovascular disorders [11].

1.2 Transport of the Blood-Brain Barrier

Early studies using electron microscopy combined with tracers demonstrated that there are several important differences between brain endothelial cells and their peripheral counterparts [12]. First, they exhibit very few endocytotic vesicles which reduce the ability of hydrophobic molecules to transport across the endothelial cells from blood into the brain; this is called transcellular transport and it is very limited in the BBB [1]. Free membrane diffusion only applies to small hydrophobic molecules such as ethanol [4]. Essential nutrients are transported through carrier-mediated transporters; for example, GLUT-1 is responsible for the transport of glucose from the blood side to the brain. Other examples include monocarboxylic acid transporter MCT1, large neutral amino-acid transporter LAT1, and sodium-coupled nucleoside transporter CNT2 [4].

Second, intercellular junctions, specifically the tight junctions, formed between adjacent endothelial cells in the brain severely restrict the transport of hydrophilic molecules, which we call paracellular transport. Brain endothelial tight junctions are formed with occludin and a family of claudins such as claudin-1 and claudin-5; these protein strands are then connected to the cells through zonula occludens proteins [13]. It is worth noting that the changes of expression level of a certain tight junction protein do not always reflect changes in the transport properties through the paracellular route [4]. However, changes in the structure of these tight junction proteins can affect BBB function. For example, erroneous distribution of tight junction proteins in the internal and external membrane of brain endothelial cells will result in altered polarity of glucose transporter GLUT-1 resulting in stroke-prone spontaneously hypertensive conditions with no changes in occludin, claudin-1, clduain-5 and zonula occludens protein-1 expression [4].

Finally, efflux transporters such as the P-glycoproteins are expressed in the BBB and have been studied extensively [14, 15]. It has been found that this particular transporter possesses broad specificity and is able to recognize hundreds of compounds ranging from 330 daltons up to 4000 daltons in size [16]. Its primary function is to capture diffusing molecules transcellularly from the blood side to the brain tissue and pump them back to the blood side against their concentration gradients at the expense of ATP. The existence of P-glycoproteins, even though are essential to keep the brain tissue from contacting potential toxins, they are detrimental to the delivery of therapeutic agents to the brain. One such example is the treatment of brain tumor. Chemotherapeutic agents such as paclitaxel and doxorubicin have been determined to be substrates of the P-glycoprotein [17, 18]. As a

result, even though improved cancer therapeutics have been able to prolong the survival of patients with systemic cancer, the incidence of brain metastatic disease is increasing [15]. Furthermore, due to the restrictive transport of chemotherapeutic agents resulting in minimal drug concentration in the brain and the intrinsic resistance to chemotherapies of primary brain malignancies, there are currently very limited options for effective drug delivery into the brain for treatment of brain tumor [15].

1.3 Alternative Drug Delivery Methods to the BBB

The inability of conventional drug molecules to across the BBB has, in some cases, forced drug development programs to go forward without the consideration of BBB transport at all [10]. This led to the development of craniotomy-based drug delivery method where a hole is drilled in the head, and drugs are directly administered to the brain, thus bypassing the BBB altogether. However, drug molecules administered this way tend to stay at the injection site and cannot effectively penetrate the brain parenchyma. With such limited penetration capability, only 1% of the brain volume is reached, making this method ineffective against most, if not all, brain diseases.

Clinical research has also shown that osmotic modification of the BBB can increase the delivery of drug molecules, specifically chemotherapeutic agents for the treatment of brain tumors. Typically 1.4 M mannitol solution is introduced into the system by intracarotid infusion resulting in the opening of tight junctions at the BBB due to increased osmotic pressure at the apical side of the capillaries [19]. This method, coupled with

intravenous infusion of chemotherapeutic agents, has been found to prolong survival of patients with high-grade gliomas by 10-12 months [19]; however, this therapeutic method is associated with cognitive deterioration or changes in the central nervous system (CNS) detectable by Magnetic Resonance Imaging [20].

In comparison to the limitations of methods such as the craniotomy-based drug delivery system and osmotic modification of the BBB, if drug molecules administered intravenously or intracarotidly are capable of taking advantage of the transport systems, they have the potential to become much more effective at penetrating the BBB while minimizing side effects at the same time. Drug molecules capable of such maneuvers have the ability to reach nearly all of the neurons in the brain since every neuron is supported by its own capillary vessel [10]; however, it requires innovative drug-targeting systems that have the capability of traversing through the BBB. Development of such system cannot begin until detailed molecular and cellular biology of the BBB are revealed; and obtaining such information requires an accurate and cost-effective *in vitro* BBB model that can be used repeatedly for drug screening and experimentation.

1.4 Current *In Vitro* Blood-Brain Barrier Models

Since BBB is a transport barrier that has the capability to even restrict the movement of ions, the simplest form of measuring paracellular transport "tightness" is to assess the trans-endothelial electrical resistance [4]. While the earliest measurements on cultured monolayers of brain endothelial cells were published in 1987 by using Ussing chamber [21, 22], the methodology has become much easier since then through the widely

available semi-porous membrane inserts and the "chopstick" electrodes acting as Volt-Ohm resistance meters. These laboratory equipments allow repeated and rapid measurements of TEER. TEER is calculated as resistance measured (Ω) multiplied by the area of endothelial monolayer (cm^2) [4]. Another important measurement for evaluating paracellular transport is permeability using a fluorescently labeled or radioactive hydrophilic molecule [4]. A typically permeability value is evaluated by putting the marker molecule in the apical side of the endothelial monolayer and let it diffuse as a function of time. At the end of the time period, permeability is calculated by using the concentrations, volumes, surface area, and duration. It has a unit of cm/s.

Realizing the importance of *in vitro* BBB models, many groups have attempted to construct such model using both primary and immortalized cell lines. Primary endothelial cells isolated from bovine, human, porcine, and rodent are typically used in modeling the BBB [4]. Among all such established models, one porcine model demonstrated relatively high TEER and low permeability [4], which are key characteristics of the BBB. Despite the ethical questions and the logistical difficulties of obtaining human brain tissue, there have been reports of established human BBB models; these models, however, are less robust than porcine models according to published data [4]. All primary models suffer from several disadvantages. Primary cells are expensive to obtain and the reconstitution process is time consuming. Furthermore, the homogeneity of obtained cells is difficult to determine, and can be easily contaminated with neighboring cell types such as the pericytes [4].

In recent years, immortalized brain endothelial cell lines have been more commonly used than primary cell lines due to their ease of manipulation and reproducibility. There are

currently more than 20 endothelial cell lines available and virtually all of them have been used to establish *in vitro* BBB models with published results [4]. Many of these models utilize transwell system, which is the standard tool for *in vitro* drug screening. The major issue that such models suffer is leaky monolayer formation which results in low TEER and high permeability values. Since these models did not generate BBB characteristics, it is very difficult to use them for BBB related studies. We believe that the reasons for the failed mimicry of the restrictive transport properties of the BBB can be due to the formation of "loose" tight junctions between adjacent endothelial cells, lower expressions of specific carriers, or limited cell viability. This can be attributed to the lack of proper micro-environments and efficient integration of endothelial and neural cells in a model that allow cell-to-cell communication necessary to induce the proper differentiation of brain capillary endothelial cells, formation of restrictive tight junctions, and functional expression of different transporters at the levels present *in vivo*.

In 2008, Cucullo and colleagues published a dynamic *in vitro* model of the BBB that utilizes astrocyte co-culture and pulsatile flow, both of which are key environmental factors that influence the development and regulation of BBB [23]. The model demonstrated high TEER values similar to that of primary porcine endothelial cell culture model and low permeability measured by using paracellular transport markers such as mannitol and sucrose. Curiously, co-culture of endothelial cells with astrocytes was not required to obtain BBB-like characteristics in this model [23]. While technical difficulties involved with the model set-up, such as the handling and cost of the hollow fibers used for cell seeding and flow parameters that are inconsistent with *in vivo* capillary conditions, do

exist, the model itself proved that micro-environments are the most important factors that dictate the proliferation and differentiation of endothelial cells. Therefore, in order to develop an accurate *in vitro* model of the BBB focus should be set upon recreating the micro-environments of brain endothelial cells instead of manipulating innate cellular properties.

REFERENCES

1. Rubin, L.L. and J.M. Staddon, *The Cell Biology of the Blood-Brain Barrier.* Annual Review of Neuroscience, 1999. **22**: p. 11-28.
2. Dermietzel, R., D.C. Spray, and M. Nedergaard, *Blood-Brain Barrier: From Ontogeny to Artificial Interfaces*. Vol. 1. 2006, Weinheim, Germany: WILEY-VCH.
3. Persidsky, Y., et al., *Blood-Brain Barrier: Structural Components and Function Under Physiologic and Pathologic Conditions.* Journal of Neuroimmune Pharmacology, 2006. **1**(3): p. 223-236.
4. Deli, M.A., et al., *Permeability Studies on In Vitro Blood-Brain Barrier Models: Physiology, Pathology, and Pharmacology.* Cellular and Molecular Neurobiology, 2005. **25**(1): p. 59-127.
5. Abbott, N.J., *Astrocyte-endothelial interactions and blood-brain barrier permeability.* Journal of Anatomy, 2002. **200**(6): p. 629-638.
6. Abbott, N.J., L. Ronnback, and E. Hansson, *Astrocyte-endothelial interactions at the blood-brain barrier.* Nature Reviews Neuroscience, 2006. **7**: p. 41-53.
7. Allt, G. and J.G. Lawrenson, *Pericytes: Cell Biology and Pathology.* Cells Tissues Organs, 2001. **169**(1): p. 1-11.
8. Armulik, A., G. Genove, and C. Betsholtz, *Pericytes: developmental, physiological, and pathological perspectives, problems, and promises.* Developmental Cell, 2011. **21**(2): p. 193-215.

9. Betsholtz, C., P. Lindblom, and H. Gerhardt, *Role of pericytes in vascular morphogenesis.* Mechanisms of Angiogenesis Experientia Supplementum, 2005. **94**(115-125).

10. Pardridge, W.M., *Blood-Brain Barrier Drug Targeting: The Future of Brain Drug Development.* Molecular Interventions, 2003. **3**(2): p. 90-105.

11. Pardridge, W.M., *Why is the global CNS pharmaceutical market so under-penetrated?* DDT, 2002. **7**(1): p. 5-7.

12. Reese, T.S. and M.J. Karnovsky, *Fine Structural Localization of a Blood-Brain Barrier to Exogenous Peroxidase.* The Journal of Cell Biology, 1967. **34**: p. 207-217.

13. Brown, R.C., A.P. Morris, and R.G. O'Neil, *Tight Junction Protein Expression and Barrier Properties of Immortalized Mouse Brain Microvessel Endothelial Cells.* Brain Research, 2007. **1130**(1): p. 17-30.

14. Ueda, K., et al., *Human P-glycoprotein Transports Cortisol, Aldosterone, and Dexamethasone, but Not Progesterone.* The Journal of Biological Chemistry, 1992. **267**(34): p. 24248-24252.

15. Deeken, J.F. and W. Loscher, *The Blood-Brain Barrier and Cancer: Transporters, Treatment, and Trojan Horses.* Clinical Cnacer Research, 2007. **13**: p. 1663-1674.

16. Aller, S.G., et al., *Structure of P-glycoprotein Reveals a Molecular Basis for Poly-Specific Drug Binding.* Science, 2009. **323**(5922): p. 1718-1722.

17. Gallo, J.M., et al., *The Effect of P-glycoprotein on Paclitaxel Brain and Brain Tumor Distribution in Mice.* Cancer Research 2003. **63**: p. 5114-5117.

18. Shiraki, N., et al., *Increase in Doxorubicin Cytotoxicity by Inhibition of P-glycoprotein Activity with Lomerizine.* Biological and Pharmaceutical Bulletin, 2001. **24**(5): p. 555-557.

19. Nag, S., *The Blood-Brain Barrier: Biology and Research Protocols*. 2003, Totowa, New Jersey: Humana Press Inc.

20. Roman-Goldstein, S., et al., *MR and Cognitive Testing of Patients Undergoing Osmotic Blood-Brain Barrier Disruption with Intraarterial Chemotherapy.* American Journal of Neuroradiology, 1995. **16**(3): p. 543-553.

21. Hart, M.N., et al., *Differential opening of the brain endothelial barrier following neutralization of the endothelial luminal anionic charge in vitro.* Journal of Neuropathology & Experimental Neurology, 1987. **46**(141-153).

22. Rutten, M.J., R.L. Hoover, and M.J. Karnovsky, *Electrical resistance and macromolecular permeability of brain endothelial monolayer cultures.* Brain Research, 1987. **425**: p. 301-310.

23. Cucullo, L., et al., *Immortalized human brain endothelial cells and flow-based vascular modeling: a marriage of convenience for rational neurovascular studies.* Journal of Cerebral Blood Flow & Metabolism, 2008. **28**: p. 312-328.

Chapter 2

Background

2.1 Rationale for Using PDMS Microfluidic Channels for *In Vitro* Modeling

Microfluidic channels have been used in many biological applications including rapid high density sequencing [24-26], polymerase chain reaction [27-31], and detection of single molecules [32-34] since its development in the 1990s. They have been particularly useful in the development of biological assays such as particle immunoassays [35], cell-based high throughput screening for drug discovery [36], and capacitance cytometry of single eukaryotic cells [37]. The micron-scale size of these microfluidic devices offers many unique advantages including close mimicry of many *in vivo* microenvironments [38] and small volume requirement compared to conventional analysis systems [39].

Several materials have been used to fabricate these microfluidic channels such as silicon, ceramic , quartz glass, polymethyl methacrylate, SU-8, and poly(dimethylsiloxane) (PDMS) [30, 35, 36, 39-41]. The optical clarity [42], biocompatibility [43], and high oxygen diffusivity of PDMS [44] render it the most commonly used material in fabrication of microfluidic channels for biological applications. Several groups have capitalized on these advantages and used PDMS-based microfluidic channels to develop *in vitro* models of different physiological processes. For example, Sodunke *et al*. successfully conducted a study on the replication of hepatitis B virus in normal human hepatocytes using a PDMS-based microfluidic platform [45]. PDMS-based microfluidic channels also proved efficient in maintaining high and low density cultures of mammalian neuronal cells [46]. Recently, Huh *et al*. demonstrated the versatility of PDMS-based channels by creating a microfluidic airway system that simulates human airway epithelia and physiological airway flow found in the respiratory system [47].

One key limitation of these channels is the hydrophobicity of the PDMS surface, which reduces its wettability by aqueous biological fluids and affects its compatibility with cell culture. Plasma oxidation has been routinely used to introduce silanol groups on the PDMS surface to become more hydrophilic and fitting for *in vitro* cell culture [48]. However, diffusion of free uncross-linked PDMS chains from the bulk plymer to the channel surface diminishes its hydrophilic character causing the channel wall to gradually revert to its intrinsic hydrophobic nature [49]. Furthermore, exposure of oxidized PDMS surfaces to air for an extended period of time restores its hydrophobic character. Extraction of PDMS surfaces using different solvents to remove unreacted oligomers followed by

plasma oxidation was shown to increase the stability of hydrophilic PDMS surfaces by 7 days. Combination of plasma oxidation followed by treatment with $SiCl_4$ and CCl_4 gases or deposition of metal oxides have also been used to increase the stability of hydrophilic PDMS surfaces. Despite the promise of these approaches in maintaining the hydrophilic nature of oxidized PDMS surfaces, they are not routinely used in fabrication of PDMS devices particularly those developed for biological assays. An earlier study confirmed the hydrophobicity of PDMS devices when Nile Red (a hydrophobic fluorescent dye) diffused into the PDMS wall of microfluidic channels shown by the retention of the fluorescence signal after repeated washes. While this earlier study by Toepke *et al*. provides a visual evidence of molecular absorption into PDMS channels, it does not provide any quantitative methods to predict the absorption of other hydrophobic molecules into PDMS microfluidic channels. It is essential that we can understand how molecules interact with the PDMS walls before any quantitative assays are used in PDMS microfluidic channels.

2.2 Design of PDMS Microfluidic Channels for Modeling the Blood-Brain Barrier

The design of our microfluidic device incorporates two layered microfluidic channels that sandwich a polyester membrane (0.4μm pore size) along the entire length of the channel, which was used to culture b.End3 cells **(Figure 2.1)**. The device is designed to incorporate a cross section between the top and bottom channels sufficient to allow measurement of solute's permeability across b.End3 cell monolayers while maintaining an elongated geometric shape and scaled down dimensions. The elongated rectangular shaped channel serve to guide endothelial cell growth, which has been shown to enhance

endothelial cell growth and differentiation [50]. The geometry of our device also serves to mimic the blood vessel much more closely compared to the circular design of the transwells. The small dimensions (W = 2mm; L = 4cm; H = 200µm) of the 2mm-wide microfluidic channel increase the surface to volume ratio, which results in concentration of the factors secreted by brain endothelial cells and decreases the volume of the markers' solution needed for permeability studies at the same time. Therefore, the volume of the markers' solution in our microfluidic device is only 16µl in the top channel compared to 1ml in standard 12-well transwells. Our device also allows the incorporation of Ag/AgCl electrodes in both the top and bottom channels allowing real-time measurement of TEER, which is an indicator of cell monolayer integrity [51].

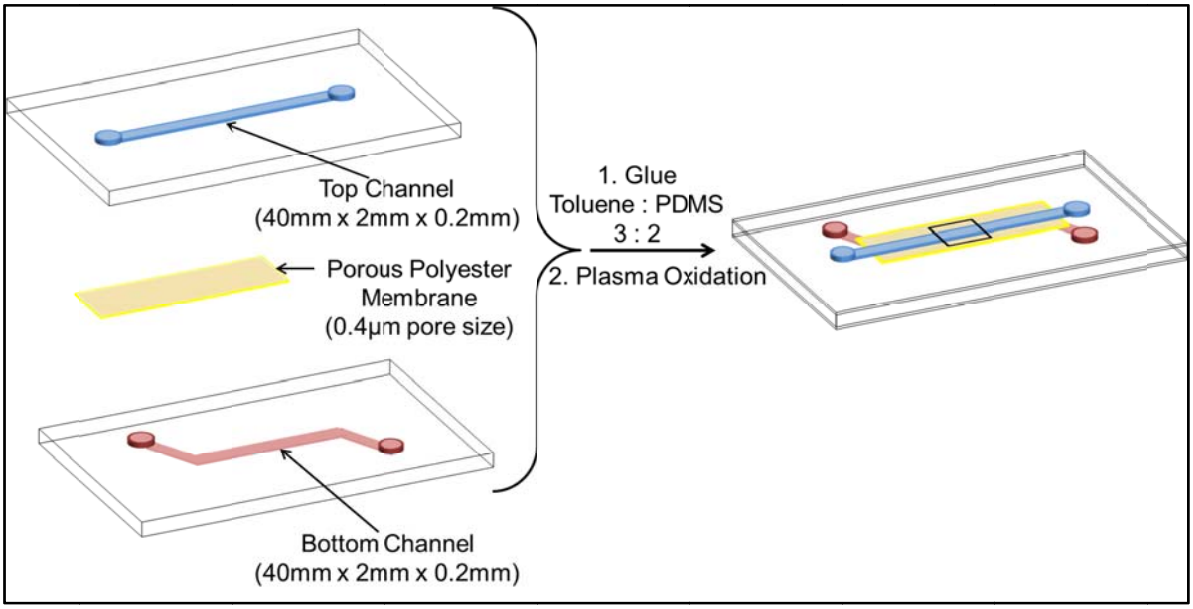

Figure 2.1: A schematic drawing of the layered PDMS (40mm x 2mm x 0.2mm) sandwiching a polyester membrane

The microfluidic devices used for culture of b.End3 cells are composed of layered microfluidic channels sandwiching a porous membrane (0.4μm pore size), which were fabricated using soft lithography following established protocols [41, 51]. Briefly, PDMS prepolymer was mixed with the curing agent at a 10 (prepolymer)/1 (curing agent) weight ratio before casting onto two 4 inch silicon wafers containing a 200μm thick positive relief pattern. The mixture was cured at 60°C for 2 hours before peeling the PDMS layer off the silicon wafer. Access holes were punched with a 16 gauge blunt syringe (1.65 mm outer diameter) forming the inlet and outlet holes for each channel. We spun coated a PDMS/toluene mixture prepared at a 3/2 weight ratio on a clean glass slide for 1 minute to generate a thin mortar layer, which was used to glue the top and bottom PDMS layers. Ag/AgCl recording electrodes were embedded in 500μm x 500μm side channels when fabricating microfluidic devices for measurement of transendothelial electrical resistance (TEER) across b.End3 monolayers following a published procedure [51]. Polyester membranes with an average pore size of 0.4μm were sandwiched between the aligned top and bottom PDMS layers and glued together before curing for 1 hour until the PDMS mortar completely hardened. Pipette tips (100μl) were inserted into the inlets and outlets of the top and bottom channels to serve as medium reservoirs before exposure to plasma oxygen for 5 minutes. Sterile fibronectin solution (25μg/ml) was loaded into the top PDMS channel for 24 hours to coat the polyester membrane followed by exposure of the microfluidic device to UV radiation for sterilization before seeding of b.End3 cells.

TEER values across b.End3 monolayers cultured in layered microfluidic channels was measured on daily basis following our published protocol [51]. Briefly, impedance

spectra were taken using an Autolab potentiostat/galvanostat at 0.1V of alternating current passing between the two embedded electrodes within layered microfluidic channels. Frequency range between 10Hz to 1.00MHz was used to yield a total of 64 impedance measurements. The control impedance spectra measured before seeding the cells were subtracted from the measured impedance spectra with b.End3 cells to eliminate their contribution to the calculated resistance. We developed a MATLAB code (The MathWorks Inc., Natick, MA) using its optimization toolbox to resolve the TEER values, which were normalized to the surface area of the cell monolayers to calculate the resistance in $\Omega.cm^2$.

2.3 Single Culture of Brain Microvascular Endothelial Cells in Layered PDMS Microfluidic Channels

Stewart and co-workers provided one of the earlier examples showing the effect of microenvironment on the barrier properties of chick capillaries implanted in quail brain and quail somite grafts [52]. They showed that chick capillaries implanted in quail brain graft displayed blood-brain barrier like properties while those implanted in quail somite graft near the skeletal muscle did not exhibit the same restrictive properties [52]. In this research, we aimed to mimic the shape and dimensions of small blood vessels in the design of our layered microfluidic channels, which will allow better cell-to-cell contact, increase the surface-to-volume ratio, minimize the dilution of secreted factors, and reduce the needed volume to evaluate the transport of different markers [41, 50, 53-55]. We can achieve this goal by adjusting the dimensions of the top channel to resemble a blood capillary while maintaining a large aspect ratio and a small total volume (17 μl). Starting with 2mm-wide

channels, it can be hypothesized that channel width and geometry can enhance b.End3 cell-to-cell contact and guide their alignment along the longitudinal axis of the channel, which is supported by previous reports utilizing microfluidic devices with similar width and height [56]. Renkin function, a frequently used mathematical model that can resolve the radius of the tight junctional pores in both endothelial and epithelial monolayers, can help demonstrate and verify that b.End3 cells cultured in PDMS microfluidic channels can indeed form "tighter" and more "restrictive" tight junctions in the radius of the intercellular space. We hope that by developing an *in vitro* model of the BBB where barrier integrity is enhanced by controlling the dimensions of the microfluidic channel without the need for flow-mediated shear stress, we can take a significant step towards the development of simplified yet robust *in vitro* models.

Previous works have indicated that geometry of the cell culture micro-environment not only can help define vascular architectures [57] and cell adhesion [58], it can also influence cell growth, differentiation, and apoptosis [50]. Therefore we hypothesized early on that the small width of the channels can induce better cell-to-cell contact and play an important role in assisting the formation of tight junctions. This effect can be demonstrated by increasing the width of the microfluidic channels from 2 mm to 4 and 8 mm. We will then evaluate TEER measurements and permeability values of marker molecules to confirm the effect of geometry has on endothelial monolayers.

2.4 Bi- and Tri-Culture Configurations in Layered PDMS Microfluidic Channels

It has long been acknowledged that both pericytes [24] and astrocytes [6] play very important roles in the differentiation and development of brain endothelial cells. Pericytes, in particular, partially surround the brain capillaries at endothelial tight junctions, and are usually found between endothelial cells and astrocyte end-feet. This strategic position allows pericytes to interact with both the endothelial cells and the astrocytes [8, 59]. Previous researches have suggested that pericytes, based on their morphology and localization, play important roles in endothelial cell function and modulation of blood flow, and they make direct contact with endothelial cells through gap and adherens junctions [7, 59, 60]. It is also important to note that at the BBB the ratio of pericytes to endothelial is one of the highest in any organ [61]. Furthermore, there are evidences in the literature that suggest pericytes are capable of secreting signaling molecules that are essential to the differentiation and contractile properties of endothelial cells [9, 62, 63]. Astrocytes, too, have been found to secrete a range of neurotrophic factors such as transforming growth factor-β (TGFβ) [6], glial-derived neurotrophic factor (GDNF) [64], and basic fibroblast growth factor (bFGF) [6]. It has been found that these factors can induce many aspects of the BBB phenotype in endothelial cells *in vitro* [2, 6, 10]. At the same time, endothelial-derived factor such as leukaemia inhibitory factor (LIF) has been documented to induce the differentiation of astrocytes [65]. The cross-interaction between endothelial cells and astrocytes are mutually beneficial and ensures the differentiation of both BBB and astrocytic development.

Based on the importance of pericytes and astrocytes on endothelial differentiation, we want to design our bi- and tri-culture configurations to examine the feasibility of culturing b.End3 cells together with pericytes and astrocytes and whether these co-culture configurations can induce BBB-like transport properties. For our bi-culture configuration, our goal will be to mimic the close promixity of endothelial cells and the pericytes; therefore we will culture pericytes on the back-side of the semi-porous membrane, where the endothelial cells are growing on, in the microfluidic devices. This configuration ensures that b.End3 cells and pericytes are in close contact with each other in the condition that is similar to the conditions *in vivo*. For our tri-culture configuration, we will add astrocytes to the bottom layer of the channels. While the astrocytes are not in direct contact with the endothelial-pericyte layers, the secreted neurotrophic factors that are so critical to the BBB development still reaches the b.End3 cells through diffusion; again, creating a similar condition to the *in vivo* conditions. To further validate the effects of astrocytes on endothelial-pericyte layers, we will modify our original device and change the height of the bottom channel from 0.2mm to 0.6mm and 1mm. The purpose of modifying the bottom channel is to increase the distance between the astrocytes and the endothelial-pericyte layers and increase the volume of the bottom channel in order to subject the secreted neurotrophic factors to dilution.

REFERENCES

1. Liu, S., et al., *The Role of Pericytes in Blood-Brain Barrier Function and Stroke.* Current Pharmaceutical Design, 2012. **18**: p. 3653-3662.
2. Simpson, P.C., et al., *High-throughput genetic analysis using microfabricated 96-sample capillary array electrophoresis microplates.* Proceedings of the National Academy of Sicences, 1998. **95**(5): p. 2256-2261.
3. Woolley, A.T. and R.A. Mathies, *Ultra-High-Speed DNA Sequencing Using Capillary Electrophoresis Chips.* Analytical Chemistry, 1995. **67**(20): p. 3676-3680.
4. Burns, M.A., et al., *An Integrated Nanoliter DNA Analysis Device.* Science, 1998. **282**: p. 484-487.
5. Cheng, J., et al., *Degenerate oligonucleotide rpimed-PCR and capillary electrophoretic analysis of human DNA on microchip-based devices.* Analytical Biochemistry, 1998. **257**: p. 101-106.
6. Kopp, M.U., A.J.d. Mello, and A. Manz, *Chemical Amplification: Continuous-Flow PCR on a Chip.* Science, 1998. **280**(5366): p. 1046-1048.
7. Northrup, M.A., et al., *A miniature analytical instrument for nucleic acids based on micromachined silicon reaction chambers.* Analytical Chemistry, 1998. **70**: p. 912-922.
8. Waters, L.C., et al., *Multiple Sample PCR Amplification and Electrophoretic Analysis on a Microchip.* Analytical Chemistry, 1998. **70**: p. 5172.
9. Chou, H.P., et al., *A microfabricated device for sizing and sorting DNA molecules.* Proceedings of the National Academy of Sciences, 1999. **96**(1): p. 11-13.

10. Dörre, K., et al., *Techniques for single molecule sequencing.* Bioimaging, 1997. **5**: p. 139-152.

11. Effenhauser, C.S., et al., *Integrated Capillary Electrophoresis on Flexible Silicone Microdevices: Analysis of DNA Restriction Fragments and Detection of Single DNA Molecules on Microchips.* Analytical Chemistry, 1997. **69**(17): p. 3451-3457.

12. Han, J.-H. and J.-Y. Yoon, *Reusable, polyethylene glycol-structured microfluidic channel for particle immunoassays.* Journal of Biological Engineering, 2009. **3**(6): p. 1-6.

13. Upadhyaya, S. and P.R. Selvaganapathy, *Microfluidic devices for cell based high throughput screening.* Lab on a Chip, 2010. **10**: p. 341-348.

14. Sohn, L.L., et al., *Capacitance cytometry: Measuring biological cells one by one.* Proceedings of the National Academy of Sciences, 2000. **97**(20): p. 10687-10690.

15. Fiddes, L.K., et al., *A circular cross-section PDMS microfluidics system for replication of cardiovascular flow conditions.* Biomaterials, 2010. **31**: p. 3459-3464.

16. Tung, Y.-C., et al., *Small volume low mechanical stress cytometry using computer-controlled Braille display microfluidics.* Lab on a Chip, 2007. **7**: p. 1497-1503.

17. Abate, A.R., et al., *Glass coating of PDMS microfluidic channels by sol-gel methods.* Lab on a Chip, 2008. **8**: p. 516-518.

18. Chueh, B.-h., et al., *Leakage-Free Bonding of Porous Membranes into Layered Microfluidic Array Systems.* Analytical Chemistry, 2007. **79**(9): p. 3504-3508.

19. Huszank, R., et al., *Fabrication of optical devices in poly(dimethylsiloxane) by proton microbeam.* Optics Communications, 2009. **283**: p. 176-180.

20. Thangawng, A.L., et al., *An ultra-thin PDMS membrane as a bio/micro-nano interface: fabrication and characterization.* Biomedical Microdevices, 2007. **9**: p. 587-595.

21. Cox, M.E. and B. Dunn, *Oxygen Diffusion in Poly(dimethyl Siloxane) using Fluorescence Quenching. I. Measurement Technique and Analysis.* Journal of Polymer Science: Part A: Polymer Chemistry, 1986. **24**: p. 621-636.

22. Sodunke, T.R., M.J. Bouchard, and H.M. Noh, *Microfluidic platform for hepatitis B viral replication study.* Biomedical Microdevices, 2007.

23. Millet, L.J., et al., *Microfluidic devices for culturing primary mammalian neurons at low densities.* Lab on a Chip, 2007. **7**: p. 987-994.

24. Huh, D., et al., *Acoustically detectable cellular-level lung injury induced by fluid mechanical stresses in microfluidic airway systems.* Proceedings of the National Academy of Sciences, 2007. **104**(48): p. 18886-18891.

25. McDonald, J.C., et al., *Fabrication of microfluidic systems in poly(dimethylsiloxane).* Electrophoresis, 2000. **21**(1): p. 27-40.

26. Eddington, D.T., J.P. Puccinelli, and D.J. Beebe, *Thermal aging and reduced hydrophobic recovery of polydimethylsiloxane.* Sensors and Actuators B, 2006. **114**: p. 170-172.

27. Huang, S. and D.E. Ingber, *Shape-Dependent Control of Cell Growth, Differentiation, and Apoptosis: Switching between Attractors in Cell Regulatory Networks.* Experimental Cell Research, 2000. **261**: p. 91-103.

28. Douville, N.J., et al., *Fabrication of Two-Layered Channel System with Embedded Electrodes to Measure Resistance Across Epithelial and Endothelial Barriers.* Analytical Chemistry, 2010. **82**(6): p. 2505-2511.

29. Stewart, P.A. and M.J. Wiley, *Developing Nervous Tissue Induces Formation of Blood-Brain Barrier Characteristics in Invading Endothelial Cells: A Study Using Quail-Chick Transplantation Chimeras.* Developmental Biology, 1981. **84**: p. 183-192.

30. Anene-Nzelu, C.G., et al., *Scalable alignment of three-dimensional cellular constructs in a microfluidic chip.* Lab on a Chip, 2013. **13**: p. 4124-4133.

31. Stins, M.F., J. Badger, and K.S. Kim, *Bacterial invasion and transcytosis in transfected human brain microvascular endothelial cells.* Microbial Pathogenesis, 2001. **30**: p. 19-28.

32. Augustin, H.G., *Methods in Endothelial Cell Biology*. 2004, New York: Springer.

33. Booth, R. and H. Kim, *Characterization of a microfluidic in vitro model of the blood-brain barrier (uBBB).* Lab on a Chip, 2012. **12**: p. 1784-1792.

34. Baker, B.M., et al., *Microfluidics embedded within extracellular matrix to define vascular architectures and pattern diffusive gradients.* Lab on a Chip, 2013. **13**(16): p. 3246-3252.

35. Green, J.V., et al., *Effect of channel geometry on cell adhesion in microfluidic devices.* Lab on a Chip, 2009. **9**(5): p. 677-685.

36. Abbott, N.J., L. Ronnback, and E. Hansson, *Astrocyte-endothelial interactions at the blood-brain barrier.* Nature Reviews Neuroscience, 2006. **7**: p. 41-53.

37. Diaz-Flores, L., et al., *Pericytes. Morphofunction, interactions and pathology in a quiescent and activated mesenchymal cell niche.* Histology and Histopathology, 2009. **24**: p. 909-969.

38. Armulik, A., G. Genove, and C. Betsholtz, *Pericytes: developmental, physiological, and pathological perspectives, problems, and promises.* Developmental Cell, 2011. **21**(2): p. 193-215.

39. Allt, G. and J.G. Lawrenson, *Pericytes: Cell Biology and Pathology.* Cells Tissues Organs, 2001. **169**(1): p. 1-11.

40. Fujimoto, K., *Pericyte-endothelial gap junctions in developing rat cerebral capillaries: a fine structural study.* The Anatomical Record, 1995. **242**(4): p. 562-565.

41. Frank, R.N., T.J. Turczyn, and A. Das, *Pericyte Coverage of Retinal and Cerebral Capillaries.* Investigative Ophthalmology, 1990. **31**(6): p. 999-1007.

42. Krueger, M. and I. Bechmann, *CNS pericytes: Concepts, misconceptions, and a way out.* Glia, 2009. **58**(1): p. 1-10.

43. Betsholtz, C., P. Lindblom, and H. Gerhardt, *Role of pericytes in vascular morphogenesis.* Mechanisms of Angiogenesis Experientia Supplementum, 2005. **94**(115-125).

44. Lai, C.-H. and K.-H. Kuo, *The critical component to establish in vitro BBB model: Pericyte.* Brain Research Reviews, 2005. **50**: p. 258-265.

45. Igarashi, Y., et al., *Glial Cell Line-Derived Neurotrophic Factor Induces Barrier Function of Endothelial Cells Forming the Blood-Brain Barrier.* Biochemical and Biophysical Research Communications, 1999. **261**(1): p. 108-112.

46. Pardridge, W.M., *Blood-Brain Barrier Drug Targeting: The Future of Brain Drug Development.* Molecular Interventions, 2003. **3**(2): p. 90-105.

47. Dermietzel, R., D.C. Spray, and M. Nedergaard, *Blood-Brain Barrier: From Ontogeny to Artificial Interfaces*. Vol. 1. 2006, Weinheim, Germany: WILEY-VCH.

48. Mi, H., H. Haeberle, and B.A. Barres, *Induction of Astrocyte Differentiation by Endothelial Cells.* The Journal of Neuroscience, 2001. **21**(5): p. 1538-1547.

Chapter 3

Quantitative Analysis of Molecular Absorption into PDMS Microfluidic Channels

3.1 INTRODUCTION

Microfluidic channels have been used in many biological applications including rapid high density sequencing,[1-3] polymerase chain reaction,[4-8] and detection of single molecules[9-11] since its development in the 1990s. They have been particularly useful in the development of biological assays such as particle immunoassays,[12] cell-based high throughput screening for drug discovery,[13] and capacitance cytometry of single eukaryotic cells.[14] The micron-scale size of these microfluidic devices offers many unique advantages including close mimicry of many *in vivo* microenvironments[15, 16] and small volume requirement[17, 18] compared to conventional analysis systems.

Several materials have been used to fabricate these microfluidic channels such as silicon,[19-21] ceramic,[22] quartz glass,[23-26] polymethyl methacrylate,[27, 28] SU-

8,[29] and poly(dimethylsiloxane; PDMS).[30, 31] The optical clarity,[32] biocompatibility,[33] and high oxygen diffusivity[34] of PDMS render it the most commonly used material in fabrication of microfluidic channels for biological applications. Several groups have capitalized on these advantages and used PDMS-based microfluidic channels to develop *in vitro* models of different physiological processes. For example, Sodunke *et al* successfully conducted a study on the replication of hepatitis B virus in normal human hepatocytes using a PDMS-based microfluidic platform.[35] PDMS-based microfluidic channels also proved efficient in maintaining high and low density cultures of mammalian neuronal cells.[36] Recently, Huh *et al* demonstrated the versatility of PDMS-based channels by creating a microfluidic airway system that simulates human airway epithelia and physiological airway flow found in the respiratory system.[37]

One key limitation of these channels is the hydrophobicity of the PDMS surface, which reduces its wettability by aqueous biological fluids and affects its compatibility with cell culture.[31] Plasma oxidation has been routinely used to introduce silanol groups on the PDMS surface to become more hydrophilic and fitting for *in vitro* cell culture.[31] However, diffusion of free uncross-linked PDMS chains from the bulk polymer to the channel surface diminishes its hydrophilic character causing the channel wall to gradually revert to its intrinsic hydrophobic nature.[38] Furthermore, exposure of oxidized PDMS surfaces to air for an extended period of time restores its hydrophobic character.[31] Extraction of PDMS surfaces using different solvents to remove unreacted oligomers followed by plasma oxidation was shown to increase the stability of hydrophilic PDMS surfaces by seven days.[39] Combination of plasma oxidation followed by treatment with

$SiCl_4$ and CCl_4 gases[40] or deposition of metal oxides[41] have also been used to increase the stability of hydrophilic PDMS surfaces. Despite the promise of these approaches in maintaining the hydrophilic nature of oxidized PDMS surfaces, they are not routinely used in fabrication of PDMS devices particularly those developed for biological assays. An earlier study confirmed the hydrophobicity of PDMS devices when Nile Red (a hydrophobic fluorescent dye) diffused into the PDMS wall of microfluidic channels shown by the retention of the fluorescence signal after repeated washes.[42] While this earlier study by Toepke *et al.* provides a visual evidence of molecular absorption into PDMS channels, it does not provide any quantitative methods to predict the absorption of other hydrophobic molecules into PDMS microfluidic channels.

In this report, we provide a quantitative correlation between the partition coefficient (log P) of a series of marker molecules and their absorption into microfluidic PDMS channels at pH 7.0 as a function of solution temperature (25 ºC and 37 ºC) and incubation time (0.5, 1, 2.5, and 4.5 hours). The partition coefficient, log P, of a given molecule depends on its chemical structure and the associated hydrophilic/hydrophobic balance.[43] Log P is experimentally determined by the ratio between molecule's concentration in a hydrophobic solvent (octanol) and concentration in a hydrophilic solvent (water) upon dissolution and reaching equilibrium in this biphasic solvent system as shown in equation 1.[43]

$$\log P = \log \frac{[\text{solute in octanol}]}{[\text{solute in water}]} \quad \text{----------Eq 1}$$

Molecules with high log P value such as Nile Red (log P = 5.0)[44] are highly hydrophobic and can easily partition into lipid bilayers[45] and absorb into hydrophobic PDMS

surfaces.[42] However, the majority of pharmaceutical and diagnostic agents have significantly lower log P values than 5 to achieve aqueous solubility and absorption from the gastrointestinal tract.[46] Consequently, there is a need to establish a relationship between log P of model solute molecules and their absorption into PDMS to predict the effect of molecular absorption of different therapeutic or diagnostic molecules on the accuracy and reproducibility of *in vitro* assays performed in microfluidic PDMS devices.

We selected five molecules with log P values that span the established log P range of current pharmaceutical agents[46, 47] and are commonly used as markers to assess the viability and barrier properties of epithelial and endothelial monolayers **(Figure 3.1)**.

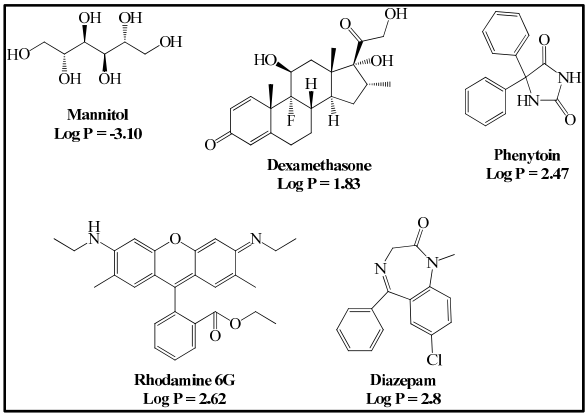

Figure 3.1: Chemical structure and log P values of the selected marker molecules.

Mannitol is a hydrophilic small molecular weight molecule with six hydroxyl groups and a log P value of -3.10.[48] Mannitol permeates across epithelial and endothelial barriers through the aqueous pores in the tight junction complexes and is routinely used as a paracellular permeability marker.[49] Dexamethasone is a glucocorticoid with a potent

anti-inflammatory effect.[50] Phenytoin is an anti-epileptic drug that is used to suppress abnormal brain activity including epileptic seizures.[51] Dexamethasone and phenytoin are moderately hydrophobic drug molecules with log P values of 1.83 and 2.47, respectively.[52, 53] Both dexamethasone and phenytoin are substrates for the P-glycoprotein (P-gp) efflux pump present on the luminal side of intestinal epithelial cells, vascular endothelial cells, and cancer cells.[54-56] Both molecules are routinely used to assess the functional expression of the P-gp efflux pump in epithelial and endothelial monolayers used as *in vitro* screening tools.[54, 55] Rhodamine 6G is a hydrophobic, membrane-permeable, fluorescent dye with a log P of 2.62 that has been used to evaluate membrane potential based on its fluorescence intensity.[57] Diazepam is a hydrophobic drug molecule with log P of 2.8,[58] which allows it to freely diffuse across the cell membrane and is consequently used as a marker of transcellular permeability across epithelial and endothelial cell monolayers.[59] Diazepam is routinely used as a sedative, anticonvulsant, anxiolytic, and skeletal muscle relaxant.[60] These molecules were selected to span the log P range of major pharmaceutical agents (log P ~ 2.43).[47] Furthermore, we evaluated the effect of TiO_2[61] and glass[62] coatings on the absorption of hydrophobic molecules into PDMS channels.

3.2 MATERIALS AND METHODS

3.2.1 Materials

Poly(dimethylsiloxane) (Sylgard 184) was purchased from Dow Corning (Midland, MI). SU-850 was purchased from MicroChem (Newton, MA). Titanium (IV) isopropoxide, Tetraethyl orthosilicate (TEOS), and Methyltriethyoxysilane (MTES) were purchased from Sigma Aldrich (St. Louis, MO). [14C]-D-Mannitol (100 μCi/ml) and [3H]-Phenytoin (1 mCi/ml) were purchased from Moravek Biochemicals and Radiochemicals (Brea, CA). [3H]-Diazepam (1 mCi/ml) and [3H]-Dexamethasone (1 mCi/ml) were purchased from American Radiolabeled Chemicals, Inc. (St. Louis, MO). Rhodamine 6G was purchased from Invitrogen (Carlsbad, CA). All chemicals were used as delivered without further purification.

3.2.2 Design and Fabrication of Microfluidic Channels

Microfluidic channels were fabricated using soft lithography following established procedures.[63] Briefly, PDMS prepolymer was mixed with the curing agent at a weight ratio of 10 (prepolymer):1 (curing agent) and was cast onto a 4 inches silicon wafer containing a 200 μm thick positive relief pattern. A single wafer was patterned to contain 5 evenly spaced microfluidic channels where each channel is 40 mm x 2 mm x 200 μm (L x W x H) **(Figure 3.2)**.

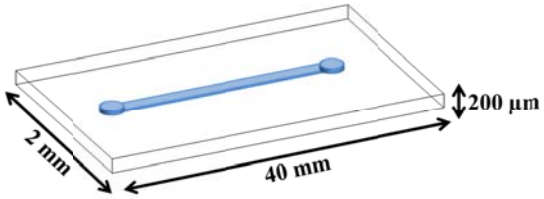

Figure 3.2: Schematic illustration of a single PDMS microfluidic channel.

The PDMS layer and a solid PDMS slab with similar composition were cured overnight for 12 hours at 60 °C. Access holes were punched with a 16 gauge blunt syringe (1.65 mm outer diameter) forming the inlet and outlet holes for each channel. PDMS prepolymer was used to bond the PDMS slab and channel upon exposure to plasma oxygen for 30 seconds. Prior to their use, fabricated PDMS channels were exposed to plasma oxygen for 5 minutes and immediately loaded with 15 µl of phosphate-buffered saline (PBS) solution.

3.2.3 Assessment of Markers Absorption

To measure the absorption of each molecule, 3 µl of [3H]-Diazepam (2.67 µM), [14C]-D-Mannitol (11.3 µM), or Rhodamine 6G (52.2 µM) stock solutions were mixed with 12 µl of PBS and loaded into the PDMS channels. Given the high specific activity of [3H]-Phenytoin (6.67 µM) and [3H]-Dexamethasone (0.0076 µM), only 0.3 µl of the stock solution was mixed with 14.7 µl of PBS solution before loading into the PDMS channel. Loaded channels were incubated at 25 °C and 37 °C for 0.5, 1, 2.5, and 4.5 hours. All concentrations are selected based on the minimum amount required for detection of these molecules in solution. The loaded marker solution was retrieved from each channel

followed by washing the channel with 15 μl of fresh PBS for 12 consecutive times at different time points and immediately analyzed using liquid scintillation counting (Beckman LS 6500, Beckman Coulter Inc., Brea, CA) for radiolabeled markers or the Fluoroskan Ascent FL plate reader (Thermo Fisher Scientific Inc., Waltham, MA) for Rhodamine 6G. The amount of each marker present in the collected washes was normalized to that initially loaded into each channel to determine % absorption of different markers. Absorption rate (%/min/cm^2) of each molecule was calculated by normalizing the % absorbed to the incubation time and channel surface area.

3.2.4 TiO_2 and Glass Coating of PDMS Channels

TiO_2 coating of PDMS channels was done following established protocols.[61] Briefly, PDMS microfluidic channels were filled with 2-propanol by applying a negative pressure of approximately 50 kPa at one end of the reservoirs while the remaining one was filled with 2-propanol. A mixture of 1:1 v/v of Titanium (IV) isopropoxide and 2-proponal was prepared and pumped through the channel for 1 minute to replace the loaded 2-propanol. The reservoirs were then allowed to dry in order to properly apply the TiO_2 coating to the surface of PDMS channels.

For glass coating, water (adjusted to pH 4.5 with HCl), TEOS, MTES, and ethanol were mixed at a 1:1:1:1 v/v to prepare the pre-conversion sol mixture following published procedures.[62] This solution was heated in a microwave oven for 15 seconds before incubating at 65 °C for 12 hours. Channels were oxidized by oxygen plasma for 5 minutes to generate hydroxyl groups on the PDMS surface to allow covalent coupling between

PDMS and siloxanes. The channels were immediately filled with pre-converted sol mixture and placed on a hot plate at 100 °C for approximately 1 minute to coat the channel surface. The sol solution was removed from the channel using a vacuum pump leaving the desired glass coating on the PDMS surface.

3.3 RESULTS AND DISCUSSION

3.3.1 Absorption of Mannitol in PDMS Microfluidic Channels

All channels used in the absorption experiments were fabricated using the same master. Channels were used 30-60 minutes after their plasma oxidation and they were easily loaded with PBS solution and remained intact throughout the absorption experiments. Channel consistency is maintained by using the same amount of PDMS for fabrication (50 g of PDMS prepolymer for 5 channels). All channels are then baked in the oven using the same master. Channel quality is checked by loading PBS solution and examined under the microscope at 10x magnification to confirm the absence of air bubbles. Microfluidic channels trapping any bubbles were immediately discarded.

Mannitol absorption into PDMS channels varied based on the incubation temperature and time **(Figure 3.3)**. The total amount of [14C]-mannitol retrieved from each channel in the initial collection (IC) and subsequent washes with fresh PBS were normalized to the amount of [14C]-mannitol loaded into the same channel and the difference represents the % of mannitol molecules absorbed into the PDMS surface **(Figure 3.3)**. Results show that 66%-82% of the loaded mannitol was retrieved after incubation for

0.5-4.5 hours in PDMS microfluidic channels at 25 °C **(Figure 3.3A)**. In comparison, 92% - 100% of the loaded mannitol was retrieved after incubation in similar microfluidic channels at 37 °C for the same incubation periods **(Figure 3.3B)**. Results show similar percentages of mannitol retrieval from PDMS channels at all incubation times regardless of the solution temperature **(Figure 3.3A & 3.3B)**. However, results show higher percentages of mannitol retrieval upon incubation at 37 °C compared to that observed at 25 °C, which is attributed to the formation of hydrogen bonds between the silanol's OH groups displayed on the surface of oxidized PDMS and the six hydroxyl groups of mannitol molecules at lower temperature. Elevating solution temperature from 25 °C to 37 °C provides sufficient energy to break the hydrogen bonds and increase mannitol retrieval at different time points **(Figure 3.3B)**.

We calculated the increase in solution energy due to temperature increase from 25 °C to 37 °C using the following heat capacity equation:

$$Q = \int_{T1}^{T2} Cp\, dT = Cp \times (T2 - T1) \text{----------Eq 2}$$

where Q is the thermal energy resulting from the temperature difference, T2 is the elevated temperature (37 °C), T1 is the standard room temperature (25 °C), and Cp is the specific heat capacity for the mannitol solution, which is assumed to be equal to water (4.18 $Jg^{-1}K^{-1}$) given that mannitol was dissolved in PBS. The calculated thermal energy as a result of temperature difference is 50.18 Jg^{-1}.

Using the heat calculated in equation 2, we calculated the energy available from the elevated temperature to mannitol molecules (15 µl with density similar to water) loaded in the microfluidic channels using equation 3.

$E_t = Q \times m$ ----------Eq 3

Where E_t is the available energy and m is the mass of the mannitol solution. Based on equation 2, increasing the solution temperature from 25 °C to 37 °C provides 0.75 J of additional energy (E_t) to the loaded mannitol solution.

Earlier research showed that (O — H - - - O) hydrogen bond has 21 $kJ.mol^{-1}$ and requires a dissociation energy of 3.49×10^{-20} J.[64, 65] Based on the specific activity of [14C]-D-Mannitol (100 μCi/ml; 60×10^{3} uCi/mmol), the number of mannitol molecules loaded in each microfluidic channel is 3.01×10^{15} molecules. These molecules will form 2.05×10^{16} hydrogen bonds and require 0.72×10^{-3} J to dissociate assuming that each of the OH groups of loaded mannitol molecules formed a hydrogen bond with a silanol group on the PDMS surface. Earlier calculations show that increasing the solution temperature from 25 °C to 37 °C provides 0.75 J, which is 1000-fold higher than the energy required to break the maximum number of hydrogen bonds formed between the loaded mannitol molecules and the OH groups displayed on the PDMS surface.

Absorption of mannitol and other molecules depend on the incubation time and the total surface area of PDMS microfluidic channels. Consequently, we normalized the percentage of absorbed molecules to the incubation period (minutes) and the PDMS surface area (cm^2) to calculate the absorption rate (%/min/cm^2) of different markers to extrapolate these findings to other microfluidic devices with different architectures and geometry. Results show that the absorption rate of mannitol dropped with the increase in incubation time and regardless of the incubation temperature, which indicates high absorption rate of mannitol molecules into the PDMS surface shortly after loading the channel **(Figure 3.3C)**.

Mannitol absorption into PDMS channels clearly shows the effect of incubation temperature with a statistically higher absorption rate at 25 ºC compared to that at 37 ºC **(Figure 3.3C)**. Results show that mannitol (log P = -3.1) exhibit low net absorption (< 10%) and absorption rate (0.63%/min/cm^2) into microfluidic PDMS channels and can be used in different quantitative assays in PDMS microfluidic channels.

(A)

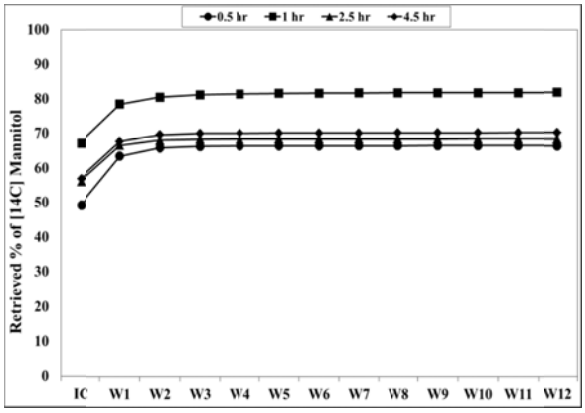

(B)

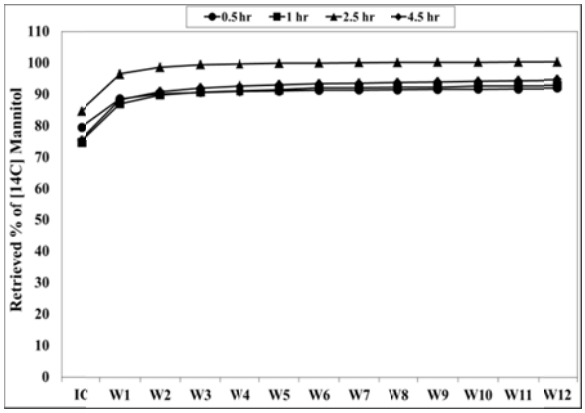

(C)

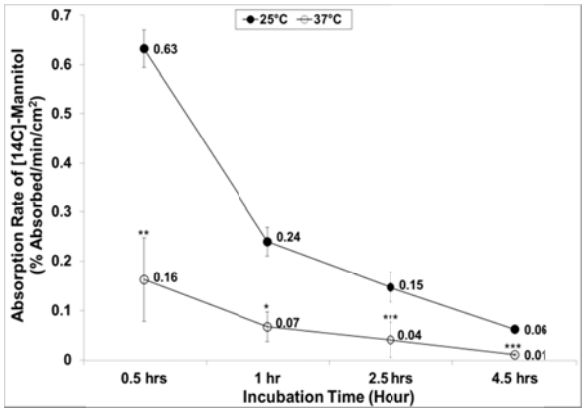

Figure 3.3: Cumulative amount of [14C]-Mannitol retrieved in the initial collection (IC) and subsequent washes (W) normalized to the total amount of mannitol loaded into microfluidic PDMS channels incubated at (A) 25 °C and (B) 37 °C for 0.5 (●), 1.0 (■), 2.5 (▲), and 4.5 (♦) hours. (C) Absorption rate of [14C]-Mannitol into PDMS microfluidic channels at 25 °C (●) and 37 °C (○) for 0.5, 1, 2.5, and 4.5 hours. Results are the average ± the standard error of the mean collected from 5 different channels. Statistical difference in mannitol absorption rate as a function of solution temperature at a given incubation time point is identified by * when $p < 0.05$, ** when $p < 0.01$, and *** when $p < 0.001$.

3.3.2 Absorption of Phenytoin and Dexamethasone in PDMS Microfluidic Channels

Phenytoin (log P = 2.47) and dexamethasone (Log P = 1.83) are moderately hydrophobic drug molecules that are substrates for the P-gp efflux pump. Results show that absorption of phenytoin and dexamethasone into PDMS microfluidic channels increased with the increase in incubation time and solution temperature **(Figures 3.4 & 3.5)**. For instance, absorption of phenytoin increased from 8% (92% retrieved) to 22% (78% retrieved) of the loaded solute molecules after incubation for 0.5 and 4.5 hours in PDMS channels at 25 °C, respectively **(Figure 3.4A)**. Phenytoin exhibited a similar absorption profile at 37 °C with 6% and 28% of the loaded solute molecules absorbed in the PDMS channel after incubation for 0.5 and 4.5 hours, respectively **(Figure 3.4B)**. Results show

that phenytoin's absorption rate at 37 °C was higher than that observed at 25 °C **(Figure 3.4C)** except at 0.5 hours, which can be attributed to the increase in solution thermal energy causing an increase in the kinetic energy of phenytoin molecules and their diffusivity into PDMS surface.[66]

(A)

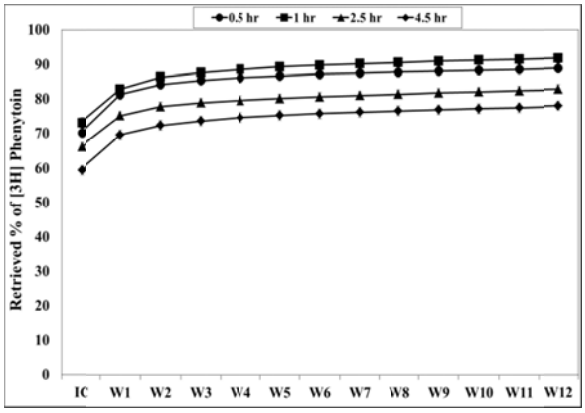

(B)

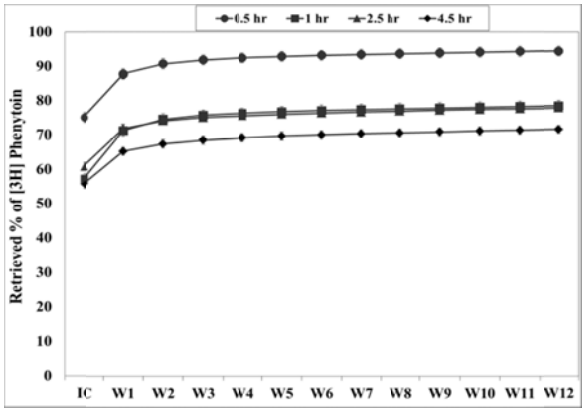

(C)

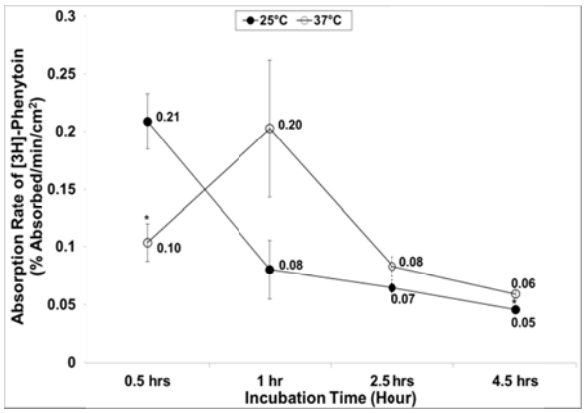

Figure 3.4: Cumulative amount of [3H]-Phenytoin retrieved in the initial collection (IC) and subsequent washes (W) normalized to the total amount of phenytoin loaded into microfluidic PDMS channels incubated at (A) 25 °C and (B) 37 °C for 0.5 (●), 1.0 (■), 2.5 (▲), and 4.5 (♦) hours. (C) Absorption rate of [3H]-Phenytoin into PDMS microfluidic channels at 25 °C (●) and 37 °C (○) for 0.5, 1, 2.5, and 4.5 hours. Results are the average ± the standard error of the mean collected from 5 different channels. Statistical difference in phenytoin absorption rate as a function of solution temperature at a given incubation time point is identified by * when $p < 0.05$, ** when $p < 0.01$, and *** when $p < 0.001$.

Similarly, absorption of dexamethasone increased from 6% (94% retrieved) to 18% (82% retrieved) upon incubation in PDMS channels at 25 °C for 0.5 and 4.5 hours, respectively **(Figure 3.5A)**. Dexamethasone exhibited a similar absorption profile at 37 °C with 2% and 30% of the loaded solute molecules absorbed in the PDMS channel after incubation for 0.5 and 4.5 hours, respectively **(Figure 3.5B)**. Similar to phenytoin, results show that phenytoin's absorption rate at 37 °C was higher than that observed at 25 °C **(Figure 3.5C)** except at 0.5 hours. It also indicates continuous absorption of solute molecules into PDMS surface throughout the incubation period **(Figure 3.5C)**. These results collectively indicate that moderately hydrophobic molecules like phenytoin and

dexamethasone can be used in quantitative assays in PDMS microfluidic devices with short analysis time (< 0.5 hours) when absorption of these solute molecules is insignificant.

(A)

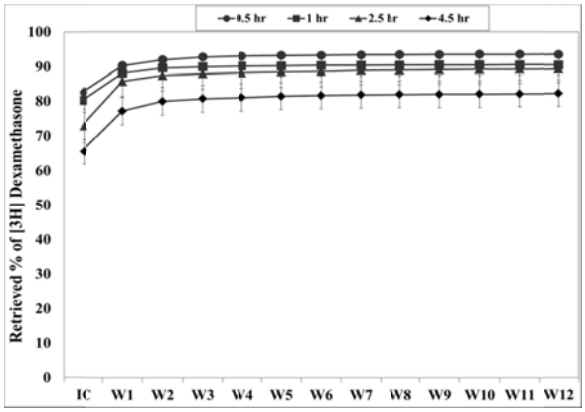

(B)

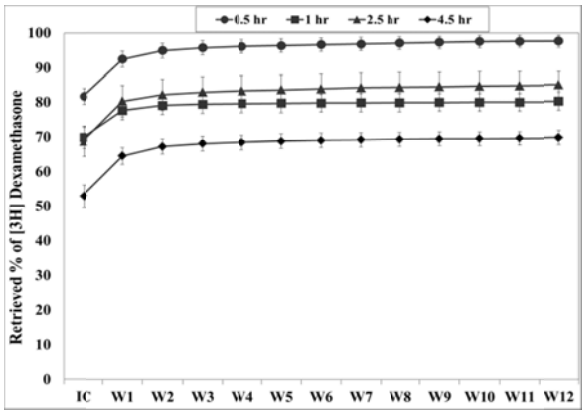

(C)

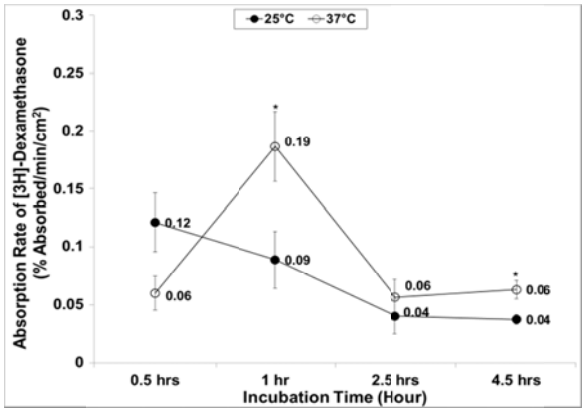

Figure 3.5: Cumulative amount of [3H]-Dexamethasone retrieved in the initial collection (IC) and subsequent washes (W) normalized to the total amount of dexamethasone loaded into microfluidic PDMS channels incubated at (A) 25 °C and (B) 37 °C for 0.5 (●), 1.0 (■), 2.5 (▲), and 4.5 (♦) hours. (C) Absorption rate of [3H]-Dexamethasone into PDMS microfluidic channels at 25 °C (●) and 37 °C (○) for 0.5, 1, 2.5, and 4.5 hours. Results are the average ± the standard error of the mean collected from 5 different channels. Statistical difference in dexamethasone absorption rate as a function of solution temperature at a given incubation time point is identified by * when $p < 0.05$, ** when $p < 0.01$, and *** when $p < 0.001$.

3.3.3 Absorption of Rhodamine 6G and Diazepam in PDMS Microfluidic Channels

Rhodamine 6G (log P = 2.62) and diazepam (log P = 2.8) are highly hydrophobic drug molecules that freely diffuse across the lipid bilayers of mammalian cell membranes and are routinely used to assess transcellular transport across epithelial and endothelial monolayers.[57, 60, 67] Results show that rhodamine 6G and diazepam exhibit extensive absorption into PDMS channels at 25 °C and 37 °C and all incubation time points **(Figures 3.6 & 3.7)**. For example, 77% and 80% of the loaded rhodamine 6G molecules were absorbed in PDMS channels regardless of the incubation time at 25 °C and 37 °C, respectively **(Figures 3.6A & 3.6B)**. This is further emphasized in **Figure 3.6C** showing

the high absorption rate of 1.44 %/min/cm^2 at 25 °C and 1.46 %/min/cm^2 37 °C of rhodamine 6G upon incubation in PDMS channels for 0.5 hours. Similarly, 90% and 95% of the loaded diazepam molecules absorbed into PDMS channels upon incubation at 25 °C and 37 °C, respectively **(Figure 3.7A & 3.7B)**. Results show that diazepam absorption into PDMS increased with the increase in incubation temperature shown by the significant increase in diazepam's absorption rate from 1.67%/min/cm^2 at 25 ºC to 1.79%/min/cm^2 at 37 ºC upon incubation for 0.5 hours **(Figure 3.7C)**. These results clearly indicate that rhodamine 6G and diazepam exhibit rapid and extensive absorption into PDMS microfluidic channels, which will reduce the effective concentration of solute molecules present in solution and may influence the accuracy of different *in vitro* assays utilizing these markers.

(A)

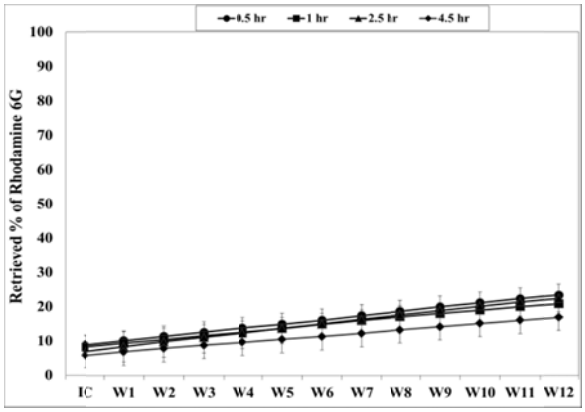

(B)

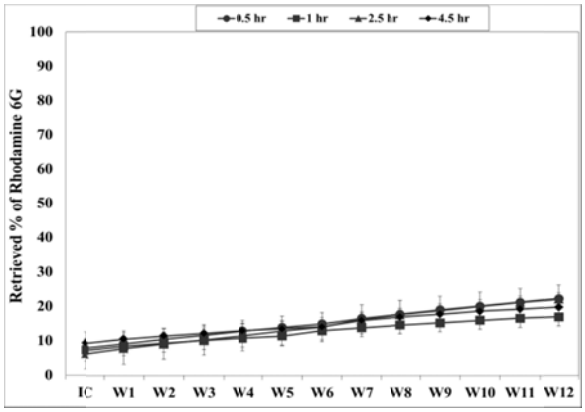

(C)

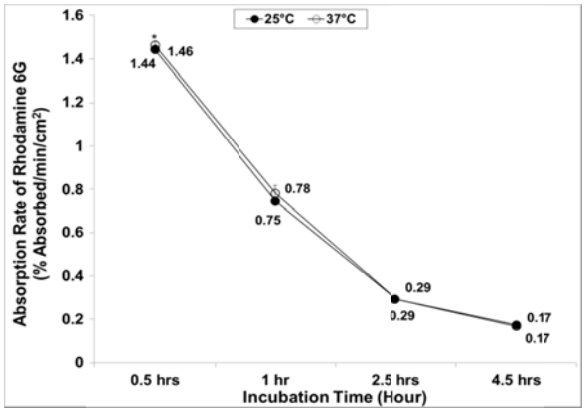

Figure 3.6: Cumulative amount of rhodamine 6G retrieved in the initial collection (IC) and subsequent washes (W) normalized to the total amount of rhodamine 6G loaded into microfluidic PDMS channels incubated at (A) 25 °C and (B) 37 °C for 0.5 (●), 1.0 (■), 2.5 (▲), and 4.5 (♦) hours. (C) Absorption rate of rhodamine 6G into PDMS microfluidic channels at 25 °C (●) and 37 °C (○) for 0.5, 1, 2.5, and 4.5 hours. Results are the average ± the standard error of the mean collected from 5 different channels. Statistical difference in rhodamine 6G absorption rate as a function of solution temperature at a given incubation time point is identified by * when $p < 0.05$, ** when $p < 0.01$, and *** when $p < 0.001$.

(A)

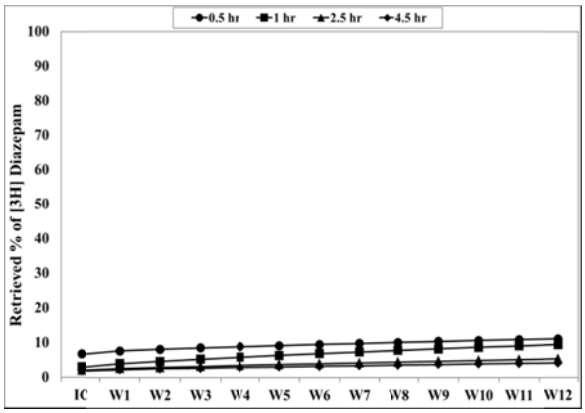

(B)

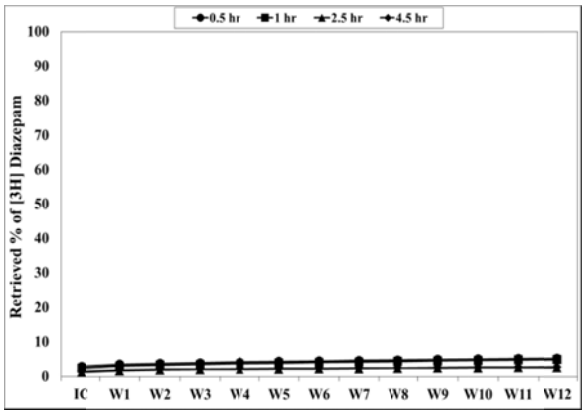

(C)

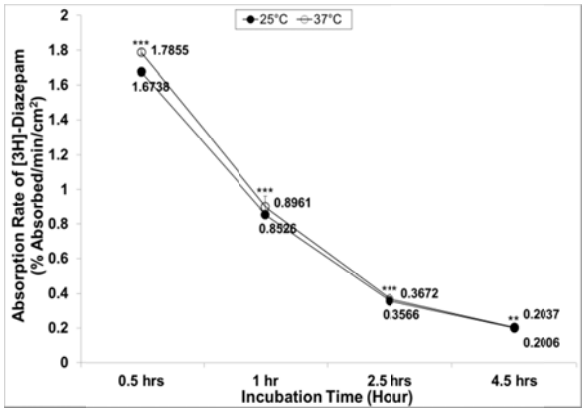

Figure 3.7: Cumulative amount of [3H]-Diazepam retrieved in the initial collection (IC) and subsequent washes (W) normalized to the total amount of diazepam loaded into

microfluidic PDMS channels incubated at (A) 25 °C and (B) 37 °C for 0.5 (●), 1.0 (■), 2.5 (▲), and 4.5 (♦) hours. (C) Absorption rate of [3H]-Diazepam into PDMS microfluidic channels at 25 °C (●) and 37 °C (○) for 0.5, 1, 2.5, and 4.5 hours. Results are the average ± the standard error of the mean collected from 5 different channels. Statistical difference in diazepam absorption rate as a function of solution temperature at a given incubation time point is identified by * when $p < 0.05$, ** when $p < 0.01$, and *** when $p < 0.001$.

3.3.4 Correlation between Log P and Absorption in PDMS Microfluidic Channels

The partition coefficient, log P, of a given molecule depends on the hydrophilic/hydrophobic balance, which is dictated by its chemical structure. This report describes the absorption of a series of markers with different degrees of hydrophobicity reflected by their log P values, which span the log P range of the majority of therapeutic and diagnostic agents.[46, 47] Correlating the log P of different markers with their absorption profile will allow the prediction of absorption of therapeutic molecules in PDMS microfluidic devices as a function of incubation time and solution temperature. Results show that mannitol exhibited the lowest absorption (95% retrieval) in PDMS channels upon incubation for 0.5 hours at 37 ºC, which is not surprising given its hydrophilic nature (log P = -3.1) **(Figure 3.8A)**. Dexamethasone (log P = 1.83) and phenytoin (log P = 2.47) also exhibited low absorption (> 90% retrieval) into PDMS channels upon incubation for 0.5 hours at 37 ºC. In comparison, increasing the log P of investigated molecules to 2.62 (rhodamine 6G) and 2.8 (diazepam) led to a substantial increase in molecular absorption in PDMS channels under the same experimental conditions. These results suggest that there is a log P "threshold" between 2.47 and 2.62 where molecules with log P < 2.47 exhibit minimal absorption into PDMS surfaces whereas those with log P > 2.62 get extensively absorbed into PDMS channels.

To better elucidate the difference in markers hydrophobicity, we used log P values to calculate the concentration of different marker molecules in octanol (equation 1) and normalized the concentration of each marker in this organic layer to that of mannitol. Results show that the calculated concentration of dexamethasone, phenytoin, rhodamine 6G, and diazepam is ~85,000-, 372,000, 525,000-, 794,000-folds the concentration of mannitol partitioning into the organic octanol layer, respectively, which clearly shows the significant difference in hydrophobicity of different molecules. Further, it shows the significant difference in hydrophobicity between phenytoin and rhodamine 6G despite the small difference in their log P values, which suggests that there is a log P "threshold" for extensive absorption into PDMS microfluidic devices. The relationship between log P of different markers and their observed absorption into PDMS microfluidic devices was consistent at all incubation time points up to 4.5 hours **(Figure 3.8)**.

Our results are supported by earlier studies by Lee *et al* who examined the compatibility of different aqueous and organic solvents with PDMS-based microfluidic devices by measuring the partition of multiple organic solutes between bulk PDMS and different organic solvents.[68] Results of this investigation showed that aqueous solutions of rhodamine B (log P = 2.74)[67] and fluorescein (log P = -0.67)[69] exhibited different absorption profiles into bulk PDMS.[68] Specifically, fluorescein was not absorbed into PDMS whereas 60% of rhodamine B molecules got absorbed into bulk PDMS under the same experimental conditions.[68] These earlier results are in agreement with our findings and support the notion that absorption into PDMS depends on the solute's log P value. It is important to note that an analysis of over 3000 drug candidates between 1960-2000 showed

that the mean log P value for these therapeutic molecules is approximately 2.43,[47] which is similar to the log P threshold identified in this report. This suggests that approximately 50% of current drugs can be used in different *in vitro* assays that utilize microfluidic PDMS devices without exhibiting appreciable absorption into PDMS surface. However, drugs with log P values > 2.62 should be carefully evaluated before using them in any quantitative assays that utilize PDMS devices to eliminate the effect of their absorption into PDMS wall on the accuracy of the results.

(A)

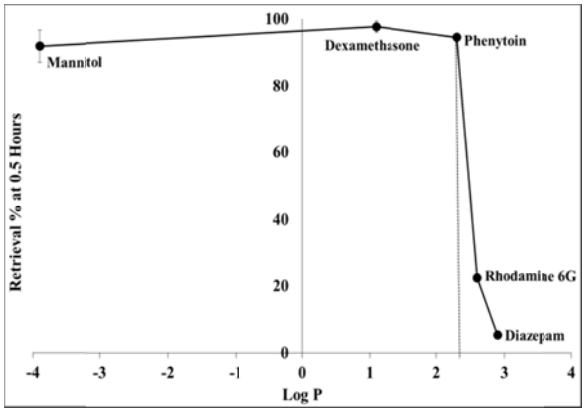

(B)

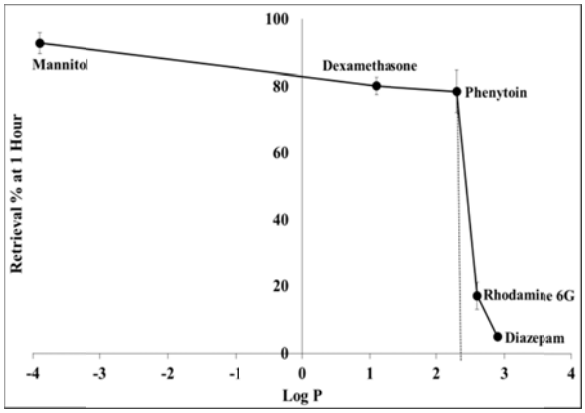

(C)

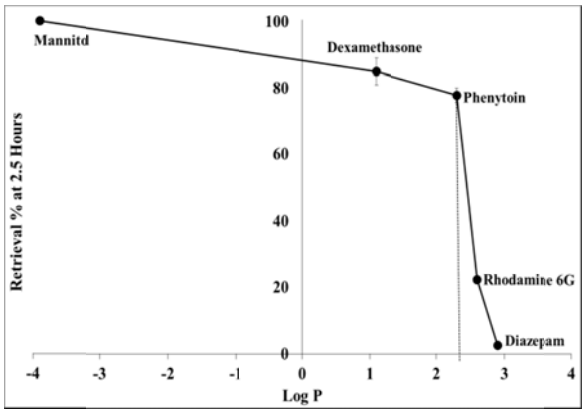

(D)

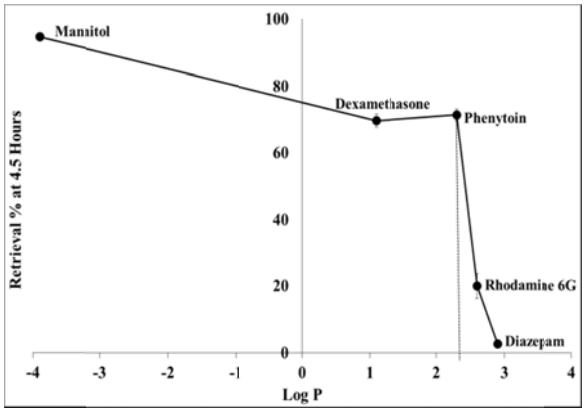

Figure 3.8: The relationship between the retrieved percentage of each marker molecules and its log P value after incubation in microfluidic PDMS channels for (A) 0.5, (B) 1.0, (C) 2.5, and (D) 4.5 hours at 37 °C. Results are the average ± the standard error of the mean collected from 5 different channels.

3.3.5 Effect of TiO_2 and Glass Coating on Absorption in PDMS Channels

Culbertson and Weitz groups showed that TiO_2 and glass coatings prevent the diffusion of rhodamine B (log P = 2.74)[67] into the PDMS walls of microfluidic channels. This was indicated by the localization of the fluorescence signal to lumen of the channel compared to uncoated channels, which showed extensive fluorescence staining of the

PDMS walls.[58, 59] Earlier studies showed that the contact angle for uncoated Sylgard 184 PDMS 110º, which indicates the high hydrophobicity of the PDMS surface.[61] However, TiO_2- and glass-coated PDMS channels have a significantly lower contact angle of 61º and 35º, respectively.[61, 70] Consequently, we evaluated the effect of TiO_2 and glass coatings on diazepam (log P = 2.8) absorption into microfluidic PDMS channels upon incubation for 0.5 hour at 37 ºC **(Figure 3.9)**. Results show that the percentage of retrieved diazepam increased from 4% for uncoated PDMS channels to 8% and 18% in TiO_2- and glass-coated channels, respectively **(Figure 3.9A)**. Therefore, diazepam absorption rate decreased significantly from 1.79 %/min/cm^2 for uncoated PDMS channels to 1.73 %/min/cm^2 and 1.57 %/min/cm^2 in TiO_2- and glass-coated channels, respectively **(Figure 3.9B)**. However, the decrease in diazepam absorption in TiO_2- and glass-coated channels did not match the low absorption rate of marker molecules with log P < 2.47. These results suggest the potential of TiO_2 and glass coatings in reducing the absorption of hydrophobic molecules (log P > 2.62) but coating conditions (e.g. number and thickness of coating layers) need to be further optimized to inhibit molecular absorption into microfluidic PDMS channels.

(A)

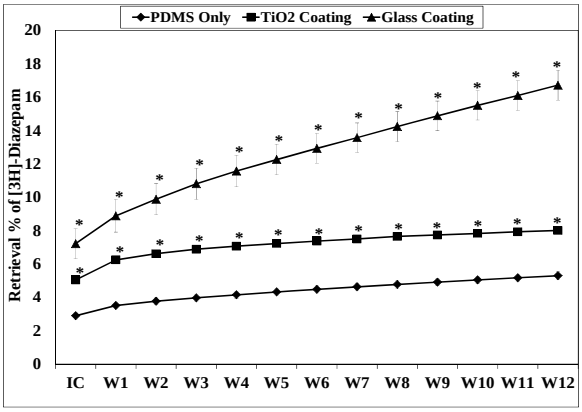

(B)

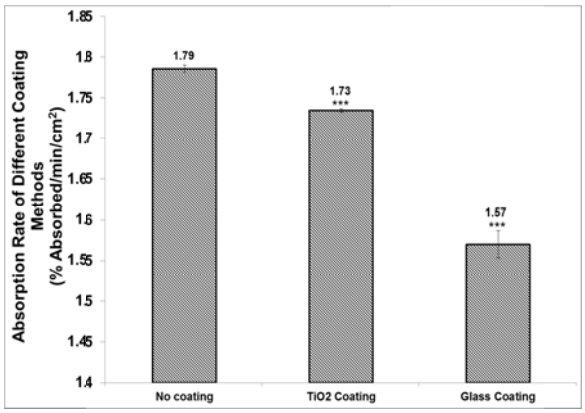

Figure 3.9: (A) Cumulative amount of [3H]-Diazepam retrieved in the initial collection (IC) and subsequent washes (W) normalized to the total amount of diazepam loaded into uncoated (♦), TiO_2-coated (■), and glass-coated (▲) microfluidic PDMS channels for 0.5 hour at 37 °C. (B) Absorption rate of [3H]-Diazepam into uncoated and TiO_2- and glass-coated PDMS microfluidic channels upon incubation for 0.5 hour at 37 °C. Results are the average ± the standard error of the mean collected from 5 different channels. Statistical difference in diazepam absorption rate as a function of channel coating is identified by * when $p < 0.05$, ** when $p < 0.01$, and *** when $p < 0.001$.

3.4 CONCLUSIONS

Our results provide a quantitative correlation between the log P of a series of markers and their absorption in microfluidic PDMS channels as a function of incubation time and temperature. Results show molecules with log P < 2.47 exhibit minimal absorption (< 10%) into PDMS channels whereas molecules with log P > 2.62 exhibit extensive absorption in the same channels. Further, TiO_2 and glass coatings reduce the absorption of [3H]-Diazepam (log P = 2.8) in microfluidic PDMS channels. However, reduction in diazepam absorption to match the low levels observed with hydrophilic molecules (log P < 2.47) requires a systemic investigation of the effect of coating parameters on net molecular absorption. These results clearly show the significance of

considering the log P of different solute molecules before using them in quantitative assays in microfluidic PDMS devices.

REFERENCES

1. Simpson, P.C., et al., *High-throughput genetic analysis using microfabricated 96-sample capillary array electrophoresis microplates.* PNAS, 1998. **95**(5): p. 2256-2261.
2. Woolley, A.T. and R.A. Mathies, *Ultra-high-speed DNA sequencing using capillary electrophoresis chips.* Anal. Chem., 1995. **67**: p. 3676-3680.
3. Liu, S., et al., *Optimization of high-speed DNA sequencing on microfabricated capillary electrophoresis channels.* Anal. Chem., 1999. **71**: p. 566-573.
4. Kopp, M.U., A.J.d. Mello, and A. Manz, *Chemical Amplification: Continuous-Flow PCR on a Chip.* Science, 1998. **280**(5366): p. 1046-1048.
5. Waters, L.C., et al., *Multiple sample PCR amplification and electrophoretic analysis on a microchip.* Anal. Chem., 1998. **70**: p. 5172.
6. Burns, M.A., et al., *An Integrated Nanoliter DNA Analysis Device.* Science, 1998. **282**: p. 484-487.
7. Northrup, M.A., et al., *A miniature analytical instrument for nucleic acids based on micromachined silicon reaction chambers.* Anal. Chem., 1998. **70**: p. 912-922.
8. Cheng, J., et al., *Degenerate oligonucleotide rpimed-PCR and capillary electrophoretic analysis of human DNA on microchip-based devices.* Anal. Biochem., 1998. **257**: p. 101-106.
9. Effenhauser, C.S., et al., *Integrated capillary electrophoresis on flexible silicone microdevices: analysis of DNA restriction fragments and detection of single DNA molecules on microchips.* Anal. Chem., 1997. **69**(17): p. 3451-3457.

10. Chou, H.P., et al., *A microfabricated device for sizing and sorting DNA molecules.* PNAS, 1999. **96**(1): p. 11-13.

11. Dörre, K., et al., *Techniques for single molecule sequencing.* Bioimaging, 1997. **5**: p. 139-152.

12. Han, J.-H. and J.-Y. Yoon, *Reusable, polyethylene glycol-structured microfluidic channel for particle immunoassays.* J. Biol. Eng., 2009. **3**(6).

13. Upadhyaya, S. and P.R. Selvaganapathy, *Microfluidic devices for cell based high throughput screening.* Lab Chip, 2010. **10**: p. 341-348.

14. Sohn, L.L., et al., *Capacitance cytometry: Measuring biological cells one by one.* PNAS, 2000. **97**(20): p. 10687-10690.

15. Fiddes, L.K., et al., *A circular cross-section PDMS microfluidics system for replication of cardiovascular flow conditions.* Biomaterials, 2010. **31**: p. 3459-3464.

16. Lima, R., et al., *In vitro blood flow in a rectangular PDMS microchannel: experimental observations using a confocal micro-PIV system.* Biomed. Microdevices, 2008. **10**: p. 153-167.

17. Prakash, A.R., et al., *Small volume PCR in PDMS biochips with integrated fluid control and vapour barrier.* Sens. Actuators, B, 2006. **113**: p. 398-409.

18. Tung, Y.-C., et al., *Small volume low mechanical stress cytometry using computer-controlled Braille display microfluidics.* Lab Chip, 2007. **7**: p. 1497-1503.

19. Cheng, J., et al., *Analysis of ligase chain reaction products amplified in a silicon-glass chip using capillary electrophoresis.* J. Chromatogr., 1996. **732**(1): p. 151-158.

20. Shoffner, M.A., et al., *Chip PCR. I. Surface passivation of microfabricated silicon-glass chips for PCR.* Nucleic Acids Res., 1996. **24**(2): p. 375-379.

21. Cheng, J., et al., *Chip PCR. II. Investigation of different PCR amplification systems in microfabricated silicon-glass chips.* Nucleic Acids Res., 1996. **24**(2): p. 380-385.

22. Rebenklau, L., K.-J. Wolter, and S. Howitz. *Realization of hybrid microfluidic systems using standard LTCC process*. in *Electronic Components and Technology Conference*. 2000. Las Vages, NV.

23. Harrison, D.J., et al., *Capillary electrophoresis and sample injection systems integrated on a planar glass chip.* Anal. Chem., 1992. **64**(17): p. 1926-1932.

24. Effenhauser, C.S., A. Manz, and H.M. Widmer, *Glass chips for high-speed capillary electrophoresis separations with submicrometer plate heights.* Anal. Chem., 1993. **65**(19): p. 2637-2642.

25. Seiler, K., D.J. Harrison, and A. Manz, *Planar glass chips for capillary electrophoresis: repetitive sample injection, quantitation, and separation efficiency.* Anal. Chem., 1993. **65**(10): p. 1481-1488.

26. Fan, Z.H. and D.J. Harrison, *Micromachining of capillary electrophoresis injectors and separators on glass chips and evaluation of flow at capillary intersections.* Anal. Chem., 1994. **66**(1): p. 177-184.

27. Becker, H. and C. Gartner, *Polymer microfabrication methods for microfluidic analytical applications.* Electrophoresis, 2000. **21**(1): p. 12-26.

28. Ko, J.S., et al., *A polymer-based microfluidic device for immunosensing biochips.* Lab Chip, 2003. **3**(2): p. 106-113.

29. Zhang, J., et al., *Polymerization optimization of SU-8 photoresist and its applications in microfluidic systems and MEMS.* J. Micromech. Microeng., 2001. **11**(1): p. 20-26.

30. Jong, J.d., R.G.H. Lammertink, and M. Wessling, *Membranes and microfluidics: a review.* Lab Chip, 2006. **6**: p. 1125-1139.

31. McDonald, J.C., et al., *Fabrication of microfluidic systems in poly(dimethylsiloxane).* Electrophoresis, 2000. **21**: p. 27-40.

32. Huszank, R., et al., *Fabrication of optical devices in poly(dimethylsiloxane) by proton microbeam.* Opt. Commun., 2009. **283**(1): p. 176-180.

33. Thangawng, A.L., et al., *An ultra-thin PDMS membrane as a bio/micro-nano interface: fabrication and characterization.* Biomed. Microdevices, 2007. **9**(4): p. 587-595.

34. Cox, M.E. and B. Dunn, *Oxygen diffusion in poly(dimethyl Siloxane) using fluorescence quenching. I. measurement technique and analysis.* J. Polym. Sci., Part A: Polym. Chem., 1986. **24**: p. 621-636.

35. Sodunke, T.R., M.J. Bouchard, and H.M. Noh, *Microfluidic platform for hepatitis B viral replication study.* Biomed. Microdevices, 2007.

36. Millet, L.J., et al., *Microfluidic devices for culturing primary mammalian neurons at low densities.* Lab Chip, 2007. **7**: p. 987-994.

37. Huh, D., et al., *Acoustically detectable cellular-level lung injury induced by fluid mechanical stresses in microfluidic airway systems.* PNAS, 2007. **104**(48): p. 18886-18891.

38. Eddington, D.T., J.P. Puccinelli, and D.J. Beebe, *Thermal aging and reduced hydrophobic recovery of polydimethylsiloxane.* Sens. Actuators, B, 2006. **114**: p. 170-172.

39. Vickers, J.A., M.M. Caulum, and C.S. Henry, *Generation of hydrophilic poly(dimethylsiloxane) for high-performance microchip electrophoresis.* Analytical Chemistry, 2006. **78**: p. 7446-7452.

40. Bodas, D. and C. Khan-Malek, *Formation of more stable hydrophilic surfaces of PDMS by plasma and chemical treatments.* Microelectronic Engineering, 2006. **83**(4-9): p. 1277-1279.

41. Zhou, J., A.V. Ellis, and N.H. Voelcker, *Recent developments in PDMS surface modification for microfluidic devices.* Electrophoresis, 2010. **31**: p. 2-16.

42. Toepke, M.W. and D.J. Beebe, *PDMS absorption of small molecules and consequences in microfluidic applications.* Lab Chip, 2006. **6**: p. 1484-1486.

43. Leo, A., C. Hansch, and D. Elkins, *Parition coefficients and their uses.* Chem. Rev., 1971. **71**(6): p. 525-616.

44. Kuchler, S., et al., *Influence of nanocarrier type and size on skin delivery of hydrophilic agents.* Int. J. Pharm., 2009. **377**: p. 169-172.

45. Fowler, S.D. and P. Greenspan, *Application of nile red, a fluorescent hydrophobic probe, for the detection of neutral lipid deposits in tissue sections: comparison with oil red o.* J. Histochem. Cytochem., 1985. **33**(8): p. 833-836.

46. Lipinski, C.A., et al., *Experimental and computational approaches to estimate solubility and permeability in drug discovery and development settings.* Adv. Drug Deliv. Rev., 2001. **46**: p. 3-26.

47. Proudfoot, J.R., *The evolution of synthetic oral drug properties.* Bioorg. Med. Chem. Lett., 2005. **15**(4): p. 1087-1090.

48. Collett, A., et al., *Modulation of the permeability of H_2 receptor antagonists cimetidine and ranitidine by P-glycoprotein in rat intestine and the human colonic cell line caco-2.* J. Pharmacol. Exp. Ther., 1999. **288**(1): p. 171-178.

49. Deli, M.A., et al., *Permeability studies on in vitro blood-brain barrier models: physiology, pathology, and pharmacology.* Cell. Mol. Neurobiol., 2004. **25**(1): p. 59-127.

50. Schmelzeisen, R. and J.-C. Frolich, *Prevention of postoperative swelling and pain by dexamethasone after operative removal of impacted third molar teeth.* Eur. J. Clin. Pharmacol., 1993. **44**: p. 275-277.

51. Hardman, J.G., L.E. Limbird, and A.G. Gilman, *Goodman & Gilman's the pharmacological basis of therapeutics, 10th edition*. 2001, New York: McGraw-Hill.

52. Paturi, J., et al., *Transdermal and intradermal iontophoretic delivery of dexamethasone sodium phosphate: quantification of the drug localized in skin.* J. Drug Target., 2010. **18**(2): p. 134-140.

53. Bereczki, A., et al., *Determination of phenytoin in plasma by molecularly imprinted solid-phase extraction.* J. Chromatogr. A, 2001. **930**: p. 31-38.

54. Ueda, K., et al., *Human p-glycoprotein transports cortisol, aldosterone, and dexamethasone, but not progesterone.* J. Biol. Chem., 1992. **267**(34): p. 24248-24252.

55. Baltes, S., et al., *Differences in the transport of the antiepileptic drugs phenytoin, levetiracetam and carbamazepine by human and mouse P-glycoprotein.* Neuropharmacology, 2007. **52**: p. 333-346.

56. Yang, H.-w., et al., *Increased P-glycoprotein function and level after long-term exposure of four antiepileptic drugs to rat brain microvascular endothelial cells in vitro.* Neurosci. Lett., 2008. **434**(3): p. 299-303.

57. Mandala, M., et al., *The fluorescent cationic dye rhodamine 6G as a probe for membrane potential in bovine aortic endothelial cells.* Anal. Biochem., 1998. **274**: p. 1-6.

58. Hansch, C., P.G. Sammes, and J.B. Taylor, *Comprehensive medicinal chemistry: the rational design, mechanistic study & therapeutic applications of chemical compounds*. Vol. 6. 1990, Oxford: Pergamon Press.

59. Neuhaus, W., et al., *Validation of in vitro cell culture models of the blood-brain barrier: tightness characterization of two promising cell lines.* J. Pharm. Sci., 2008. **97**(12): p. 5158-5175.

60. Mandrioli, R., L. Mercolini, and M.A. Raggi, *Benzodiazepine metabolism: an analytical perspective.* Curr. Drug. Metab., 2008. **9**(8): p. 827-844.

61. Roman, G.T. and C.T. Culbertson, *Surface engineering of poly(dimethylsiloxane) microfluidic devices using transition metal sol-gel chemistry.* Langmuir, 2006. **22**: p. 4445-4451.

62. Abate, A.R., et al., *Glass coating for PDMS microfluidic channels by sol-gel methods.* Lab Chip, 2008. **8**: p. 516-518.

63. Duffy, D.C., et al., *Rapid Prototyping of Microfluidic Systems in Poly(dimethylsiloxane).* Anal. Chem., 1998. **70**: p. 4974-4984.

64. Emsley, J., *Very strong hydrogen bonds.* Chem. Soc. Rev., 1980. **9**: p. 91-124.

65. Markovitch, O. and N. Agmon, *Structure and energetics of the hydronium hydration shells.* J. Phys. Chem. A, 2007. **111**(12): p. 2253-2256.

66. Kittel, C. and H. Kroemer, *Thermal physics*. 2nd ed. 1980: W. H. Freeman Company.

67. Tetko, I.V., et al., *Virtual computational chemistry laboratory - design and description.* J. Comput. Aided Mol. Des., 2005. **19**: p. 453-463.

68. Lee, J.N., C. Park, and G.M. Whitesides, *Solvent compatibility of poly(dimethylsiloxane)-based microfluidic devices.* Anal. Chem., 2003. **75**: p. 6544-6554.

69. Cheruvu, N.P.S., S.P. Ayalasomayajula, and U.B. Kompella, *Retinal delivery of sodium fluorescein, budesonide & celecoxib following subconjunctival injection.* Drug Devel. Deliv., 2003. **3**(6).

70. Li, M. and D.P. Kim, *Silicate glass coated microchannels through a phase conversion process for glass-like electrokinetic performance.* Lab on a Chip, 2011. **11**: p. 1126-1131.

Chapter 4

Development of an *In Vitro* Model of the Blood-Brain Barrier in Layered Microfluidic Channels

4.1 Introduction

The endothelial cells lining the capillaries that supply the brain with oxygen and nutrients present a highly regulated barrier known as the blood-brain barrier (BBB) [1, 2]. These endothelial cells are characterized by thick cell membranes, few endocytic vesicles, absence of fenestrae, and highly organized tight junctions, which restrict molecules' diffusion from the blood circulation into the brain [1, 2]. These endothelial cells along with other supporting cells that contribute to the BBB integrity such as astrocytes [3], neurons [1], pericytes [2], and microglial cells [4] are collectively known as the neurovascular unit, which control the permeability of the BBB [3]. The integrity and function of the BBB is also regulated by several environmental conditions including flow-induced shear stress [1],

endothelial cell-to-cell contact [5], communication within the neurovascular unit [4], and the local concentration of secreted chemical factors [3]. The restrictive nature of the BBB allows only 2% of small molecular weight (< 500 Daltons) drugs to permeate from the systemic circulation and achieve therapeutic concentrations in the brain [6]. However, large molecular weight drugs (e.g. peptides, proteins, and nano-medicines) generally fail to diffuse across the BBB [1, 2]. Therefore, treatment of several neurological disorders such as Alzheimer disease, Huntington disease, stroke, and brain cancer is limited by the lack of new drug molecules that can effectively permeate across the BBB and achieve the desired therapeutic concentration in diseased brain cells [6].

Several groups focused their research efforts on understanding the cellular and molecular mechanisms that control and regulate the integrity and function of the BBB [7]. Other investigations relied on computational and experimental studies to predict the chemical structure and properties of an ideal drug candidate that can diffuse across the BBB [2, 6]. These mechanistic investigations catalyzed the development of *in vitro* models to represent the BBB [6, 7]. Many *in vitro* BBB models are established by culturing the endothelial cells on porous polycarbonate or polyester membranes with variable pore size using the conventional transwells system [7]. However, these endothelial monolayers typically exhibit low trans-endothelial electrical resistance (TEER) and high permeability values indicating the formation of a "leaky" barrier that is not representative of the BBB *in vivo* [7], which prompted the development of more sophisticated models that can mimic a complete neurovascular unit.

Microfluidic channels have been used to create many *in vitro* assays due to their ability to closely mimic the *in vivo* microenvironment [8] and utilize a small volume of the studied analytes compared to conventional analytical tools [9]. Poly(dimethylsiloxane) or PDMS is a commonly used material for fabrication of microfluidic channels used for cell culture due to its optical clarity [10], biocompatibility [11], and high oxygen diffusivity [12]. For example, embedding Ag/AgCl electrodes in the upper and lower microfluidic PDMS channels allowed real time quantitative assessment of the integrity of epithelial and endothelial cells cultured in layered microfluidic channels by monitoring the change in monolayer resistance [13].

In this article, we report the successful culture of mouse brain endothelial cells (b.End3) in layered microfluidic PDMS devices to develop a new *in vitro* BBB model that better mimics the restrictive transport behavior observed *in vivo*. We rely on the geometry and dimensions of the PDMS channels to drive the formation of a "restrictive" b.End3 monolayer compared to conventional transwells. We examined the viability, morphology, and organization of b.End3 cells in layered microfludic channels as a functions of days in culture. We measured TEER across b.End3 monolayers established in layered microfluidic channels and conventional transwells as a function of days in culture as an indication of barrier integrity. We also compared the diffusion of mannitol and dextran (paracellular permeability markers) across b.End3 cell monolayers established in layered microfluidic channels to that observed in conventional transwells to investigate the difference in barrier properties among these BBB models and calculated their respective membrane porosity. In addition, we evaluated the functional expression of the P-glycoprotein (P-gp) efflux pump

by b.End3 cells in both *in vitro* models by measuring the apical-to-basolateral (AB) and basolateral-to-apical (BA) permeability of dexamethasone (a P-gp substrate) as a function of culture time.

4.2 Materials and Methods

4.2.1 Materials

Poly(dimethylsiloxane) (Sylgard 184) was purchased from Dow Corning (Midland, MI). SU-850 was purchased from MicroChem (Newton, MA). Toluene and sterile fibronectin solution were purchased from Sigma-Aldrich (St. Louis, MO). [14C]-D-mannitol (100 μCi/ml) was purchased from Moravek Biochemicals and Radiochemicals (Brea, CA). [3H]-Dexamethasone (1 mCi/ml) was purchased from American Radiolabeled Chemicals, Inc. (St. Louis, MO). Mouse brain endothelial cells (b.End3) were purchased from ATCC (Manassas, VA). Dulbecco's modified eagle medium, fetal bovine serum, 0.05% trypsin, and live/dead cytotoxicity kits were purchased from Invitrogen Life Technologies Corporation (Carlsbad, CA). FITC-labeled 40K-dextran was generously gifted by Dr. Anuska Andjelkovic-Zochowska from the Department of Pathology and Neurosurgery at the University of Michigan.

4.2.2 Design and Fabrication of Microfluidic Devices

The microfluidic devices used for culture of b.End3 cells are composed of layered microfluidic channels (W = 2, 4, or 8mm; L = 4cm; H = 200μm) sandwiching a porous

membrane (0.4μm pore size), which were fabricated using soft lithography following established protocols [13, 14]. Briefly, PDMS prepolymer was mixed with the curing agent at a 10 (prepolymer)/1 (curing agent) weight ratio before casting onto two 4 inch silicon wafers containing a 200μm thick positive relief pattern. The mixture was cured at 60°C for 2 hours before peeling the PDMS layer off the silicon wafer. Access holes were punched with a 16 gauge blunt syringe (1.65 mm outer diameter) forming the inlet and outlet holes for each channel. We spun coated a PDMS/toluene mixture prepared at a 3/2 weight ratio on a clean glass slide for 1 minute to generate a thin mortar layer, which was used to glue the top and bottom PDMS layers. Ag/AgCl recording electrodes were embedded in 500μm x 500μm side channels when fabricating microfluidic devices for measurement of transendothelial electrical resistance (TEER) across b.End3 monolayers following a published procedure [13]. Polyester membranes with an average pore size of 0.4μm were sandwiched between the aligned top and bottom PDMS layers and glued together before curing for 1 hour until the PDMS mortar completely hardened. Pipette tips (100μl) were inserted into the inlets and outlets of the top and bottom channels to serve as medium reservoirs before exposure to plasma oxygen for 5 minutes. Sterile fibronectin solution (25μg/ml) was loaded into the top PDMS channel for 24 hours to coat the polyester membrane followed by exposure of the microfluidic device to UV radiation for sterilization before seeding of b.End3 cells.

4.2.3 Cell Culture

Frozen mouse brain endothelial cells (b.End3) were thawed at 37°C before mixing with 3mL of culture medium, centrifuging at 1000rpm for 3 minutes, aspirating the supernatant, suspending the cell pellet in 10mL of culture medium, transferring cell suspension to a T75 flask, and incubating the cells in a humidified 5% CO_2 incubator at 37°C while changing the culture medium every 48 hours. Cultured b.End3 cells were passaged after reaching 80% confluence by incubating with 5mL of 0.05% Trypsin-EDTA solution for 3 minutes at 37°C to collect the cell pellet for splitting into new T75 flasks or seeding onto fibronectin-coated membranes in microfluidic devices or conventional transwells at a seeding density of 270 cells/mm^2.

4.2.4 Assessment of Viability of b.End3 Cells

Endothelial b.End3 cells cultured in layered microfluidic channels were stained using the live/dead cytotoxicity kit (Life Technologies Corporation, Carlsbad, CA) following manufacturer's protocol. Briefly, 1µL calcein AM and 1µL ethidium homodimer-1 were added to 1mL of the culture medium before adding 16µL of this mixture to b.End3 cells cultured in the top channel and incubating for 20 minutes at 37ºC under normal culture conditions. Live b.End3 cells were stained green while dead cells were stained red and both were visualized using an inverted fluorescent microscope (Nikon, New York, NY) at 500nm and 600nm, respectively. The number of live and dead b.End3 cells observed at the inlet, center, and outlet of the top microfluidic channel was counted in the fluorescent images (1.7mm x 0.88 m) captured at a 10X magnification.

The angle (θ) between cultured b.End3 cells and the longitudinal (X) axis of the top channel in captured fluorescent images (10X magnification) was measured using Photoshop CS4 (Adobe, San Jose, CA) to determine the change in cell alignment at the channel's inlet, center, and outlet as a function of culture time. The variance of the angle measurements is then calculated using equation (1) where σ^2 is the variance, N is the number of data points, x_i is each specific data point, and μ is the mean:

$$\sigma^2 = \frac{1}{N}\sum_{i=1}^{N}(x_i - \mu)^2$$ ---------- Equation 1

4.2.5 Trans-Endothelial Electrical Resistance (TEER) across b.End3 Cell Monolayers

Trans-endothelial electrical resistance (TEER) of confluent b.End3 cell monolayers cultured onto conventional transwells was measured using standard chopstick electrodes (World Precision Instruments, Sarasota, FL) while accounting for the intrinsic resistance of blank filters. Resistance across b.End3 monolayers cultured in layered microfluidic channels was measured on daily basis following our published protocol [13]. Briefly, impedance spectra were taken using an Autolab potentiostat/galvanostat at 0.1V of alternating current passing between the two embedded electrodes within layered microfluidic channels. Frequency range between 10Hz to 1.00MHz was used to yield a total of 64 impedance measurements. The control impedance spectra measured before seeding the cells were subtracted from the measured impedance spectra with b.End3 cells to eliminate their contribution to the calculated resistance. We developed a MATLAB code

(The MathWorks Inc., Natick, MA) using its optimization toolbox to resolve the TEER values, which were normalized to the surface area of the cell monolayers to calculate the resistance in $\Omega.cm^2$.

4.2.6 Paracellular Permeability across b.End3 Cell Monolayers

We investigated the transport of two paracellular permeability markers namely [14C]-mannitol (182 Da, 11.32μM) and FITC-labeled 40K-dextran (40 kDa, 0.117μM) across b.End3 cell monolayers cultured in conventional transwells and layered microfluidic channels after 3, 6, 9, 12, 15, 18, and 21 days in culture. In both transwells and layered microfluidic channels, b.End3 cells were seeded at a seeding density of 270 cells/mm^2 onto porous polyester membranes pretreated with fibronectin and allowed to grow under normal culture conditions. The culture medium was removed from the apical (top) and basolateral (bottom) compartments before washing the b.End3 monolayers twice with warm (37°C) PBS solution prior to starting the transport study. The PBS solution in the apical compartment was replaced with different marker solutions before incubating different devices at 37°C, 95% relative humidity, and 5% CO_2 for 60 minutes. The PBS solution in the receiver compartment in layered microfluidic channels and transwells was collected and replaced with fresh PBS every 10 minutes for 60 minutes. At the end of the 1 hour incubation time, PBS solutions in both the donor and receiver compartments were also collected. Collected PBS solutions containing radiolabeled markers were mixed with 1mL of the liquid scintillation fluid (GMI Inc., Ramsey, MN) and analyzed using the Beckman LS6500 Liquid Scintillation Counter (Beckman Coulter Inc., Brea, CA) to determine the

concentration of each marker using a standard calibration curve. Similarly, the fluorescence of FITC-labeled 40K-dextran was measured (λ_{ex} = 488nm and λ_{em} = 520nm) using a fluorescence plate reader (Thermo Fisher Scientific Inc., Wayne, MI) to calculate dextran concentration in collected solutions using a calibration curve.

The permeability of a given molecule across the b.End3 monolayer was calculated using the following differential equation derived from Fick's Law [15]:

$$P = \frac{V_{basolateral} \times \frac{\Delta C_{basolateral}}{\Delta t}}{A \times C_{apical}}$$ ---------- Equation 2

Where P denotes solute permeability (cm/sec), V is the PBS volume in the basolateral compartment, A is the surface area of the b.End3 monolayer, C is solute concentration in the apical compartment, and ΔC is the change in solute concentration in the basolateral compartment as a function of time. It is important to note that the transfer of solutes from the apical to the basolateral compartment does not depend on solute concentration and varies only with the incubation time.

4.2.7 Assessment of P-glycoprotein Activity in b.End3 Cell Monolayers

Functional expression of P-glycoprotein (P-gp) efflux pump by b.End3 cells cultured in transwells and layered microfluidic channels was investigated by measuring the apical-to-basolateral (AB) and basolateral-to-apical (BA) permeability of [3H]-Dexamethasone (0.004μM), which is a substrate for the P-gp efflux pump. Before starting the transport experiment, the culture medium in the apical and basolateral compartments in the transwells and channels were replaced with fresh PBS preheated at 37°C after washing

the cell monolayer twice. PBS solutions were then aspirated and replaced with [3H]-Dexamethasone in the apical (top) compartment for half of the total number of channels and transwells. The basolateral (bottom) compartment in the other half of the channels and transwells was filled with the radioactive marker. All other experimental conditions and solution retrieval procedures were similar to those used in the paracellular permeability studies. We calculated the apical-to-basolateral (AB) and basolateral-to-apical (BA) permeability of [3H]-Dexamethasone using equation 5.

4.3 RESULTS

4.3.1 Effect of Dimensions of Microfluidic Channels on b.End3 Viability and Morphology

The design of our microfluidic device incorporates two layered microfluidic channels that sandwich a polyester membrane (0.4μm pore size) along the entire length of the channel, which was used to culture b.End3 cells **(Figure 4.1A)**. The device is designed to incorporate a cross section between the top and bottom channels sufficient to allow measurement of solute's permeability across b.End3 cell monolayers while maintaining an elongated geometric shape and scaled down dimensions. The elongated rectangular shaped channel serve to guide endothelial cell growth, which has been shown to enhance endothelial cell growth and differentiation [16]. The geometry of our device also serves to mimic the blood vessel much more closely compared to the circular design of the transwells. The small dimensions (W = 2mm; L = 4cm; H = 200μm) of the 2mm-wide microfluidic

channel increase the surface to volume ratio, which results in concentration of the factors secreted by brain endothelial cells and decreases the volume of the markers' solution needed for permeability studies at the same time. Therefore, the volume of the markers' solution in our microfluidic device is only 16µl in the top channel compared to 1ml in standard 12-well transwells. Our device also allows the incorporation of Ag/AgCl electrodes in both the top and bottom channels allowing real-time measurement of TEER, which is an indicator of cell monolayer integrity [13].

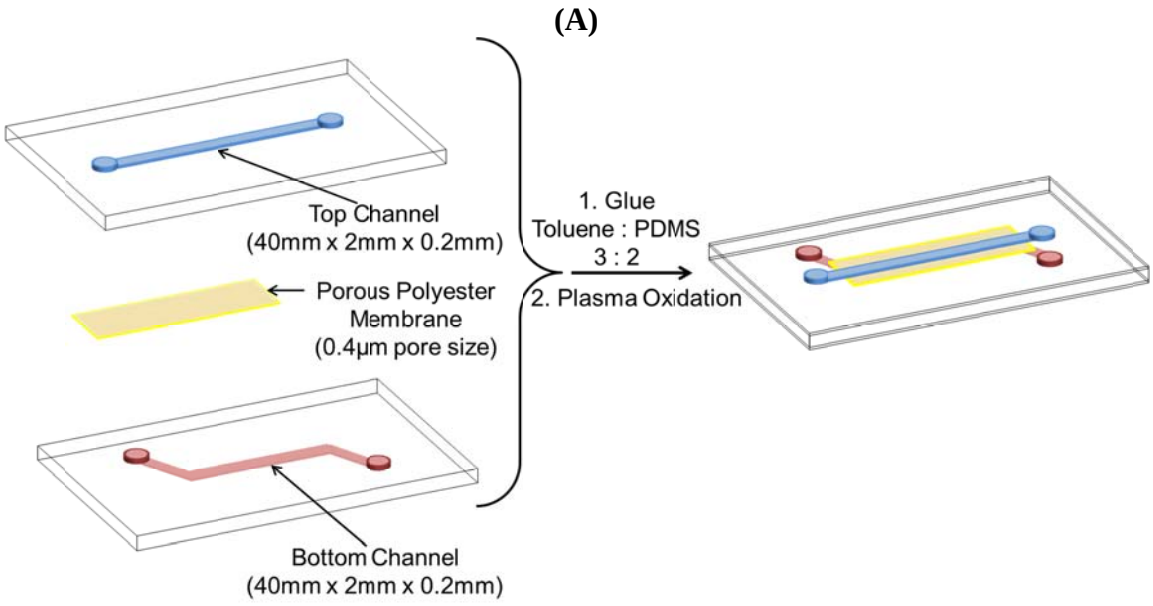

(B)

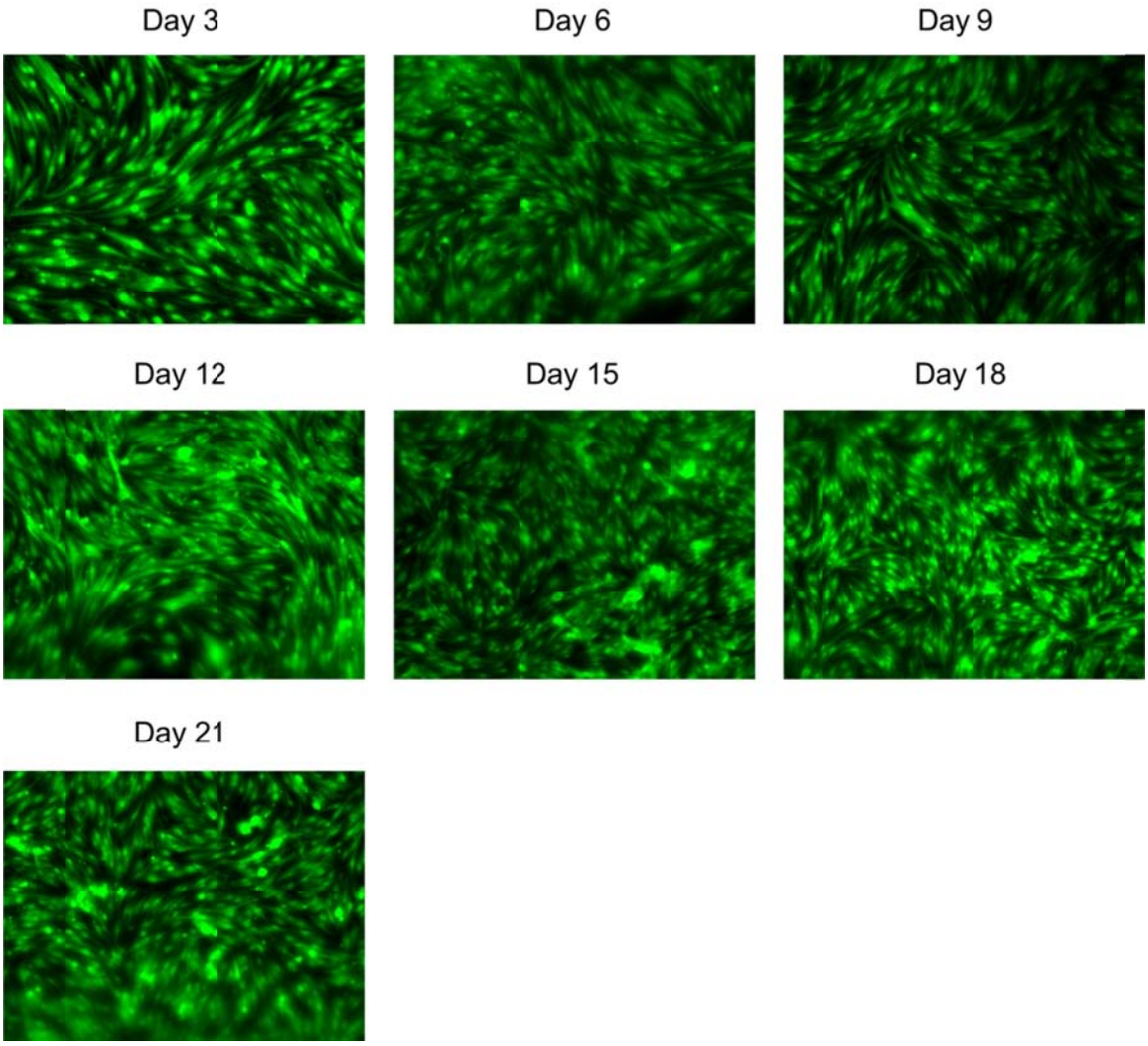

(C)

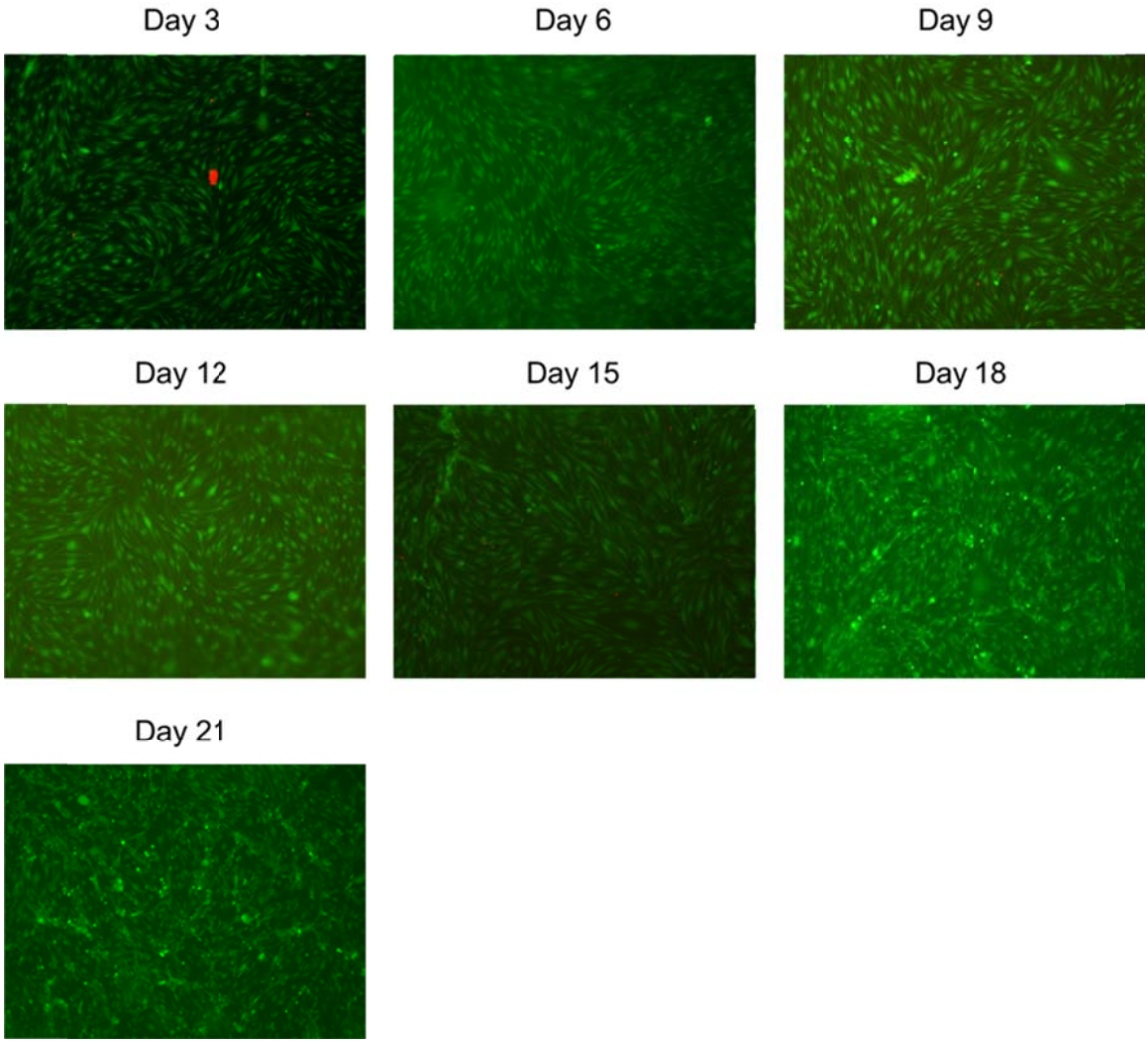

Figure 4.1: (A) A schematic drawing of the layered PDMS channels (40mm x 2mm x 0.2mm) sandwiching a polyester membrane (pore size = 400 nm). Fluorescent images (10x magnification) of b.End3 cells cultured in **(B)** 2 mm-wide layered PDMS channels and **(C)** conventional 12-well transwells at different days in culture.

Fluorescent images demonstrate the feasibility of culturing b.End3 cells in layered microfluidic devices and formation of a viable monolayer for 21 days **(Figure 4.1B)**. Our

results show that the number of viable b.End3 cells significantly increased from 435±21 cells/mm^2 after 3 days in culture to 565±35 cells/mm^2 after 6 days ($\alpha = 0.05$) and remained constant up to 21 days **(Figure 4.2A)**. Similarly, the number of b.End3 cells cultured in transwells increased from 400±25 cells/mm^2 after 3 days in culture to 538±28 cells/mm^2 after 6 days **(Figure 4.2A)**. However, the number of b.End3 cells gradually declined from 550±54 cells/mm^2 after 12 days in culture down to 473±25 cells/mm^2 after 21 days **(Figure 4.2A)**. The decline in number of viable b.End3 cells is supported by earlier reports showing shorter viability span of b.End3 cells cultured in transwells compared to microfluidic devices [17].

We measured the angle (θ) between the spindle of b.End3 cells and the longitudinal axis of the microfluidic channels as a function of days in culture. Fluorescent images of b.End3 cells show a 50° angle (θ) between b.End3 cells and the longitudinal axis of the microfluidic channels after 3 days in culture, which indicates a random organization of the cultured cells at early time points **(Figure 4.2B)**. However, this angle (θ) gradually declined with the increase in culture time reaching 28° after 21 days, which indicates gradual alignment of bEnd.3 cells along the length of the microfluidic channel that increased with culture time **(Figure 4.2B)**. In comparison, the angle (θ) between the spindle of b.End3 cells and the cross-sectional diameter of the transwells was 51° after 3 days in culture and dropped to only 44° after 21 days in culture indicating random organization of b.End3 cells throughout the culture time **(Figure 4.2B)**. The variance (σ^2) in angle measurement showed a steady decline in spindle angle for b.End3 cells cultured in microfluidic channels compared to those cultured in transwells, which further confirms the alignment of b.End3

cells along the length of the top channel **(Figure 4.2C)**. These results are in agreement with earlier reports showing the change in organization and morphology of endothelial cells when cultured in microfluidic devices, which is induced by shear stress [18] or channel's shape and size [19-23].

(A)

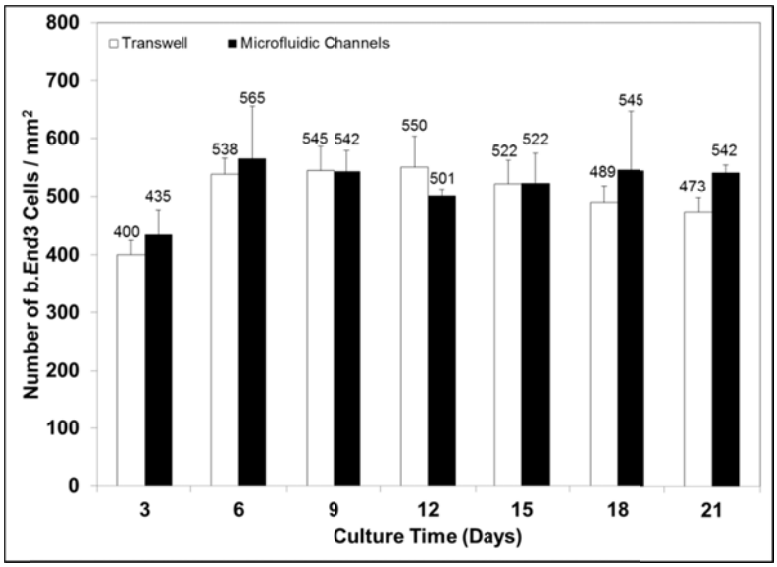

(B)

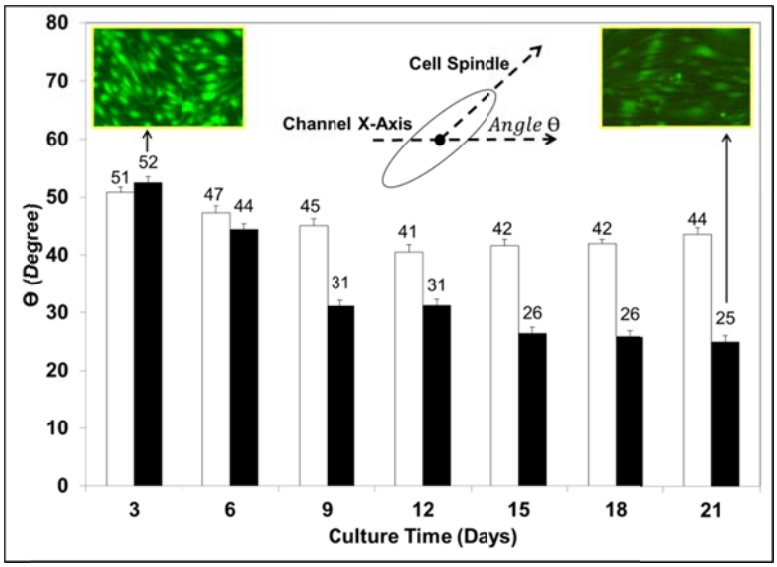

(C)

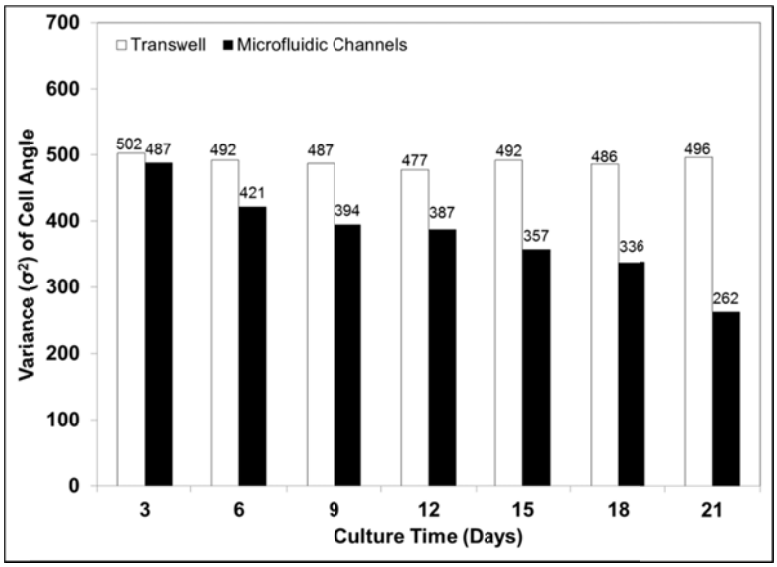

Figure 4.2: The change in **(A)** number, **(B)** angle (θ), and **(C)** variance of angle (σ^2) of b.End3 cells cultured in 12-well transwells and 2 mm-wide layered microfluidic channels as a function of days in culture.

4.3.2 TEER of b.End3 Monolayers in Transwells and Layered Microfluidic Channels

TEER values were measured using embedded Ag/AgCl electrodes in both the top and bottom PDMS layers of the microfluidic channels **(Figure 4.3A)**. TEER values were resolved by modeling the internal resistance of a cell and the capacitance of the cell membrane in series. Baseline TEER measurements across porous polyester membranes without seeding b.End3 cells were similar in layered microfluidic devices and transwells at different days in culture, which indicates that the layout of the device and composition of the culture medium (e.g. FBS serum) did not affect the calculated TEER values.

Results show that TEER across b.End3 cell monolayers established in conventional transwells starts at 29 Ohms.cm^2 after 1 day in culture and shows a slight increase reaching a maximum of 45 Ohms.cm^2 during 21 days in culture **(Figure 4.3B)**, which is similar to previous reports [24]. In comparison, TEER across b.End3 monolayers cultured in 2mm-wide microfluidic channels gradually increased from 28 Ohms.cm^2 directly after seeding to 84, 125, and 143 Ohms.cm^2 on days 1, 2, and 3, respectively **(Figure 4.3B)**. The b.End3 monolayers established in microfluidic channels maintained an average TEER of ~140 Ohms.cm^2 between days 3 and 21 in culture indicating the viability and high integrity of the formed barrier throughout this culture time **(Figure 4.3B)**. The observed 3.5-fold increase in TEER across b.End3 cell monolayers cultured in 2mm-wide microfluidic channels compared to transwells despite of the equal cell seeding density and similar culture conditions indicates the formation of a "tighter" barrier in the microfluidic devices [25].

(A)

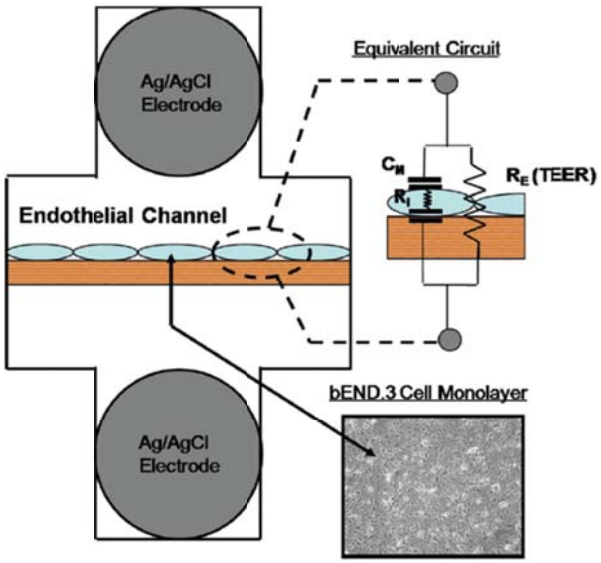

(B)

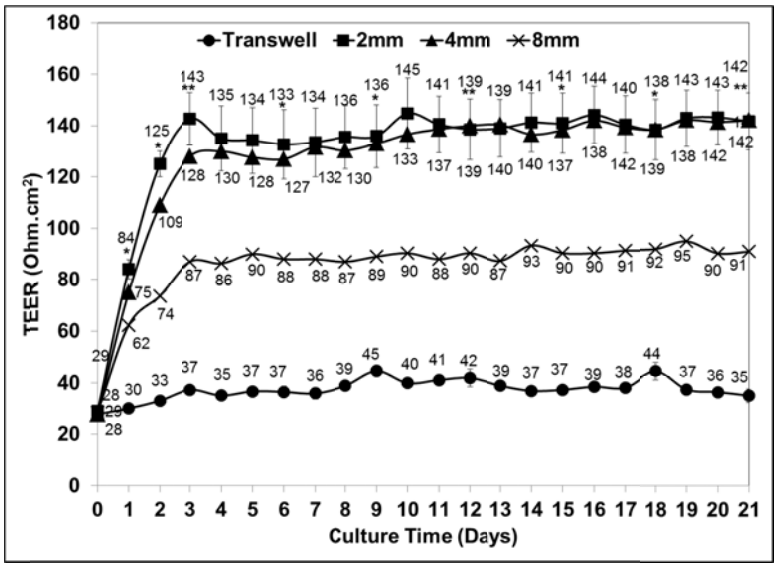

Figure 4.3: (A) is a schematic drawing showing the design of the layered microfluidic channels and the equivalent circuit model. Ag/AgCl recording electrodes are embedded on opposing sides bEnd.3 cells cultured on a polyester porous membrane. Electrical current has two parallel paths through the confluent cell monolayer. The transcellular path can be modeled by the internal resistance of a cell (RI) in series with the capacitance of the cell membranes (CM). The paracellular path is modeled by the resistor (RE) and represents the trans-endothelial electrical resistance (TEER) of the experiment [13]. **(B)** The TEER across b.End3 monolayers cultured in 12-well transwells and 2mm-, 4mm-, and 8mm-wide layered microfluidic channels at different days in culture. The * ($p<0.05$) and ** ($p<0.01$) indicate statistically higher TEER in the microfluidic channels compared to 12-well transwells at similar time points.

4.3.3 Assessment of Paracellular Permeability Across b.End3 Cell Monolayers

We investigated the transport of [14C]-mannitol and 40K-dextran, which are standard paracellular permeability markers, across b.End3 cell monolayers cultured in conventional transwells and microfluidic channels to investigate the difference in barrier properties. Results show similar permeability of [14C]-mannitol across b.End3 cell monolayers cultured in transwells (37.1 x 10^{-6} cm/s) and 2mm-wide microfluidic channels

(31.8 x 10^{-6} cm/s) after 3 days in culture **(Figure 4.4A)**. However, permeability of [14C]-mannitol across b.End3 cell monolayers cultured in microfluidic channels gradually decreased with the increase in culture time compared to the observed [14C]-mannitol permeability across b.End3 cell monolayers cultured in conventional transwells **(Figure 4.4A)**. For example, permeability of [14C]-mannitol across b.End3 cell monolayers cultured in 2mm-wide microfluidic channels dropped to 13.8 x 10^{-6} cm/s compared to 36.7 x 10^{-6} cm/s observed in transwells after 6 days in culture (2.7-fold decrease in permeability) **(Figure 4.4A)**. After 9 days in culture, permeability of [14C]-mannitol across b.End3 cell monolayers cultured in 2mm-wide microfluidic channels dropped further to 3.4 x 10^{-6} cm/s compared to 27.7 x 10^{-6} cm/s observed in the transwells (8.2-fold decrease in permeability) **(Figure 4.4A)**. Permeability of [14C]-mannitol across b.End3 cell monolayers cultured in 2mm-wide microfluidic channels was 3.2 x 10^{-6}, 3.3 x 10^{-6}, 3.3 x 10^{-6}, and 3.5 x 10^{-6} cm/s after 12, 15, 18, and 21 days in culture, respectively, which is 5.7- to 15.1-fold lower than the observed permeability across b.End3 cell monolayers cultured in 12-well transwells at the same time points **(Figure 4.4A)**.

Results show similar permeability of 40K-dextran across b.End3 cell monolayers cultured in transwells (2.3 x 10^{-6} cm/s) and 2mm-wide microfluidic channels (2.0 x 10^{-6} cm/s) after 3 days in culture **(Figure 4.4B)**. However, permeability of 40K-dextran across b.End3 cell monolayers cultured in microfluidic channels gradually decreased with the increase in culture time compared to the observed 40K-dextran permeability across b.End3 cell monolayers cultured in conventional transwells **(Figure 4.4B)**. For example, permeability of 40K-dextran across b.End3 cell monolayers cultured in 2mm-wide

microfluidic channels dropped to 0.6 x 10^{-6} cm/s compared to 1.7 x 10^{-6} cm/s observed in transwells after 6 days in culture (2.8-fold decrease in permeability) **(Figure 4.4B)**. After 9 days in culture, permeability of 40K-dextran across b.End3 cell monolayers cultured in 2mm-wide microfluidic channels dropped further to 0.1 x 10^{-6} cm/s compared to 1.1 x 10^{-6} cm/s observed in the transwells (11-fold decrease in permeability) **(Figure 4.4B)**. Permeability of 40K-dextran across b.End3 cell monolayers cultured in 2mm-wide microfluidic channels remained constant at 0.1 x 10^{-6} cm/s between 12 and 21 days in culture, which is 15- to 21-fold lower than the observed permeability across b.End3 cell monolayers cultured in 12-well transwells at the same time points **(Figure 4.4B)**.

The permeability profiles of [14C]-mannitol and 40K-dextran across b.End3 cell monolayers established in 2mm-wide microfluidic device indicate the development of a stable and "restrictive" barrier after 9 days in culture, which retains its integrity for up to 21 days **(Figure 4.4, Panels A & B)**. In comparison, b.End3 cell monolayers established in 12-well transwells achieve their maximum integrity (i.e. lowest permeability) on day 9 but rapidly lose their integrity as indicated by the increase in permeability of [14C]-mannitol and 40K-dextran on the following days in culture **(Figure 4.4, Panels A & B)**. It is also important to note that b.End3 monolayers established in 2mm-wide microfluidic channels can discriminate between small molecules like mannitol and macromolecules like dextran shown by the > 30-fold higher mannitol permeability. This size selectivity towards diffusing molecules indicates the formation of tight junction complexes between adjacent endothelial cells in our microfluidic channels, which is one of the key properties of the BBB *in vivo* [1, 2].

(A)

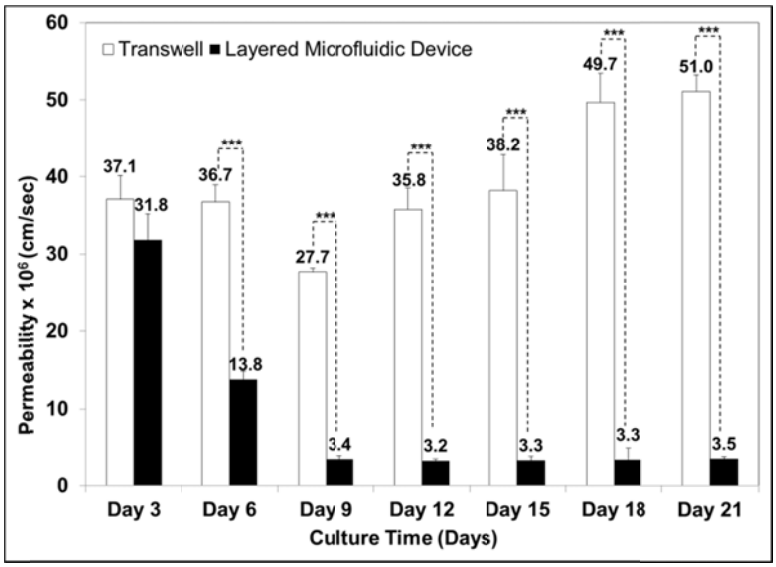
Transwell ■ Layered Microfluidic Device
Permeability x 10⁶ (cm/sec)
60
50
40
30
20
10
0
37.1
31.8
36.7
13.8
27.7
3.4
35.8
3.2
38.2
3.3
49.7
3.3
51.0
3.5
***
Day 3
Day 6
Day 9
Day 12
Day 15
Day 18
Day 21
Culture Time (Days)

(B)

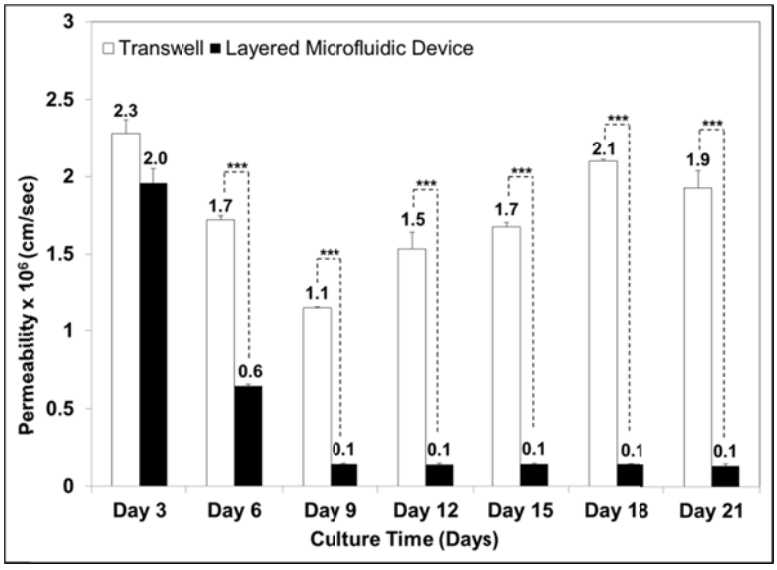
Transwell ■ Layered Microfluidic Device
Permeability x 10⁶ (cm/sec)
3
2.5
2
1.5
1
0.5
0
2.3
2.0
1.7
0.6
1.1
0.1
1.5
0.1
1.7
0.1
2.1
0.1
1.9
0.1
***
Day 3
Day 6
Day 9
Day 12
Day 15
Day 18
Day 21
Culture Time (Days)

(C)

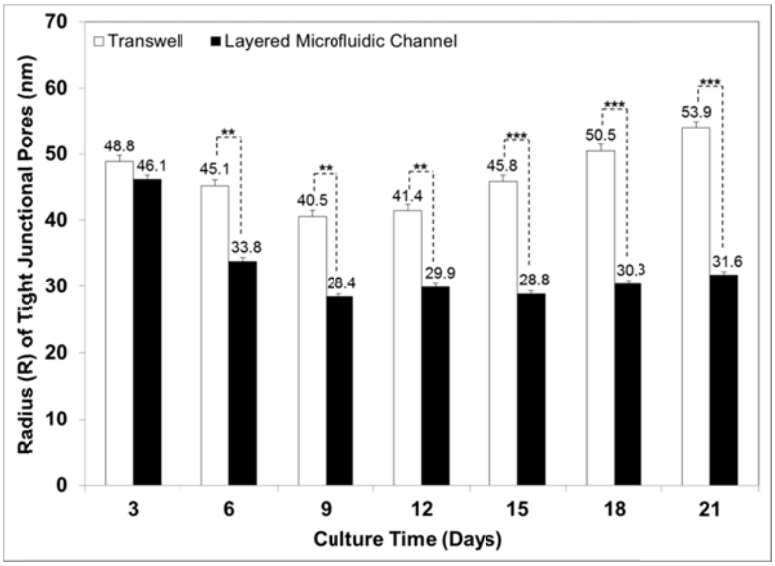

Figure 4.4: Permeability of **(A)** [14C]-mannitol and **(B)** 40K-dextran across b.End3 monolayers cultured in 12-well transwells and 2mm-wide layered microfluidic channels at different days in culture. The *** indicates a statistically lower permeability ($p<0.005$) across b.End3 monolayers cultured in 2mm-wide microfluidic channels compared to the permeability of the same marker across 12-well transwells at similar time points. **(C)** Radius of the pores of the tight junctions (R) in b.End3 monolayers cultured in 12-well transwells and 2mm-wide layered microfluidic channels at different days in culture. The ** indicates a statistically lower radius (R) ($p<0.01$) of the pores in the tight junctions of b.End3 monolayers established in the 2mm-wide microfluidic devices compared to 12-well transwells.

4.3.4 Porosity of b.End3 Cell Monolayers

The observed lower permeability of [14C]-mannitol and 40K-dextran across b.End3 monolayers cultured in 2mm-wide layered microfluidic channels compared to the b.End3 monolayers established in transwells indicates the formation of a more "restrictive" barrier (i.e. lower porosity of the tight junctions) in the microfluidic devices. By modeling the intercellular space between adjacent endothelial cells as water-filled channels, we

calculated the radius (R) of the pores of the tight junctions using the following Renkin function equation.

$$F\left(\frac{r}{R}\right) = (1-\frac{r}{R})^2[1 - 2.104\left(\frac{r}{R}\right) + 2.09\left(\frac{r}{R}\right)^3 - 0.95\left(\frac{r}{R}\right)^5] \quad \text{---------- Equation 3}$$

Where the Renkin function $[F\left(\frac{r}{R}\right)]$ mathematically describes the relationship between the radius of the diffusing molecule (r) and the pore radius of the tight junctions (R) [26].

The following flux equation provides a relationship between the permeability (P) of a diffusing marker molecule and the Renkin function $[F\left(\frac{r}{R}\right)]$.

$$P = \frac{\epsilon D F(\frac{r}{R})}{\delta} \quad \text{---------- Equation 4}$$

where ϵ is the porosity of the b.End3 monolayer, D is the diffusion coefficient of the evaluated marker molecule, and δ is the distance traversed by the marker molecule down a concentration gradient [26]. We used the diffusion coefficients (D) of mannitol (9.65×10^{-6} cm/s) and 40K-dextran (5.1×10^{-7} cm/s) with our permeability results **(Figure 4.4, Panels A&B)** to solve equation 4 for the Renkin function $F(\frac{r}{R})$ and $\frac{\epsilon}{\delta}$ at different time points. We used Matlab R2009a to solve the $F(\frac{r}{R})$ polynomial (Equation 3) and obtain R assuming that the radii (r) of mannitol and 40K-dextran are 0.34nm [27] and 3nm [28], respectively.

Results show that the average radius of the tight junctions pores (R) for b.End3 cell monolayers cultured in transwells drops from 48.8 to 45.1 and 40.5 nm after 3, 6, and 9 days in culture, respectively **(Figure 4.4C)**. At longer time points, the radius of the tight junctions pores (R) for b.End3 cell monolayers cultured in transwells gradually increases reaching 53.9 nm after 21 days in culture **(Figure 4.4C)**. In comparison, the radius of the

tight junctions pores (R) for b.End3 cell monolayers cultured in layered microfluidic channels started at 46.1 nm after 3 days in culture and gradually decreased to 33.8 nm (day 6), 28.4 nm (day 9), and remained relatively constant for 21 days in culture **(Figure 4.4C)**. Lower porosity (R) of b.End3 monolayers established in layered microfluidic channels compared to conventional transwells is statistically significant ($\alpha = 0.005$) and confirms the formation of a restrictive barrier in the microfluidic device.

4.3.5 Effect of Channel Width on Barrier Properties of b.End3 monolayers

Earlier reports relied on flow-mediated shear stress to align endothelial cells with the direction of the flow, which increased the expression and localization of tight junctions proteins between adjacent cells resulting in the formation of more restrictive models of the BBB *in vitro* [17, 18, 29, 30]. Other reports showed the ability to direct endothelial cells to follow the shape of microfluidic devices used for their culture [19-23]. Therefore, we hypothesized that controlling the narrow width of the microfluidic channels (2mm) used for culture of b.End3 cells will direct the cells to align along the longitudinal axis of the channel, which will enhance cell-cell contact, formation of the tight junctions, and result in the formation of a restrictive barrier without incorporating complex accessories to allow laminar flow through our channels. Alignment of b.End3 cells **(Figure 4.2B)**, high TEER values **(Figure 4.3B)**, and low permeability of [14C]-mannitol and 40K-dextran across b.End3 cell monolayers established in 2mm-wide microfluidic channels clearly indicate the formation of a viable and restrictive barrier in our microfluidic devices. To further validate the role of channel width in guiding b.End3 cell alignment and formation of a restrictive

BBB, we fabricated layered microfluidic channels that are 4mm and 8mm wide while keeping the same channel's length (4cm) and height (200μm) and used them for culture of b.End3 cells under the same experimental conditions.

Results show that increasing channel width to 4mm did not cause a significant change in TEER across b.End3 cell monolayers compared to those cultured in 2mm-wide channels **(Figure 4.3B)**. However, increasing channel width to 8mm (4 folds) caused a significant drop in TEER values compared to b.End3 monolayers established in 2mm-wide channels **(Figure 4.3B)**. Specifically, TEER started at 28 Ohms.cm^2 directly after seeding and gradually increased to reach 62, 74, 87 Ohms.cm^2 on days 1, 2, and 3, respectively, before stabilizing around 90 Ohms.cm^2 till day 21 **(Figure 4.3B)**. This dramatic drop in TEER values despite of identical seeding density and culture conditions clearly show the contribution of channel width to the organization of b.End3 cells in the channels and their ability to form a tight monolayer.

We investigated the permeability of [14C]-mannitol across b.End3 monolayers established in 4mm- and 8mm-wide microfluidic channels and compared the results to those observed in 2mm-wide channels **(Figure 4.5)**. Specifically, permeability of [14C]-mannitol was 5.01 x 10^{-6}, 5.28 x 10^{-6}, 5.12 x 10^{-6}, 3.75 x 10^{-6}, and 5.13 x 10^{-6} on day 9, 12, 15, 18, and 21, respectively, which are statistically higher than mannitol permeability across b.End3 cell monolayers established in 2mm-wide channels **(Figure 4.5)**. Permeability of [14C]-mannitol across b.End3 cell monolayers established in 8mm-wide channels were ~3-fold higher than that observed in 2mm-wide channels reaching 12.1 x 10^{-6}, 12.5 x 10^{-6}, 11.5 x 10^{-6}, 10.8 x 10^{-6}, and 12.2 x 10^{-6} cm/s on days 9, 12, 15, 18, and 21,

respectively **(Figure 4.5)**. It is important to note that permeability of [14C]-mannitol across b.End3 monolayers established in 2mm-, 4mm-, and 8mm-wide channels was investigated at the same concentration (11.32μM). These results indicate the role of channel width in controlling cell behavior and mediating the formation of restrictive monolayers in 2mm-wide channels.

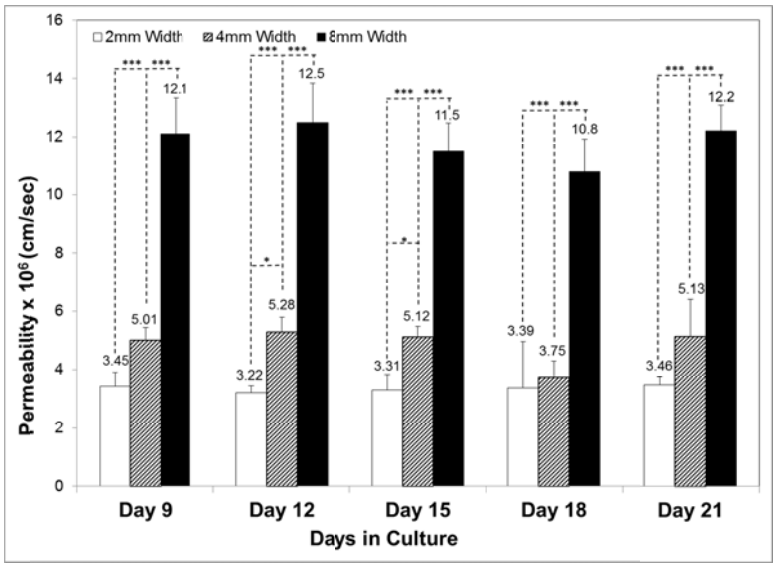

Figure 4.5: Permeability of [14C]-mannitol across b.End3 monolayers cultured in 2mm-, 4mm-, and 8mm-wide microfluidic channels at different days in culture where * indicates a statistically lower permeability ($p<0.05$) across b.End3 monolayers in 4mm- and 8mm-wide channels compared to the monolayers established in 2mm-wide channels.

4.3.6 Functional Expression of P-glycoprotein by b.End3 Cells

We measured the apical-to-basolateral (AB) and basolateral-to-apical (BA) permeability of [3H]-Dexamethasone, which is a substrate for the P-gp efflux pump across b.End3 cell monolayers established in conventional 12-well transwells and 2mm-wide microfluidic channels. Functional expression of the P-gp on the apical side of b.End3 cells

would decrease dexamethasone's AB permeability and increase its BA permeability **(Figure 4.6)**. Therefore, we calculated dexamethasone's Efflux Ratio (ER) across b.End3 monolayers using the following equation.

$$ER = \frac{Permeability_{BA}}{Permeability_{AB}}$$ ---------- Equation 5

Results show high BA permeability of dexamethasone across b.End3 monolayers cultured in transwells after 6 days in culture with an ER ranging between 1.1-1.4, which indicates low functional expression of the P-gp efflux pump. In comparison, functional expression of the P-gp by b.End3 cells cultured in 2mm-wide microfluidic channels is observed on day 12 and persists for 21 days, which is indicated by the calculated ER of 1.8 to 2.2 **(Figure 4.6)**. Higher ER observed with b.End3 cells cultured in 2mm-wide microfluidic channels compared to that observed with the monolayers cultured in transwells indicates higher expression and activity of the P-gp pump, which is characteristic of the BBB *in vivo* [31].

(A)

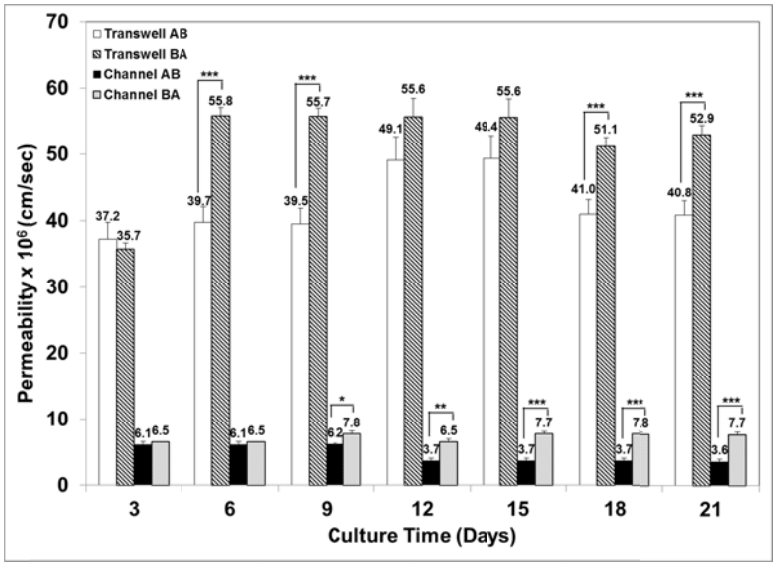

(B)

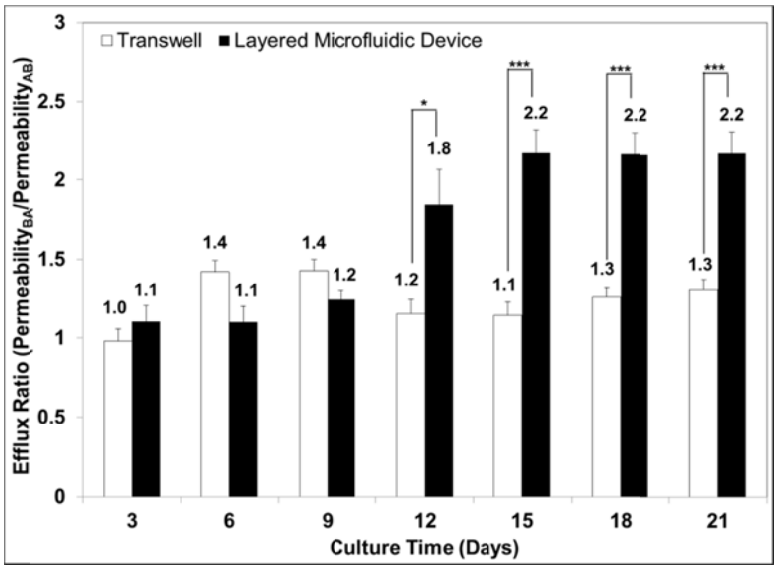

Figure 4.6: (A) Apical-to-basolateral (AB) and basolateral-to-apical (BA) permeability of [3H]-dexamethasone across b.End3 monolayers cultured in 12-well transwells and 2mm-wide layered microfluidic channels at different days in culture. The * ($p<0.05$), ** ($p<0.01$), and *** ($p<0.005$) indicate statistical difference in dexamethasone AB and BA permeability. **(B)** Comparison between the ER of [3H]-dexamethasone across b.End3 monolayers cultured in 12-well transwells and 2mm-wide layered microfluidic channels at different days in culture. The * ($p<0.05$) and *** ($p<0.005$) indicate a statistically higher ER in b.End3 monolayers cultured in 2mm-wide microfluidic channels compared to 12-well transwells.

4.4 DISCUSSION

Stewart and co-workers provided one of the earlier examples showing the effect of microenvironment on the barrier properties of chick capillaries implanted in quail brain and quail somite grafts [32]. They showed that chick capillaries implanted in quail brain graft displayed blood-brain barrier like properties while those implanted in quail somite graft near the skeletal muscle did not exhibit the same restrictive properties [32]. In this research, we aimed to mimic the shape and dimensions of small blood vessels in the design of our

layered microfluidic channels, which will allow better cell-to-cell contact, increase the surface-to-volume ratio, minimize the dilution of secreted factors, and reduce the needed volume to evaluate the transport of different markers [14, 16, 33-35]. We achieved this goal by adjusting the dimensions of the top channel to resemble a blood capillary while maintaining a large aspect ratio and a small total volume (17 µl). Starting with 2mm-wide channels, it appears that channel width and geometry enhance b.End3 cell-to-cell contact and guide their alignment along the longitudinal axis of the channel, which is supported by previous reports utilizing microfluidic devices with similar width and height [17]. Alignment of b.End3 cells and enhanced cell-to-cell contact in 2mm-wide layered microfluidic channels enhanced barrier properties as shown by the 2.5-folds increase in TEER compared to b.End3 cells cultured in conventional transwells. Further, b.End3 monolayers cultured in 2mm-wide layered microfluidic channels retained their viability and integrity for 21 days. In comparison, b.End3 cells cultured in the transwells maintained their integrity for only 6-10 days after their seeding indicated by the increase in 40K-dextran and [14C]-mannitol permeability at longer days in culture. The observed short span of barrier integrity in the transwells is supported by earlier reports [36] [35]. Renkin function, a frequently used mathematical model that can resolve the radius of the tight junctional pores in both endothelial and epithelial monolayers, clearly demonstrated that b.End3 cells cultured in 2mm-wide microfluidic channels indeed form “tighter” and more “restrictive” tight junctions shown by the ~1.5-fold reduction in the radius of the intercellular space. While the *in vivo* tight junctional pores have been shown to be 0.8 nm [37], developing an *in vitro* model of the BBB where barrier integrity is enhanced by

controlling the dimensions of the microfluidic channel without the need for flow-mediated shear stress is a significant step towards the development of simplified yet robust *in vitro* models.

Previous works have indicated that geometry of the cell culture micro-environment not only can help define vascular architectures [21] and cell adhesion [38], it can also influence cell growth, differentiation, and apoptosis [16]. It was further supported by the fact that geometry of cell-to-cell contact, which our channel design has affected through angle alignment of b.End3 cell culture, can also affect tight junction formations [39]. Therefore we hypothesized early on that the cell alignment observed through fluorescent images was a result of small width of the channels and plays an important role in assisting the formation of tight junctions. This effect was demonstrated by increasing the width of the microfluidic channels from 2 mm to 4 and 8 mm. The dramatic drop in TEER values and the corresponding increase in permeability of [14C]-mannitol across b.End3 cell monolayers established in 8mm-wide channels compared to the monolayers established in 2mm-channels clearly indicate the formation of “loose” junctions and a more “leaky” barrier. Furthermore, the observed low AB permeability and high BA permeability of dexamethasone across b.End3 monolayers cultured in 2mm-wide microfluidic channels confirm the expression of functional P-gp by cultured cells starting on day 12 and retained till 21 days in culture.

4.5 CONCLUSIONS

We report the successful culture of brain endothelial cells (b.End3) in layered microfluidic channels forming a viable monolayer that exhibits restrictive transport properties indicated by higher TEER values and lower mannitol and dextran permeability compared to b.End3 monolayers cultured in conventional transwells. Further, b.End3 cells cultured in microfluidic devices express functional P-gp at higher levels compared to transwells. Therefore, b.End3 cell monolayers cultured in the described microfluidic devices is a representative *in vitro* model of the blood-brain barrier.

REFERENCES

1. Dermietzel, R., D.C. Spray, and M. Nedergaard, *Blood-Brain Barrier: From Ontogeny to Artificial Interfaces*. Vol. 1. 2006, Weinheim, Germany: WILEY-VCH.
2. Pardridge, W.M., *Blood-Brain Barrier Drug Targeting: The Future of Brain Drug Development.* Molecular Interventions, 2003. **3**(2): p. 90-105.
3. Abbott, N.J., L. Ronnback, and E. Hansson, *Astrocyte-endothelial interactions at the blood-brain barrier.* Nature Reviews Neuroscience, 2006. **7**: p. 41-53.
4. Dermietzel, R., D.C. Spray, and M. Nedergaard, *Blood-Brain Barrier: From Ontogeny to Artificial Interfaces*. Vol. 2. 2006, Weinheim, Germany: WILEY-VCH.
5. Cines, D.B., et al., *Endothelial Cells in Physiology and in the Pathophysiology of Vascular Disorders.* Journal of the American Society of Hematology, 1998. **91**(10): p. 3527-3561.
6. Pardridge, W.M., *Why is the global CNS pharmaceutical market so under-penetrated?* DDT, 2002. **7**(1): p. 5-7.
7. Deli, M.A., et al., *Permeability Studies on In Vitro Blood-Brain Barrier Models: Physiology, Pathology, and Pharmacology.* Cellular and Molecular Neurobiology, 2004. **25**(1): p. 59-127.
8. Fiddes, L.K., et al., *A circular cross-section PDMS microfluidics system for replication of cardiovascular flow conditions.* Biomaterials, 2010. **31**: p. 3459-3464.
9. Tung, Y.-C., et al., *Small volume low mechanical stress cytometry using computer-controlled Braille display microfluidics.* Lab on a Chip, 2007. **7**: p. 1497-1503.

10. Huszank, R., et al., *Fabrication of optical devices in poly(dimethylsiloxane) by proton microbeam.* Optics Communications, 2009. **283**: p. 176-180.

11. Thangawng, A.L., et al., *An ultra-thin PDMS membrane as a bio/micro-nano interface: fabrication and characterization.* Biomedical Microdevices, 2007. **9**: p. 587-595.

12. Cox, M.E. and B. Dunn, *Oxygen Diffusion in Poly(dimethyl Siloxane) using Fluorescence Quenching. I. Measurement Technique and Analysis.* Journal of Polymer Science: Part A: Polymer Chemistry, 1986. **24**: p. 621-636.

13. Douville, N.J., et al., *Fabrication of Two-Layered Channel System with Embedded Electrodes to Measure Resistance Across Epithelial and Endothelial Barriers.* Analytical Chemistry, 2010. **82**(6): p. 2505-2511.

14. Chueh, B.-h., et al., *Leakage-Free Bonding of Porous Membranes into Layered Microfluidic Array Systems.* Analytical Chemistry, 2007. **79**(9): p. 3504-3508.

15. Cucullo, L., et al., *Immortalized human brain endothelial cells and flow-based vascular modeling: a marriage of convenience for rational neurovascular studies.* Journal of Cerebral Blood Flow & Metabolism, 2008. **28**: p. 312-328.

16. Huang, S. and D.E. Ingber, *Shape-Dependent Control of Cell Growth, Differentiation, and Apoptosis: Switching between Attractors in Cell Regulatory Networks.* Experimental Cell Research, 2000. **261**: p. 91-103.

17. Booth, R. and H. Kim, *Characterization of a microfluidic in vitro model of the blood-brain barrier (uBBB).* Lab on a Chip, 2012. **12**: p. 1784-1792.

18. Booth, R., S. Noh, and H. Kim, *A multiple-channel, multiple-assay platform for characterization of full-range shear stress effects on vascular endothelial cells.* Lab on a Chip, 2014. **14**(11): p. 1880-1890.

19. Wang, X.-Y., et al., *Engineering interconnected 3D vascular networks in hydrogels using molded sodium alginate lattice as the sacrificial template.* Lab on a Chip, 2014. **14**(15): p. 2709-2716.

20. Tung, C.-k., et al., *A contact line pinning based microfluidic platform for modelling physiological flows.* Lab on a Chip, 2013. **13**(19): p. 3876-3885.

21. Baker, B.M., et al., *Microfluidics embedded within extracellular matrix to define vascular architectures and pattern diffusive gradients.* Lab on a Chip, 2013. **13**(16): p. 3246-3252.

22. van der Meer, A.D., et al., *Three-dimensional co-cultures of human endothelial cells and embryonic stem cell-derived pericytes inside a microfluidic device.* Lab on a Chip, 2013. **13**(18): p. 3562-3568.

23. Huang, Z., et al., *Microfabrication of cylindrical microfluidic channel networks for microvascular research.* Biomedical Microdevices, 2012. **14**(5): p. 873-883.

24. Fang, H., et al., *Immortalized mouse brain endothelial cell line Bend.3 displays the commparative barrier characteristics as the primary brain microvascular endothelial cells.* Chinese Journal of Contemporary Pediatrics, 2010. **12**(6): p. 474-478.

25. Brown, R.C., A.P. Morris, and R.G. O'Neil, *Tight Junction Protein Expression and Barrier Properties of Immortalized Mouse Brain Microvessel Endothelial Cells.* Brain Research, 2007. **1130**(1): p. 17-30.

26. Adson, A., et al., *Quantitative Approaches To Delineate Paracellular Diffusion in Cultured Epithelial Cell Monolayers.* Journal of Pharmaceutical Sciences, 1994. **83**(11): p. 1529-1536.

27. Ghandehari, H., et al., *Size-Dependent Permeability of Hydrophilic Probes Across Rabbit Colonic Epithelium.* The Journal of Pharmacology and Experimental Therapeutics, 1997. **280**(2): p. 747-753.

28. Yuan, W., et al., *Non-invasive measurement of solute permeability in cerebral microvessels of the rat.* Microvascular Research, 2009. **77**: p. 166-173.

29. Walsh, T.G., et al., *Stabilization of brain microvascular endothelial barrier function by shear stress involves VE-cadherin signaling leading to modulation of pTyr-occludin levels.* Journal of Cellular Physiology, 2011. **226**(11): p. 3053-3063.

30. Colgan, O.C., et al., *Regulation of bovine brain microvascular endothelial tight junction assembly and barrier function by laminar shear stress*. Vol. 292. 2007. H3190-H3197.

31. Slosky, L.M., et al., *Acetaminophen Modulates P-Glycoprotein Functional Expression at the Blood-Brain Barrier by a Constitutive Androstane Receptor–Dependent Mechanism.* Molecular Pharmacology, 2013. **84**(5): p. 774-786.

32. Stewart, P.A. and M.J. Wiley, *Developing Nervous Tissue Induces Formation of Blood-Brain Barrier Characteristics in Invading Endothelial Cells: A Study Using*

Quail-Chick Transplantation Chimeras. Developmental Biology, 1981. **84**: p. 183-192.

33. Anene-Nzelu, C.G., et al., *Scalable alignment of three-dimensional cellular constructs in a microfluidic chip.* Lab on a Chip, 2013. **13**: p. 4124-4133.
34. Stins, M.F., J. Badger, and K.S. Kim, *Bacterial invasion and transcytosis in transfected human brain microvascular endothelial cells.* Microbial Pathogenesis, 2001. **30**: p. 19-28.
35. Augustin, H.G., *Methods in Endothelial Cell Biology*. 2004, New York: Springer.
36. Li, G., et al., *Permeability of Endothelial and Astrocyte Cocultures: In Vitro Blood-Brain Barrier Models for Drug Delivery Studies.* Annals of Biomedical Engineering, 2010. **38**(8): p. 2499-2511.
37. Miller, R.D., et al., *Miller's Anesthesia, 7th Edition*. 2009: Elsevier Health Sciences.
38. Green, J.V., et al., *Effect of channel geometry on cell adhesion in microfluidic devices.* Lab on a Chip, 2009. **9**(5): p. 677-685.
39. Anderson, J.M. and C.M.V. Itallie, *Physiology and Function of the Tight Junction.* Cold Spring Harbor Perspectives in Biology, 2009: p. 1-16.

Chapter 5

Development of a 3D *In Vitro* Model of the Blood-Brain Barrier in Layered Microfluidic Channels

5.1 INTRODUCTION

The endothelial cells lining the capillaries that supply the brain with oxygen and nutrients present a highly regulated transport barrier known as the blood-brain barrier (BBB). These endothelial cells are characterized by thick cell membranes, low number of endocytic vesicles, absence of fenestrae, and highly organized tight junctions that restrict molecular diffusion across the paracellular space [1-3]. The integrity and function of the BBB is regulated by several factors including endothelial cell-to-cell contact [4], communication with other supporting cell types such as astrocytes and pericytes [2], and the local concentration of secreted chemical factors [5, 6]. Due to the presence of this highly functional barrier, only 2% of small-molecule drugs (< 500 Daltons) can cross the BBB to achieve their effective concentrations and nearly none of the existing large-

molecule drugs can cross the BBB [7]. Only a few central nervous system (CNS) disorders, such as depression, epilepsy, chronic pain, and affective disorders, respond to clinical treatments by the 2% of small-molecule drugs that we have; on the other hand, many more serious CNS disorders cannot be effectively treated by these small therapeutic molecules [7].

The inability of conventional drug molecules to cross the BBB has, in some cases, forced drug development programs to go forward without the consideration of BBB transport at all. This led to the development of craniotomy-based drug delivery method where a hole is drilled in the head, and drugs are directly administered to the brain, thus bypassing the BBB altogether [7]. However, drug molecules administered this way tend to stay at the injection site and cannot effectively penetrate the brain parenchyma. With such limited penetration capability, only 1% of the brain volume is reached, making this method ineffective against most, if not all, brain diseases [7]. Clinical research has also shown that osmotic modification of the BBB can increase the delivery of drug molecules, specifically chemotherapeutic agents for the treatment of brain tumors. This method, coupled with intravenous infusion of chemotherapeutic agents [8], has been found to prolong survival of patients with high-grade gliomas by 10-12 months [9]; however, this therapeutic method is associated with cognitive deterioration or changes in the CNS detectable by Magnetic Resonance Imaging [10]. In comparison to the limitations of methods such as the craniotomy-based drug delivery system and osmotic modification of the BBB, if drug molecules administered intravenously or intracarotidly are capable of taking advantage of the transport systems, they have the potential to become much more effective at penetrating

the BBB while minimizing side effects at the same time. Drug molecules capable of such maneuvers have the ability to reach nearly all of the neurons in the brain since every neuron is supported by its own capillary vessel [7]; however, it requires innovative drug-targeting systems that have the capability of traversing through the BBB. Development of such system cannot begin until detailed molecular and cellular biology of the BBB are revealed; and obtaining such information requires an accurate and cost-effective *in vitro* BBB model that can be used repeatedly for drug screening and experimentation.

Realizing the importance of *in vitro* BBB models, many groups have attempted to construct such model using both primary and immortalized cell lines. Primary endothelial cells isolated from bovine, human, porcine, and rodent are typically used in modeling the BBB [4]. Among all such established models, one porcine model demonstrated relatively high trans-endothelial electrical resistance (TEER) and low permeability [4], which are key characteristics of the BBB. Despite the ethical questions and the logistical difficulties of obtaining human brain tissue, there have been reports of established human BBB models; these models, however, are less robust than porcine models according to published data [4]. All primary models suffer from several disadvantages. Primary cells are expensive to obtain and the reconstitution process is time consuming. Furthermore, the homogeneity of obtained cells is difficult to determine, and can be easily contaminated with neighboring cell types such as the pericytes [4]. In recent years, immortalized brain endothelial cell lines have been more commonly used than primary cell lines due to their ease of manipulation and reproducibility. There are currently more than 20 endothelial cell lines available and virtually all of them have been used to establish *in vitro* BBB models with published results

[4]. Many of these models utilize transwell system, which is the standard tool for *in vitro* drug screening. The major issue that such models suffer is leaky monolayer formation which results in low TEER and high permeability values. Since these models did not generate BBB characteristics, it is very difficult to use them for BBB related studies. We believe that the reasons for the failed mimicry of the restrictive transport properties of the BBB can be due to the formation of "loose" tight junctions between adjacent endothelial cells, lower expressions of specific carriers, or limited cell viability. This can be attributed to the lack of proper micro-environments and efficient integration of endothelial and neural cells in a model that allow cell-to-cell communication necessary to induce the proper differentiation of brain capillary endothelial cells, formation of restrictive tight junctions, and functional expression of different transporters at the levels present *in vivo*.

In this article, we report the successful culture of mouse brain endothelial cells (b.End3) with pericytes and astrocytes co-cultured in layered microfluidic PDMS devices to develop a new 3D *in vitro* BBB model that successfully mimics the restrictive transport properties observed *in vivo*. We rely on the dimensions of the channels and the surface to volume ratio to increase cell-to-cell contact and pericytes and astrocytes to influence the development and differentiation of the b.End3 monolayers. We compared the permeability of paracellular transport markers mannitol and urea across the monolayers to that observed *in vivo* to observe the difference in transport properties of the BBB model and calculated the Renkin function. Furthermore, we measured TEER across b.End3 monolayers established in our system to investigate the barrier integrity. We then modified the bottom layer of the channel design where astrocytes were grown in order to demonstrate the

distance effect of neutrophic factors on b.End3 monolayers cultured in layered microfluidic channels. Finally, we evaluated the functional expression of the P-glycoprotein (P-gp) efflux pump to determine the existence of these critical proteins in our BBB model.

5.2 MATERIALS AND METHODS

5.2.1 Materials

Poly(dimethylsiloxane) (Sylgard 184) was purchased from Dow Corning (Midland, MI). SU-850 was purchased from MicroChem (Newton, MA). Toluene and sterile fibronectin solution were purchased from Sigma-Aldrich (St. Louis, MO). [14C]-D-mannitol (100 μCi/ml) and [14C]-urea (100 μCi/ml) were purchased from Moravek Biochemicals and Radiochemicals (Brea, CA). [3H]-Dexamethasone (1 mCi/ml) was purchased from American Radiolabeled Chemicals, Inc. (St. Louis, MO). Mouse brain endothelial cells (b.End3) and Astrocyte type I clone (C8-D1A) were purchased from ATCC (Manassas, VA). Mouse pericytes were generously gifted by Dr. Anuska Andjelkovic from the University of Michigan. Dulbecco's modified eagle medium, fetal bovine serum, 0.05% trypsin, non-essential amino acids, and live/dead cytotoxicity kits were purchased from Invitrogen Life Technologies Corporation (Carlsbad, CA). Interferon-gamma was purchased from R&D Systems (Minneapolis, MN).

5.2.2 Design and Fabrication of Microfluidic Devices

The microfluidic devices used for culture of b.End3 cells are composed of layered microfluidic channels (W = 2mm; L = 4cm; H = 0.2, 0.6, or 1mm) sandwiching a porous membrane, which were fabricated using soft lithography following established protocols [11, 12]. Briefly, PDMS prepolymer was mixed with the curing agent at a 10 (prepolymer) / 1 (curing agent) weight ratio before casting onto two 4 inch silicon wafers containing a 200 μm thick positive relief pattern. The mixture was cured at 60 °C for 2 hours before peeling the PDMS layer off the silicon wafer. Access holes were punched with a 16 gauge blunt syringe (1.65 mm outer diameter) forming the inlet and outlet holes for each channel. We spun coated a PDMS/toluene mixture prepared at a 3/2 weight ratio on a clean glass slide for 1 minute to generate a thin mortar layer, which was used to glue the top and bottom PDMS layers. Ag/AgCl recording electrodes were embedded in 500 μm x 500 μm side channels when fabricating microfluidic devices for measurement of TEER across b.End3 monolayers following a published procedure.[12] Polyester membranes with an average pore size of 400 nm were sandwiched between the aligned top and bottom PDMS layers and glued together before curing for 1 hour until the PDMS mortar completely hardened. Pipette tips (100 μl) were inserted into the inlets and outlets of the top and bottom channels to serve as medium reservoirs before exposure to plasma oxygen for 5 minutes. Sterile fibronectin solution (25 μg/ml) was loaded into the top PDMS channel for 24 hours to coat the polyester membrane followed by exposure of the microfluidic device to UV radiation for sterilization before seeding of b.End3 cells and mouse pericyte cells.

5.2.3 Cell Culture

Mouse brain endothelial cells (b.End3) were thawed at 37 °C before mixing with 3 mL of culture medium, centrifuging at 1000 rpm for 3 minutes, aspirating the supernatant, suspending the cell pellet in 10 mL of culture medium, transferring cell suspension to a T75 flask, and incubating the cells in a humidified 5% CO_2 incubator at 37 °C while changing the culture medium every 48 hours. Cultured b.End3 cells were passaged after reaching 80% confluence by incubating with 5 mL of 0.05% Trypsin-EDTA solution for 3 minutes at 37 °C to collect the cell pellet for splitting into new T75 flasks or seeding onto fibronectin-coated membranes in microfluidic devices or conventional transwells at a seeding density of 270 cells/mm^2. Astrocytes were cultured under the same conditions using Dulbecco's Modified Eagle's Medium (30-2002) with 10% FBS based on ATCC's recommendation.

Mouse pericytes were thawed at 37 °C and directly put into a T75 flask, and incubating the cells in a humidified 5% CO_2 incubator at 31 °C while changing the culture medium every 24 hours. Cultured mouse pericytes were passaged after reaching 80% confluence by incubating with 3 mL of 0.05% Trypsin-EDTA solution for 5 minutes at 31 °C to collect the cell pellet for splitting into new T75 flasks or seeding onto back-side of the fibronectin-coated membranes in microfluidic devices or conventional transwells at a seeding density of 100 cells/mm^2.

5.2.4 Assessment of Viability of b.End3 and Pericyte Cells

Endothelial b.End3 cells, mouse pericytes, and mouse astrocytes were cultured in layered microfluidic channels were stained using the live/dead cytotoxicity kit (Life

Technologies Corporation, Carlsbad, CA) following manufacturer's protocol. Briefly, 1 μL calcein AM and 1 μL ethidium homodimer-1 were added to 1 mL of the culture medium before adding 16 μL of this mixture to b.End3 cells cultured in the top channel and incubating for 20 minutes at 37 ºC under normal culture conditions. Live b.End3 cells and pericytes were stained green while dead cells were stained red and both were visualized using a fluorescent microscope (Nikon, New York, NY) at 500 nm and 600 nm, respectively. Number of live and dead b.End3 cells observed at the inlet, center, and outlet of the top microfluidic channel was counted in the fluorescent images captured at a 10X magnification. The angle between cultured b.End3 cells and the longitudinal (X) axis of the top channel in captured fluorescent images (10X magnification) was measured using Photoshop CS4 (Adobe, San Jose, CA) to determine the change in cell alignment as a function of culture time. Similarly, we measured the shape index of cultured b.End3 cells using ImageJ 1.44p software (NIH, Washington D.C.). The variance of the angle measurements is then calculated using equation (2) where sigma^2 is the variance, N is the number of data points, xi is each specific data point, and u is the mean:

5.2.5 Trans-Endothelial Electrical Resistance across b.End3 Cell Monolayers

Trans-endothelial electrical resistance (TEER) of confluent b.End3 cell monolayers cultured onto conventional transwells was measured using standard chopstick electrodes (World Precision Instruments, Sarasota, FL) while accounting for the intrinsic resistance of blank filters. Resistance across b.End3 monolayers cultured in layered microfluidic channels were measured on daily basis following our published protocol.[12] Briefly,

impedance spectra are taken using an Autolab potentiostat/galvanostat at 0.1 V of alternating current passing between the two embedded electrodes within layered microfluidic channels. Frequency range between 10 Hz to 1.00 MHz was used to yield a total of 64 impedance measurements. The control impedance spectra measured before seeding the cells were subtracted from the measured impedance spectra with b.End3 cells to eliminate their contribution to the calculated resistance. We developed a MATLAB code (The MathWorks Inc., Natick, MA) using its optimization toolbox to resolve the TEER values, which were normalized to the surface area of the cell monolayers to calculate the resistance in $\Omega.cm^2$.

5.2.6 Paracellular Permeability across b.End3 Cell Monolayers

We investigated the transport of a paracellular permeability marker [14C]-mannitol (182 Da) across b.End3 and pericyte co-culture layer in layered microfluidic channels for 3, 6, 9, 12, 15, 18, and 21 days. Pericytes were seeded first on the reverse side of the porous polyester membranes with average pore size of 400 nm; b.End3 cells were then seeded 12 hours onto the fibronectin coated side of the same membrane under normal culture conditions. The culture medium was removed from the apical (top) and basolateral (bottom) compartments before washing the b.End3 monolayers twice with PBS solution prior to starting the transport study. PBS solution in the apical compartment was replaced with marker solution before incubating in the microfluidic devices at 37 °C, 95% relative humidity, and 5% CO_2 while shaking at transwells and layered microfluidic devices were

then placed on an orbital shaker spinning at 100 rpm inside an incubator under normal culture conditions for 60 minutes.

The PBS solution in the receiver compartment in layered microfluidic channels and transwells were collected and replaced with fresh PBS every 10 minutes. At the end of the 1 hour incubation time, PBS solutions in both the donor and receiver compartments were collected. All the collected PBS solutions were mixed with liquid scintillation fluid (GMI Inc., Ramsey, MN) and assayed using a liquid scintillation counter (GMI Inc., Ramsey, MN) to determine the concentration of each marker using a standard calibration curve.

The permeability of a given molecule across the monolayer was calculated by using a derived form of a differential equation based on Fick's Law:

$$P = \frac{V_{basolateral} \times \frac{\Delta C_{basolateral}}{\Delta t}}{A \times C_{apical}}$$ ---------- Equation 1

Note that the transfer of solutes from the apical to the basolateral side is not concentration dependent, and only varies as a function of time. The unit of measurement cm/s for permeability coefficient is commonly used.

5.2.7 Assessment of Functional P-glycoprotein in b.End3 Cell Monolayers

Functional expression of P-glycoprotein (P-gp) efflux pump by b.End3 and pericyte cells cultured in layered microfluidic channels was investigated by measuring the apical-to-basolateral (AB) permeability and basolateral-to-apical (BA) permeability of [3H]-Dexamethasone, which is a substrate for the P-gp efflux pump. Before starting the transport experiment, the culture medium in the apical and basolateral compartments in the

transwells and channels were replaced with fresh PBS at 37 °C for washing twice the cell monolayer. PBS solutions were then aspirated and replaced by [3H]-Dexamethasone at the apical (top) compartment for half of the total number of channels and transwells. The other half of channels and transwells were filled at the basolateral (bottom) compartment with the radioactively labeled marker. All other experimental conditions and solution retrieval procedures are the same as the paracellular permeability.

In addition to the apical-to-basolateral permeability, basolateral-to-apical permeability was also evaluated by putting the radioactively labeled solution in the bottom compartment, and collecting the PBS solutions from the top compartment. Efflux ratio was calculated by using basolateral-to-apical permeability divided by the apical-to-basolateral permeability. If P-glycoprotein functionality was present, the efflux ratio should be higher than 1.

5.3 RESULTS

5.3.1 Endothelial Cell Viability and Morphology

The design of our microfluidic device incorporates two layered microfluidic channels that sandwich a polyester membrane (0.4μm pore size) along the entire length of the channel, which was used to culture b.End3 cells in the top compartment. For bi-culture experiments where b.End3 cells and pericytes were used, pericytes were cultured on the back-side of the porous membrane in order to allow endothelial-pericyte contact to enhance barrier properties; for tri-culture experiments, an additional cell type - astrocytes were

cultured in the bottom compartment of the device **(Figure 5.1)**. The device incorporates a cross section between the top and bottom channels to allow measurement of solute's permeability across cell monolayers while maintaining an elongated geometric shape and small dimensions. The elongated rectangular shaped channel serves to guide endothelial cell growth, which has been shown to enhance endothelial cell growth and differentiation. The small dimensions of the channel increase the surface to volume ratio, which results in concentration of the factors secreted by different cell types and decreases the volume of the markers' solution needed for permeability studies at the same time. Our device also allows the incorporation of Ag/AgCl electrodes in both the top and bottom channels which allow real-time measurement of TEER that indicates cell monolayer integrity.

(A)

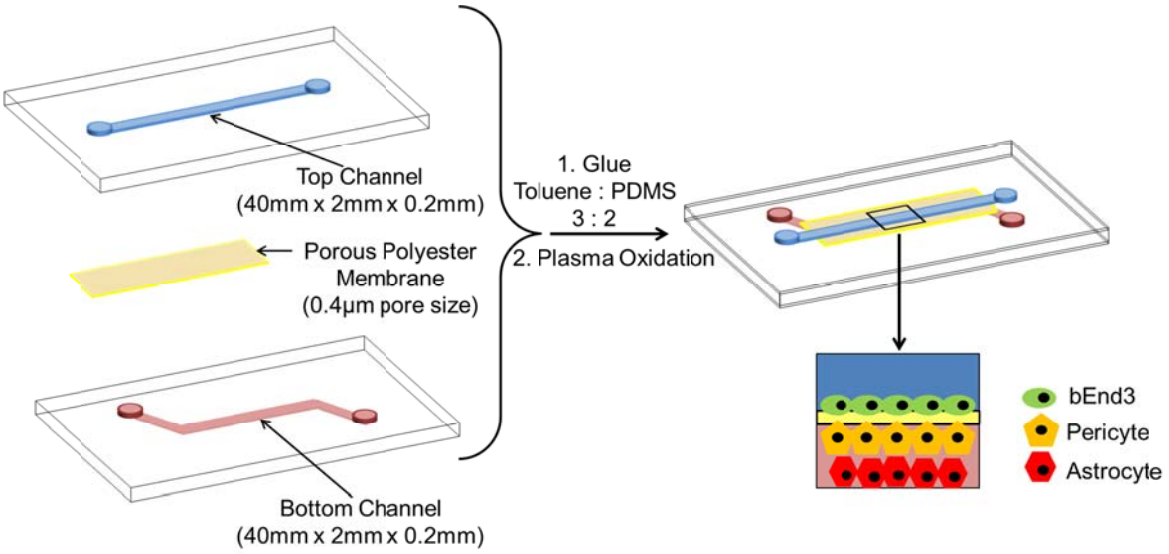

(B)

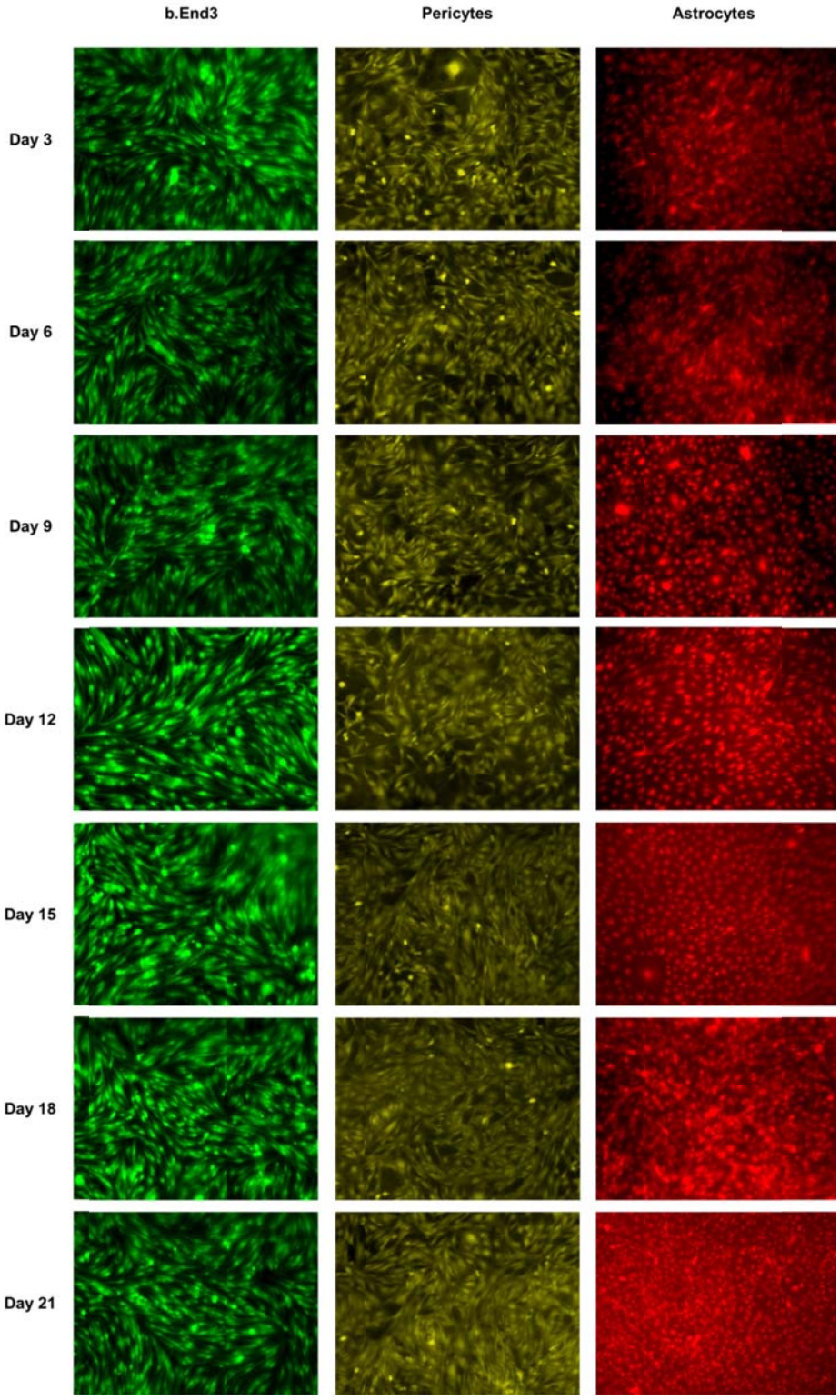
b.End3
Pericytes
Astrocytes
Day 3
Day 6
Day 9
Day 12
Day 15
Day 18
Day 21

Figure 5.1: (A) The schematic drawing of layered PDMS channel configuration with fluorescent images of b.End3, pericyte and astrocyte cells cultured in these channels (40mm x 2mm x 0.2mm) sandwiching polyester membrane filter (400 nm pore size). **(B)** b.End3, pericytes, and astrocytes stained with Live/Dead assay (Live/Dead Viability/Cytotoxicity Kit for mammalian cells, Invitrogen, Carlsbad, California) at different culture time points at 10X magnification.

Fluorescent images demonstrate the feasibility of culturing b.End3 cells with pericytes and astrocytes in layered configurations and formation of stable 3D cell layers for 21 days **(Figure 5.2A)**. Our results show that the number of viable b.End3 cells significantly increased from 499 cells/mm^2 after 3 days in culture to 627 cells/mm^2 after 6 days and remained constant up to 21 days; while pericytes increased steadily from 295 cells/mm2 after 3 days in culture to 444 cells/mm2 after 21 days for the bi-culture configuration and astrocytes also increased from 283 cells/mm2 after 3 days in culture to 369 cells/mm2 after 21 days for the tri-culture configuration. These cell numbers after 6 days indicate stable culture configurations for both of our bi-culture and tri-culture systems.

We measured the angle (θ) between the spindle of b.End3 cells and the longitudinal axis of the microfluidic channels as a function of days in culture for both the bi- and tri-culture systems. Fluorescent images of b.End3 cells show a 42°-43° angle between b.End3 cells and the longitudinal axis of the microfluidic channels after 3 days in culture, which indicates a random organization of the cultured cells at early time points for both the bi- and tri-culture configurations **(Figure 5.2B)**. However, this angle gradually decreased as a function of culture time reaching 25° and 21° after 21 days for the bi- and tri-culture configurations, respectively, which indicates gradual alignment of b.End3 cells along the length of the microfluidic channel. There is no significant difference of angle alignment

between bi- and tri-culture configurations. The variance (σ^2) in angle measurement showed a steady decline in spindle angle for b.End3 cells cultured in microfluidic channels, which further confirms the alignment of b.End3 cells along the length of the channel **(Figure 5.2C)**. Again, no significant difference was found between the bi- and tri-culture systems indicating that pericytes and astrocytes play very little role in the alignment of endothelial cells in our systems. However, these results are in agreement with earlier reports showing the change in organization and morphology of endothelial cells when cultured in microfluidic devices, which is induced by channels' shape and size [13-18].

(A)

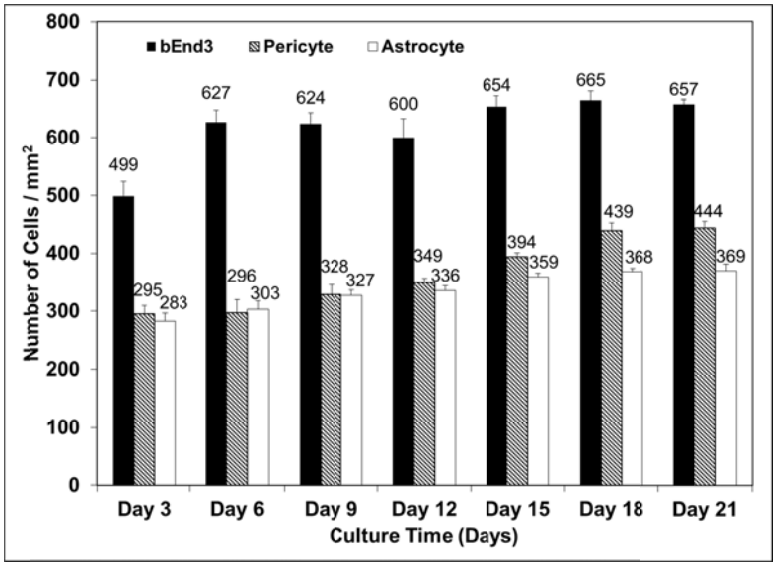

(B)

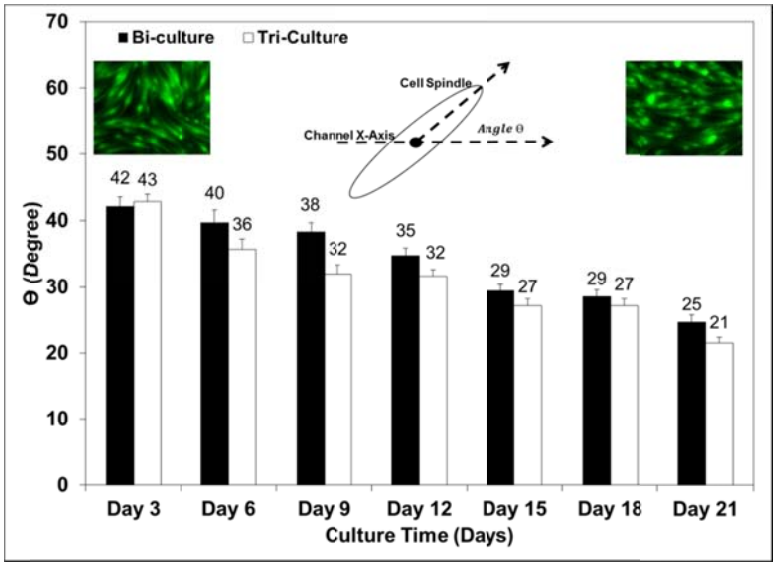

(C)

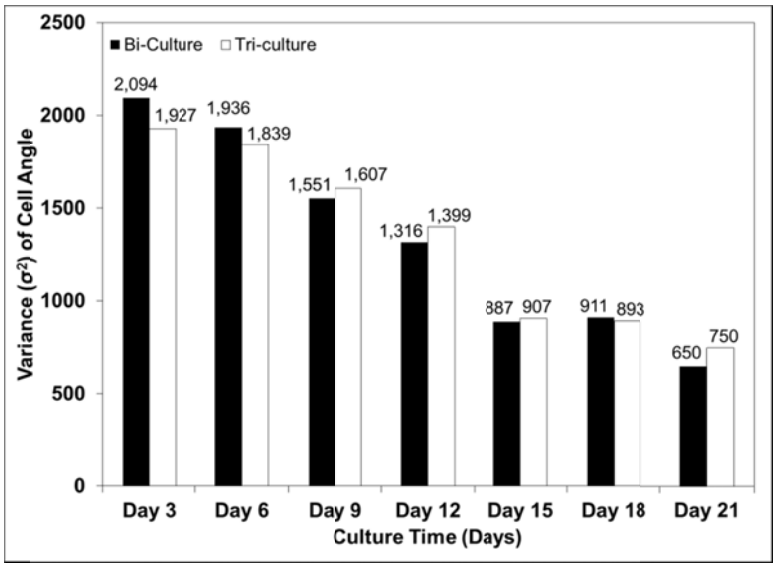

Figure 5.2: (A) Cell counts of confluent bEnd3 monolayers at 10X magnification (1.17mm x 0.88 mm field view) as a function of culture time points (days). **(B)** Angle measurements along the direction of flow of confluent bEnd3 monolayers at 10X magnification as a function of culture time points (days). **(C)** The variances of the angle measurements along the direction of flow of confluent bEnd3 monolayers at 10X magnification as a function of culture time points (days).

5.3.2 TEER of b.End3 Single Culture, b.End3-Pericyte Bi-Culture, and b.End3-Pericyte-Astrocyte Tri-Culture

TEER values were measured using embedded Ag/AgCl electrodes in both the top and bottom PDMS layers of the microfluidic channels **(Figure 5.3A)** [12]. TEER values were resolved by modeling the internal resistance of a cell and the capacitance of the cell membrane in series. Baseline TEER measurements across porous polyester membranes without seeding b.End3 cells were similar in layered microfluidic devices and transwells at different days in culture, which indicates that the layout of the device and composition of the culture medium (e.g. FBS serum) did not affect the calculated TEER values.

Our results indicate that TEER across b.End3 single culture in microfluidic channels gradually increased from 28 Ohms.cm^2 after seeding to 84, 125, and 143 Ohms.cm^2 on days 1, 2, and 3, respectively **(Figure 5.3B)**. The b.End3 monolayers established in microfluidic channels maintained an average TEER of ~140 Ohms.cm^2 between days 3 and 21 in culture. In comparison, b.End3-pericyte bi-culture configuration exhibited similar TEER value directly after seeding at 26 Ohms.cm^2 and gradually increased to 257 Ohms.cm^2 after 3 days in culture and maintained similar values through 21 days. Bi-culture TEER values were 1.8-fold higher than that of the single culture which indicates viability and higher integrity of the formed barrier throughout the culture time **(Figure 5.3B)**. Similarly, b.End3-pericyte-astrocyte tri-culture configuration exhibited similar values directly after seeding; however, after 3 days in culture, it increased even further and averaged to ~300 Ohms.cm2, 1.2-fold higher than the bi-culture configuration. Our results indicate that

pericyte plays a significant role in enhancing the "tightness" of the tight junctions in endothelial cells and astrocytes has the ability to enhance it even further.

(A)

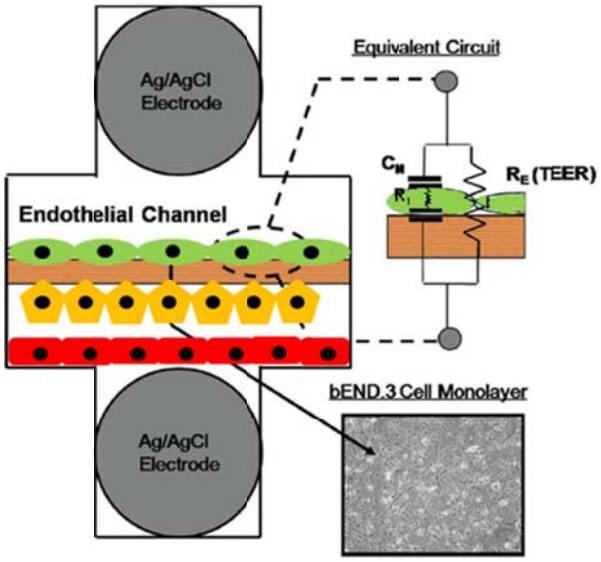

(B)

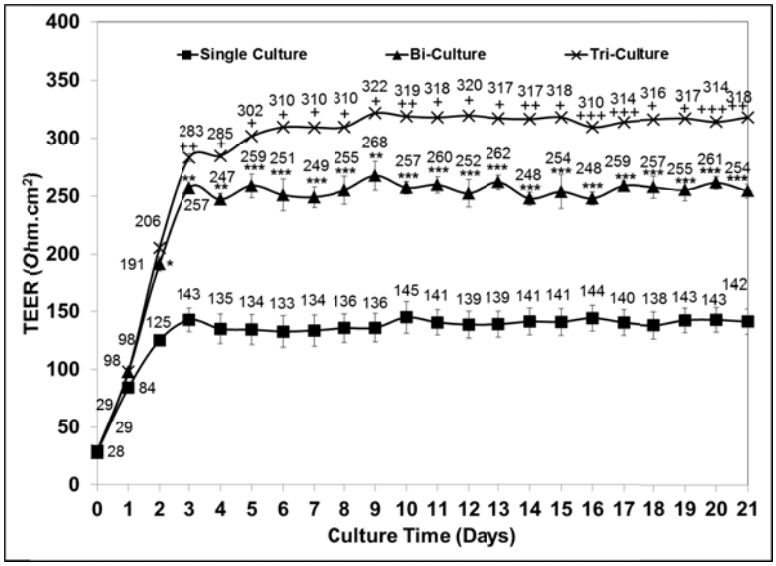

Figure 5.3: (A) Schematic drawing of electrodes implemented into layered microfluidic channels. **(B)** Comparison of TEER measurements of confluent bEnd3 monolayers cultured among single culture in layered microfluidic devices, bi-culture with pericytes, and tri-

culture with pericytes and astrocytes in layered microfluidic devices as a function of time points (days). (*: $p<0.05$; **: $p<0.01$; ***: $p<0.005$); (+: $p<0.05$; ++: $p<0.01$; +++: $p<0.005$)

5.3.3 Assessment of Paracellular Permeability Across b.End3 Cell Monolayers

We investigated the transport of standard paracellular permeability markers [14C]-mannitol and [14C]-urea across b.End3 cell monolayers cultured in layered microfluidic channels with bi- and tri-culture configurations. Our results show that permeability of [14C]-mannitol across b.End3 cell monolayers cultured in the bi-culture configuration was 1.0×10^{-6} cm/s at day 3 and day 6, it decreased by 2-fold to 0.5×10^{-6} cm/s after 9 days in culture and remained constant for the rest of the 21-day culture period **(Figure 5.4A)**. Permeability of [14C]-mannitol across b.End3 cell monolayers cultured in the tri-culture configuration demonstrated even lower permeability. At day 3 and day 6, the permeability is measured at $\sim 0.6 \times 10^{-6}$ cm/s and it decreased further to $\sim 0.3 \times 10^{-6}$ cm/s after 9 days in culture and remained constant for up to 21 days **(Figure 5.4A)**. For b.End3 single culture in the microfluidic device, the permeability value was measured at 31.8×10^{-6} cm/s; it gradually decreased with increase in culture time to 13.8×10^{-6} cm/s at day 6 and $\sim 3 \times 10^{-6}$ cm/s after 9 days in culture **(Figure 5.4A)**. The 6-fold decrease of [14C]-mannitol permeability from single culture to bi-culture indicates that pericytes play a critical role in the formation and development of "restrictive" transport properties in our microfluidic device. Further decrease of permeability values from bi-culture to tri-culture (1.7-fold) indicates that astrocytes also play an important role in the formation of a "restrictive" barrier.

Results show similar trends in permeability of [14C]-urea across bi- and tri-culture configurations. After 3 days in culture, the permeability was measured at 1.4 x 10^{-6} cm/s and 1.2 x 10^{-6} cm/s; and 1.6 x 10^{-6} cm/s and 1.4 x 10^{-6} cm/s after 6 days, respectively **(Figure 5.4B)**. However, after 9 days in culture, the permeability decreased to 1.1 x 10^{-6} cm/s and 1 x 10^{-6} cm/s for the bi- and tri-culture, respectively, and stayed constant through the 21-day culture **(Figure 5.4B)**. The permeability profiles of [14C]-mannitol and [14C]-urea across the bi- and tri-culture systems indicate the development of a stable and "restrictive" barrier after 9 days in culture and both pericytes and astrocytes play important roles in its development. It is also important to note that both the bi- and tri-culture configurations can be maintained by 21 days and the difference between permeability of [14C]-mannitol and [14C]-urea with respect to the bi- and tri-culture configurations indicate a discrimination between small molecules. This size selectivity towards paracellular markers indicates the formation of tight junction complexes between adjacent endothelial cells in our systems, which is a key characteristic of the BBB *in vivo* [2, 7].

(A)

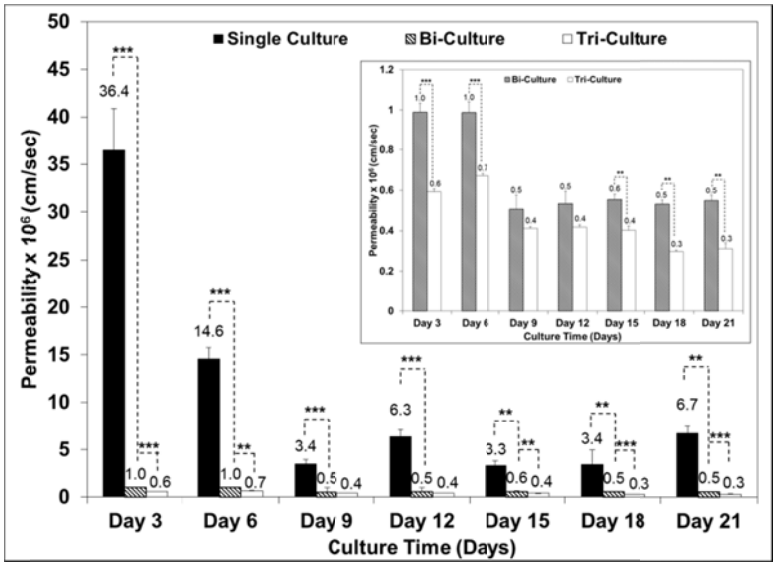
Single Culture
Bi-Culture
Tri-Culture
Permeability x 10⁶ (cm/sec)
Culture Time (Days)
Day 3
Day 6
Day 9
Day 12
Day 15
Day 18
Day 21
36.4
1.0
0.6
14.6
1.0
0.7
3.4
0.5
0.4
6.3
0.5
0.4
3.3
0.6
0.4
3.4
0.5
0.3
6.7
0.5
0.3

(B)

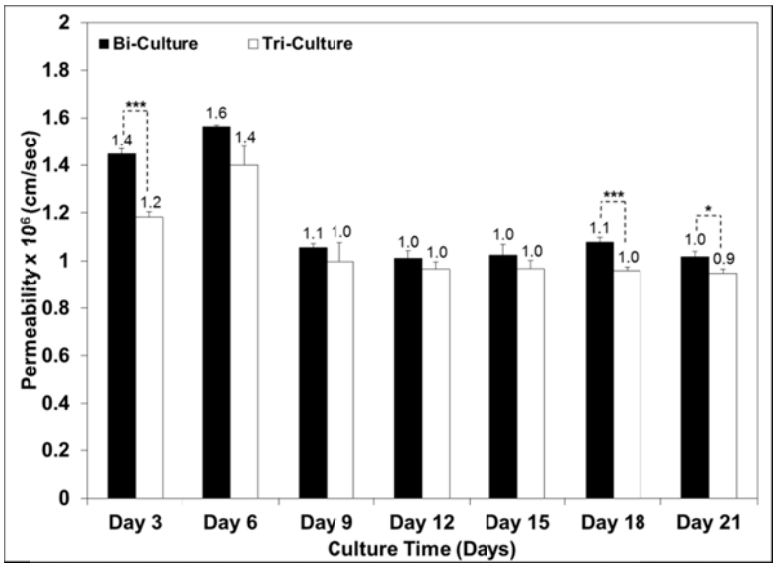
Bi-Culture
Tri-Culture
Permeability x 10⁶ (cm/sec)
Culture Time (Days)
Day 3
Day 6
Day 9
Day 12
Day 15
Day 18
Day 21
1.4
1.2
1.6
1.4
1.1
1.0
1.0
1.0
1.0
1.0
1.1
1.0
1.0
0.9

(C)

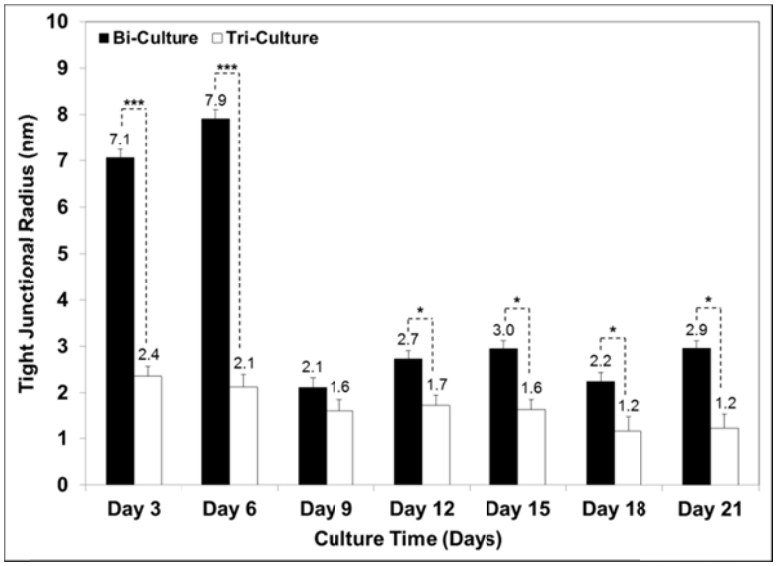

Figure 5.4: (A) Comparison between paracellular permeability of [14C]-mannitol through confluent bEnd3 monolayers with single culture, bi-cultured with pericyte, and tri-cultured with pericyte and astrocyte conditions in layered microfluidic devices as a function of culture time points (days). (*: $p<0.05$, **: $p<0.01$, ***: $p<0.005$) **(B)** Comparison between paracellular permeability of [14C]-urea through confluent bEnd3 monolayers with bi-cultured with pericyte and tri-cultured with pericyte and astrocyte conditions in layered microfluidic devices as a function of culture time points (days). (*: $p<0.05$, **: $p<0.01$, ***: $p<0.005$) **(C)** Renkin function calculation based on [14C]-mannitol and [14C]-urea permeability through confluent bEnd3 monolayers bi-cultured with pericytes and tri-cultured with percityes and astrocytes in layered microfluidic devices as a function of culture time points (days). **(*: $p<0.05$, **: $p<0.01$, ***: $p<0.005$)**

5.3.4 Porosity of Bi- and Tri-Culture Systems

The observed permeability of [14C]-mannitol and [14C]-urea across the bi- and tri-culture configurations in microfluidic channels indicate the formation of "restrictive" barriers and both pericytes and astrocytes play important roles in its development. By modeling the intercellular space between adjacent endothelial cells, we were able to calculate the radius (R) of the pores of the tight junctions using the Renkin function:

$$F\left(\frac{r}{R}\right) = (1 - \frac{r}{R})^2[1 - 2.104\left(\frac{r}{R}\right) + 2.09\left(\frac{r}{R}\right)^3 - 0.95\left(\frac{r}{R}\right)^5]$$ ---------- Equation 2

Where the Renkin function $F(\frac{r}{R})$ describes the relationship between the radius of the molecule (r) and the pore radius of the tight junction (R).

The following equation provides a relationship between the permeability (P) and the Renkin function.

$$P = \frac{\epsilon D F(\frac{r}{R})}{\delta}$$ ---------- Equation 3

where ϵ is the porosity of the b.End3 monolayer, D is the diffusion coefficient of the evaluated marker molecule, and δ is the distance traversed by the marker molecule down a concentration gradient. We used the diffusion coefficients (D) of mannitol (9.65 x 10-6 cm/s) and urea (13.8 x 10-6 cm/s) with our permeability results to solve the equation for the Renkin function and $\frac{\epsilon}{\delta}$ at different days in culture. We used Matlab R2009a to solve the polynomial equation and obtained R assuming that the radii (r) of mannitol and urea are 0.34nm [19] and 0.26nm [19, 20], respectively.

Our calculations show that the average radius of the tight junction pores (R) for the bi-culture configuration drops from 7.1nm and 7.9nm at day 3 and day 6, respectively, to 2.1nm at day 9 and is maintained constantly until day 21. In comparison, the calculated radius of the tight junction pores (R) for the tri-culture configuration drops from 2.4nm at day 3 to 2.1nm at day 6, it drops even further to 1.6nm at day 9 and is maintained until day 15 in culture. At day 18 and day 21, our data shows that the radius of the tight junction pore (R) decreases even further to 1.2nm **(Figure 5.4C)**. The lower porosity established in the tri-culture configuration compared to the bi-culture reinforces the idea that astrocytes play a

significant role in the development of "restrictive" tight junctions in the b.End3 cell layer. Since the astrocytes were seeded at the bottom layer of the channels and had no direct contact with the b.End3-pericyte layers, it can be concluded that astrocytes act through the secretion of neurotrophic factors that have the ability to influence barrier formation at the BBB [2, 5, 6].

5.3.5 Effect of Bottom Channel Height on Barrier Properties of the Tri-Culture Configuration

Based on our permeability data and calculations of the radius (R) of tight junction pores, we concluded that astrocytes act on the barrier properties through secreted neurotrophic factors. It has shown that with astrocytes in the system, the permeability of both [14C]-mannitol and [14C]-urea were lowered which indicates more "restrictive" tight junction formation; the TEER values were increased which indicates "tighter" barrier. Therefore, we hypothesized that by controlling the height of the bottom channel where the astrocytes are seeded and grown, it will affect the barrier properties of the b.End3 cells growing in the top channel through TEER measurements and permeability. To further validate the role of the astrocytes, we fabricated layered microfluidic channels that are 0.6mm and 1mm high in the bottom channel while keeping the top channel dimensions the same.

Our results show that increasing the bottom channel's height to 0.6mm decreased the TEER measurements by ~20 Ohms.cm^2 after 3 days in culture. Increasing the height to 1mm decreased the TEER measurements even further by another ~20 Ohms.cm^2 after 3

days **(Figure 5.5A)**. The incremental decline in TEER measurements that we observed with our tri-culture configuration using different height for the bottom channel where astrocytes are cultured show that distance between the astrocytes and b.End3 cells make a difference in the development of endothelial barrier properties despite identical seeding density and culture conditions. This effect demonstrates that by increasing the distance needed for the neurotrophic factors to traverse and increasing the overall volume of the bottom channel resulting in dilution of these factors, we are able to manipulate the barrier properties of the b.End3 layers.

We also investigated the permeability of [14C]-mannitol across the bi- and tri-culture configurations with modified height of 0.6mm and 1mm for the bottom channels. Specifically our data shows that with 1mm height for the bottom channel, the permeability of [14C]-mannitol in the tri-culture configuration with astrocytes shows little difference from the bi-culture configuration without astrocytes. This indicates that at a large distance and channel volume, the astrocytes are ineffective at promoting the formation of "restrictive" tight junctions. With 0.6mm height for the bottom channel, the permeability of [14C]-mannitol decreased from ~0.53 x 10^{-6} cm/s to ~0.43 x 10^{-6} cm/s at day 9, 12, 15, 18, and 21 days in culture **(Figure 5.5B)**. When we compare 0.6mm height channels with 0.2mm height channels, we found that the permeability of [14C]-mannitol decreased even further to 0.3 x 10^{-6} cm/s at the end of 21-day culture. Similar to the TEER measurements, we found incremental decline in the permeability of [14C]-mannitol which further confirms that distance between the astrocytes and b.End3 cells and dilution of these neurotrophic factors play a critical role in the effectiveness of the astrocytes in affecting the barrier

properties of the b.End3 layers: the shorter the distance and the smaller the volume, the more effective the astrocytes are.

(A)

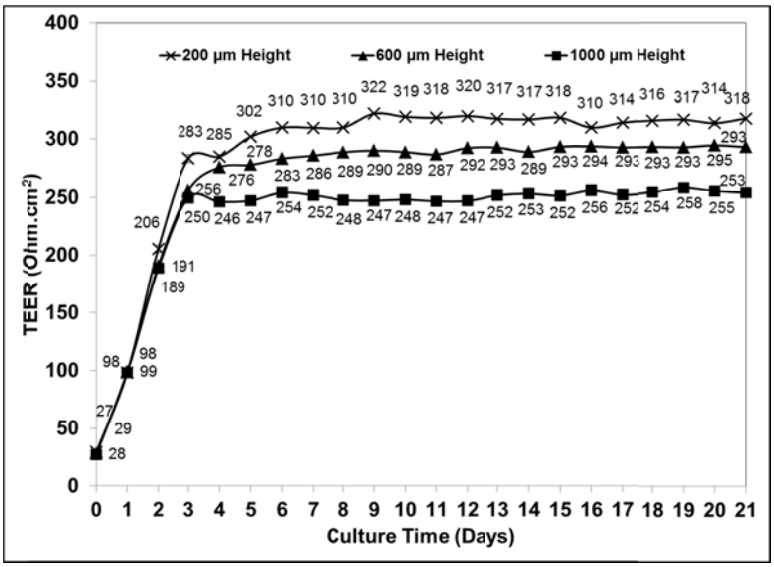

(B)

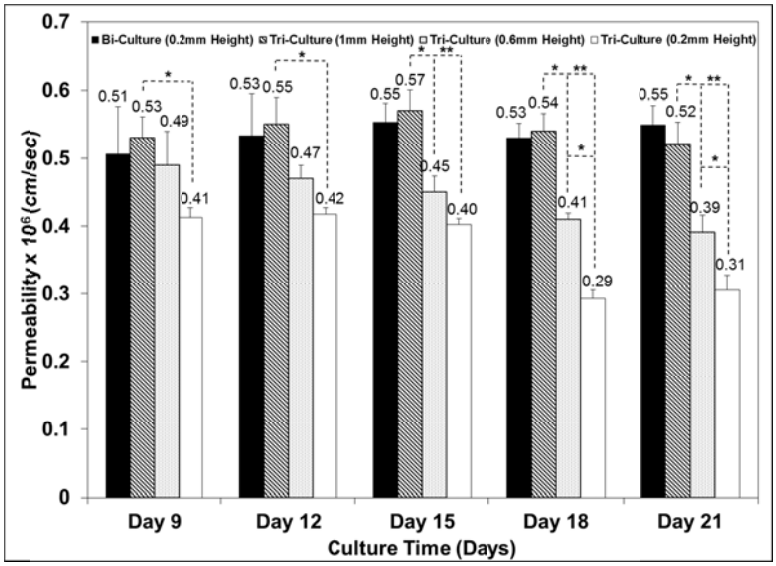

Figure 5.5: (A) Comparison of TEER measurements of confluent bEnd3 monolayers cultured in tri-culture in layered microfluidic devices with modified height of the bottom channel at 0.2mm, 0.6mm, and 1mm as a function of time points (days). (*: $p<0.05$; **: $p<0.01$; ***: $p<0.005$); (+: $p<0.05$; ++: $p<0.01$; +++: $p<0.005$) **(B)** Comparison between

paracellular permeability of [14C]-mannitol through confluent bEnd3 monolayers with tri-culture configuration in layered microfluidic devices with modified height of the bottom channel at 0.2mm, 0.6mm, and 1mm as a function of time points (days). (*: $p<0.05$; **: $p<0.01$; ***: $p<0.005$); (+: $p<0.05$; ++: $p<0.01$; +++: $p<0.005$)

5.3.6 Functional Expression of P-glycoprotein by the Bi- and Tri-Culture Systems

We measured the apical-to-basolateral (AB) and basoalteral-to-apical (BA) permeability of [3H]-Dexamethasone, which is a substrate for the P-gp efflux pump across the bi- and tri-culture configurations with regular 0.2mm height at the bottom channels. Functional expression of the P-gp on the apical side of b.End3 cells would decrease the AB permeability of dexamethasone and increase the BA permeability. Therefore, we calculated the Efflux Ratio (ER) across b.End3 cell layers using the following equation.

$$ER = \frac{Permeability_{BA}}{Permeability_{AB}}$$ ---------- Equation 4

Results show that both bi- and tri-culture configurations exhibit high BA permeability of [3H]-dexamethasone relative to its respective AB permeability **(Figure 5.6A)**. For the bi-culture configuration, the Efflux Ratio was 1.2 at day 3 and gradually increased to 2.5 at the end of the 21-day culture period. For the tri-culture configuration, the Efflux Ratio was 1.6 at day 3 and gradually increased to 4.8 at the end of 21-day **(Figure 5.6B)**. The data indicates that both the bi- and tri-culture configurations are capable of inducing the functionality of P-gp pumps; however, as a function of days in culture, the tri-culture configuration is significantly more effective at inducing P-gp activities which is another key characteristic of the BBB.

(A)

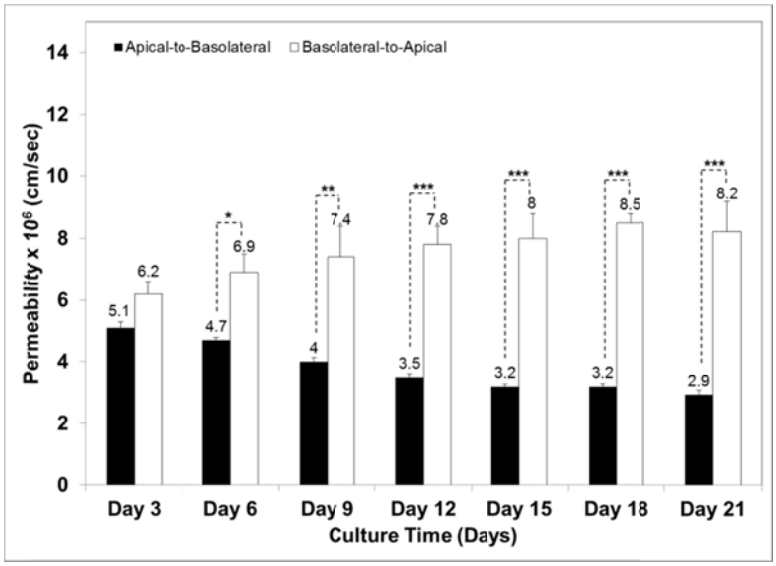
Apical-to-Basolateral
Basclateral-to-Apical
Permeability x 10⁶ (cm/sec)
14
12
10
8
6
4
2
0
5.1
6.2
4.7
6.9
4
7.4
3.5
7.8
3.2
8
3.2
8.5
2.9
8.2
*
**
***
Day 3
Day 6
Day 9
Day 12
Day 15
Day 18
Day 21
Culture Time (Days)

(B)

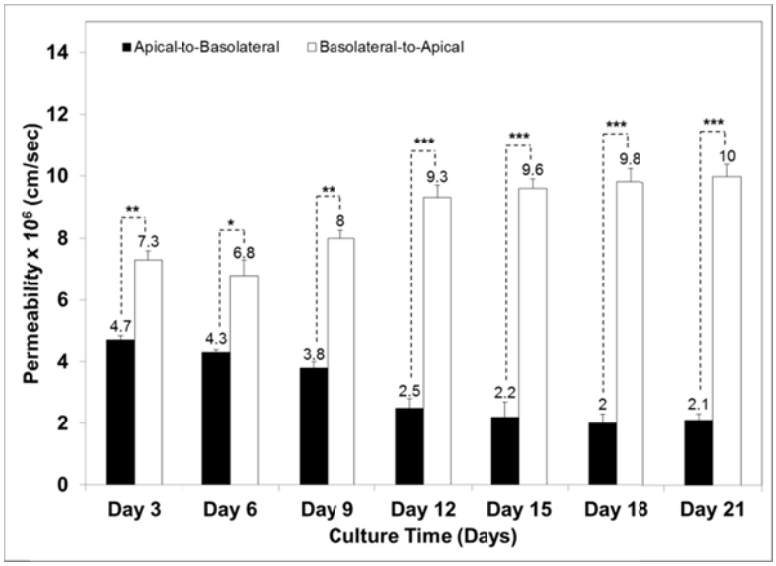
Apical-to-Basolateral
Basolateral-to-Apical
Permeability x 10⁶ (cm/sec)
14
12
10
8
6
4
2
0
4.7
7.3
4.3
6.8
3.8
8
2.5
9.3
2.2
9.6
2
9.8
2.1
10
*
**
***
Day 3
Day 6
Day 9
Day 12
Day 15
Day 18
Day 21
Culture Time (Days)

(C)

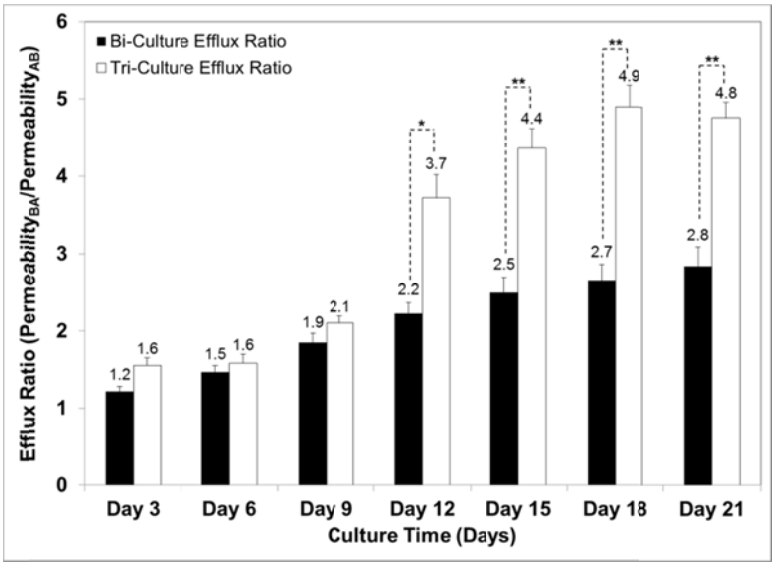

Figure 5.6: (A) Comparison between permeability of [3H]-dexamethasone through confluent bEnd3 monolayers bi-cultured with pericytes inside layered microfluidic devices from apical-to-basolateral and basolateral-to-apical as a function of culture time points (days). **(*: p<0.05, **: p<0.01, ***: p<0.005) (B)** Comparison between permeability of [3H]-dexamethasone through confluent bEnd3 monolayers tri-cultured with pericytes and astrocytes inside layered microfluidic devices from apical-to-basolateral and basolateral-to-apical as a function of culture time points (days). **(*: p<0.05, **: p<0.01, ***: p<0.005) (C)** Comparison between the efflux ratios (permeability$_{BA}$/permeability$_{AB}$) of confluent bEnd3 bi-culture and tri-cultured inside layered microfluidic channels as a function of culture time points (days).

5.4 DISCUSSION

It has long been acknowledged that both pericytes [21] and astrocytes [5] play very important roles in the differentiation and development of brain endothelial cells. Pericytes, in particular, partially surround the brain capillaries at endothelial tight junctions, and are usually found between endothelial cells and astrocyte end-feet. This strategic position allows pericytes to interact with both the endothelial cells and the astrocytes [22, 23].

Previous researches have suggested that pericytes, based on their morphology and localization, play important roles in endothelial cell function and modulation of blood flow, and they make direct contact with endothelial cells through gap and adherens junctions [22, 24, 25]. It is also important to note that at the BBB the ratio of pericytes to endothelial is one of the highest in any organ [26]. Furthermore, there are evidences in the literature that suggest pericytes are capable of secreting signaling molecules that are essential to the differentiation and contractile properties of endothelial cells [27-29]. Astrocytes, too, have been found to secrete a range of neurotrophic factors such as transforming growth factor-β (TGFβ) [5], glial-derived neurotrophic factor (GDNF) [30], and basic fibroblast growth factor (bFGF) [5]. It has been found that these factors can induce many aspects of the BBB phenotype in endothelial cells *in vitro* [2, 5, 7]. At the same time, endothelial-derived factor such as leukaemia inhibitory factor (LIF) has been documented to induce the differentiation of astrocytes [31]. The cross-interaction between endothelial cells and astrocytes are mutually beneficial and ensures the differentiation of both BBB and astrocytic development.

Based on the importance of pericytes and astrocytes on endothelial differentiation, we designed our bi- and tri-culture configurations to examine the feasibility of culturing b.End3 cells together with pericytes and astrocytes and whether these co-culture configurations can induce BBB-like transport properties. For our bi-culture configuration, our goal was to mimic the close promixity of endothelial cells and the pericytes; therefore we cultured pericytes on the back-side of the semi-porous membrane, where the endothelial cells were growing on, in the microfluidic devices. This configuration ensures that b.End3 cells and pericytes are in close contact with each other in the condition that is similar to the

conditions *in vivo*. Our results demonstrated that pericytes can in fact improve the barrier properties of b.End3 layers through TEER measurements, permeability of paracellular markers such as mannitol and urea, and porosity calculations. For our tri-culture configuration, we added astrocytes to the bottom layer of the channels. While the astrocytes are not in direct contact with the endothelial-pericyte layers, the secreted neurotrophic factors that are so critical to the BBB development still reaches the b.End3 cells through diffusion; again, creating a similar condition to the *in vivo* conditions. Our results of the tri-culture configuration show even further enhancement of the barrier properties compared to the bi-culture configuration. It is worth mentioning that when we compare our [14C]-mannitol permeability value at the end of 21 days in culture, which is 0.3 x 10^{-6} cm/s, it is very close to the *in vivo* permeability value of 0.2 x 10^{-6} cm/s [2, 32]. Similarly, our porosity calculations show the lowest tight junction radius in our tri-culture configuration to be 1.2nm, where the *in vivo* value is measured to be 0.8nm [33]. Our results indicate that by culturing b.End3 cells together with pericytes and astrocytes according to the tri-culture configuration in microfluidic devices can induce BBB transport properties very similar to the *in vivo* data.

To further validate the effects of astrocytes on endothelial-pericyte layers, we modified our original device and changed the height of the bottom channel from 0.2mm to 0.6mm and 1mm. The purpose of modifying the bottom channel is to increase the distance between the astrocytes and the endothelial-pericyte layers and increase the volume of the bottom channel in order to subject the secreted neurotrophic factors to dilution. Through TEER measurements and permeability values, we were able to clearly demonstrate that

when astrocytes are far apart from the endothelial-pericyte layers, in this instance 1mm, astrocytes have little effect on the barrier properties of b.End3 cells. This conclusion is based on the fact that [14C]-mannitol permeability shows no statistical difference between the bi-culture configuration and the tri-culture configuration utilizing 1mm height in the bottom channel. The incremental decline of TEER measurements from using 0.2mm channel to 0.6mm channel to 1mm channel also demonstrates that as astrocytes are removed farther and farther away from the endothelial-pericyte layers, its effect is diminished as a function of bottom channel height. These results clearly indicate that close proximity of astrocytes with the endothelial-pericyte layers is required to induce proper BBB characteristics within the microfluidic devices.

Finally, we demonstrated the ability of the bi- and tri-culture configurations to induce P-gp pumps by measuring the AB and BA permeability using [3H]-dexmathasone. The calculated Efflux Ratio based on permeability shows highly functional P-gp by cultured cells starting on day 15 and is maintained until day 21.

5.5 CONCLUSION

We report the successful culture of brain endothelial cells (b.End3) with pericytes in a bi-culture configuration and astrocytes with b.End3-pericyte layers in a tri-culture configuration forming a viable 3D model of the blood-brain barrier that exhibits restrictive transport properties indicated by high TEER values and low [14C]-mannitol and [14C]-urea permeability. In addition, these bi- and tri-culture configurations exhibited high P-gp functionality through the calculation of Efflux Ratio. All of the results lead us to believe

that we have created an accurate model of the BBB *in vitro* that can be utilized for drug screening and research purposes.

REFERENCES

1. Rubin, L.L. and J.M. Staddon, *The Cell Biology of the Blood-Brain Barrier.* Annual Review of Neuroscience, 1999. **22**: p. 11-28.
2. Dermietzel, R., D.C. Spray, and M. Nedergaard, *Blood-Brain Barrier: From Ontogeny to Artificial Interfaces*. Vol. 1. 2006, Weinheim, Germany: WILEY-VCH.
3. Persidsky, Y., et al., *Blood-Brain Barrier: Structural Components and Function Under Physiologic and Pathologic Conditions.* Journal of Neuroimmune Pharmacology, 2006. **1**(3): p. 223-236.
4. Deli, M.A., et al., *Permeability Studies on In Vitro Blood-Brain Barrier Models: Physiology, Pathology, and Pharmacology.* Cellular and Molecular Neurobiology, 2004. **25**(1): p. 59-127.
5. Abbott, N.J., L. Ronnback, and E. Hansson, *Astrocyte-endothelial interactions at the blood-brain barrier.* Nature Reviews Neuroscience, 2006. **7**: p. 41-53.
6. Abbott, N.J., *Astrocyte-endothelial interactions and blood-brain barrier permeability.* Journal of Anatomy, 2002. **200**(6): p. 629-638.
7. Pardridge, W.M., *Blood-Brain Barrier Drug Targeting: The Future of Brain Drug Development.* Molecular Interventions, 2003. **3**(2): p. 90-105.
8. Nag, S., *The Blood-Brain Barrier: Biology and Research Protocols*. 2003, Totowa, New Jersey: Humana Press Inc.
9. Gumerlock, M.K., et al., *Osmotic blood-brain barrier disruption and chemotherapy in the treatment of high grade malignant glioma: patient series and literature review.* Journal of Neuro-oncology, 1992. **12**(1): p. 33-46.

10. Roman-Goldstein, S., et al., *MR and Cognitive Testing of Patients Undergoing Osmotic Blood-Brain Barrier Disruption with Intraarterial Chemotherapy.* American Journal of Neuroradiology, 1995. **16**(3): p. 543-553.

11. Chueh, B.-h., et al., *Leakage-Free Bonding of Porous Membranes into Layered Microfluidic Array Systems.* Analytical Chemistry, 2007. **79**(9): p. 3504-3508.

12. Douville, N.J., et al., *Fabrication of Two-Layered Channel System with Embedded Electrodes to Measure Resistance Across Epithelial and Endothelial Barriers.* Analytical Chemistry, 2010. **82**(6): p. 2505-2511.

13. Huang, S. and D.E. Ingber, *Shape-Dependent Control of Cell Growth, Differentiation, and Apoptosis: Switching between Attractors in Cell Regulatory Networks.* Experimental Cell Research, 2000. **261**: p. 91-103.

14. Huang, Z., et al., *Microfabrication of cylindrical microfluidic channel networks for microvascular research.* Biomedical Microdevices, 2012. **14**(5): p. 873-883.

15. Baker, B.M., et al., *Microfluidics embedded within extracellular matrix to define vascular architectures and pattern diffusive gradients.* Lab on a Chip, 2013. **13**(16): p. 3246-3252.

16. Tung, C.-k., et al., *A contact line pinning based microfluidic platform for modelling physiological flows.* Lab on a Chip, 2013. **13**(19): p. 3876-3885.

17. van der Meer, A.D., et al., *Three-dimensional co-cultures of human endothelial cells and embryonic stem cell-derived pericytes inside a microfluidic device.* Lab on a Chip, 2013. **13**(18): p. 3562-3568.

18. Wang, X.-Y., et al., *Engineering interconnected 3D vascular networks in hydrogels using molded sodium alginate lattice as the sacrificial template.* Lab on a Chip, 2014. **14**(15): p. 2709-2716.

19. Ghandehari, H., et al., *Size-Dependent Permeability of Hydrophilic Probes Across Rabbit Colonic Epithelium.* The Journal of Pharmacology and Experimental Therapeutics, 1997. **280**(2): p. 747-753.

20. Cussler, E.L., *Diffusion: Mass Transfer in Fluid Systems*. 2009, Cambridge: Cambridge University Press.

21. Liu, S., et al., *The Role of Pericytes in Blood-Brain Barrier Function and Stroke.* Current Pharmaceutical Design, 2012. **18**: p. 3653-3662.

22. Diaz-Flores, L., et al., *Pericytes. Morphofunction, interactions and pathology in a quiescent and activated mesenchymal cell niche.* Histology and Histopathology, 2009. **24**: p. 909-969.

23. Armulik, A., G. Genove, and C. Betsholtz, *Pericytes: developmental, physiological, and pathological perspectives, problems, and promises.* Developmental Cell, 2011. **21**(2): p. 193-215.

24. Allt, G. and J.G. Lawrenson, *Pericytes: Cell Biology and Pathology.* Cells Tissues Organs, 2001. **169**(1): p. 1-11.

25. Fujimoto, K., *Pericyte-endothelial gap junctions in developing rat cerebral capillaries: a fine structural study.* The Anatomical Record, 1995. **242**(4): p. 562-565.

26. Frank, R.N., T.J. Turczyn, and A. Das, *Pericyte Coverage of Retinal and Cerebral Capillaries.* Investigative Ophthalmology, 1990. **31**(6): p. 999-1007.

27. Krueger, M. and I. Bechmann, *CNS pericytes: Concepts, misconceptions, and a way out.* Glia, 2009. **58**(1): p. 1-10.

28. Betsholtz, C., P. Lindblom, and H. Gerhardt, *Role of pericytes in vascular morphogenesis.* Mechanisms of Angiogenesis Experientia Supplementum, 2005. **94**(115-125).

29. Lai, C.-H. and K.-H. Kuo, *The critical component to establish in vitro BBB model: Pericyte.* Brain Research Reviews, 2005. **50**: p. 258-265.

30. Igarashi, Y., et al., *Glial Cell Line-Derived Neurotrophic Factor Induces Barrier Function of Endothelial Cells Forming the Blood-Brain Barrier.* Biochemical and Biophysical Research Communications, 1999. **261**(1): p. 108-112.

31. Mi, H., H. Haeberle, and B.A. Barres, *Induction of Astrocyte Differentiation by Endothelial Cells.* The Journal of Neuroscience, 2001. **21**(5): p. 1538-1547.

32. Preston, J.E., H. Al-Sarraf, and M.B. Segal, *Permeability of the developoing blood-brain barrier to 14C-mannitol using the rat in situ brain perfusion technique.* Developmental Brain Research, 1995. **87**: p. 69-76.

33. Ek, C.J., et al., *Functional effectiveness of the blood-brain barrier to small water soluble molecules in developing and adult opossum (Monodelphis domestica).* Journal of Comparative Neurology, 2009. **496**(1): p. 13-26.

Chapter 6

Conclusion and Future Works

This research project successfully built an *in vitro* model of the blood-brain barrier that is capable of mimicking its physiological properties *in vivo*. Through vigorous verifications, we confirmed that PDMS that is required for building flexible and cell culture friendly channels have a limit to its quantitative assay applications. We found that hydrophobic molecules having log P values larger than 2.47 will induce hydrophobic interactions with PDMS channel walls, thus making quantitative assays inaccurate. However, any molecular markers with less hydrophobicity can be safely used in microfluidic PDMS channels. Next, we designed and built our microfluidic PDMS channels in such a way that it allows both 3D cell culture configurations and quantitative assays. We initially verified the cell culture aspect of the device by culturing bEnd3 single culture monolayers. We found that by culturing bEnd3 cells inside the device, we not only were able to increase the longevity of the cell culture, we also found higher TEER values, lower paracellular permeability, and higher P-gp functionality when compared to

conventional transwells. Finally, we added pericytes to complete the bi-culture configuration and astrocytes to complete the tri-culture configuration. Both of these configurations showed closer mimicry of the BBB than the single culture, confirming the importance of both of these cell types in the development and proliferation of the BBB. Furthermore, we found that our tri-culture configuration exhibited similar paracellular permeability as the *in vivo* data collected by other research groups, and the radius of tight junctions is also close to the *in vivo* values through the use of mathematical modeling. We believe that the device in its current state can accurately model the BBB and has the potential to allow us to better understand the mechanisms involved in regulating barrier properties of single and co-culture endothelial cell monolayers, provide a tool to accurately evaluate the permeability of new drug candidates across the BBB, and allow accurate *in vitro/in vivo* correlation of drug transport profiles, which will accelerate the development of new therapies for treatment of CNS disorders.

Currently, the 3D configuration produces the most accurate results; however, it requires constant supervision and medium changes of four times a day. The constant energy required for upkeep of these channels is potentially an issue and was somewhat problematic even during the experimental stage. The immediate future work is to rectify this issue by implementing automated medium change into the system in such a way that medium can be changed automatically on a daily basis with minimal human intervention. This can be achieved by implementing a braille system into the device or adding an additional pump to the device. Once this is complete, we can culture a large array of channels simultaneously with minimal effort, which seems to be a requirement for this device to become a

commercially successful product. Furthermore, we are planning to develop a pathological model of the BBB to model the diseased condition by altering either the 3D composition or culture conditions for the cells, such as oxygen level and seeding density. We believe that if a pathological model can be developed, it will further assist us in understanding the BBB in diseased conditions and accelerating the process of drug discovery.